VNIVERSITAT DE VALÈNCIA

Departament de Química Inorgànica
Institut de Ciència Molecular

Programa de Doctorat en Química (RD 99/2011)

Estudio magnetoestructural de nuevos sistemas moleculares basados en iones metálicos $5d$ y $4f$

Tesi Doctoral

Adrián Sanchis Perucho

Directors
Francisco José Martínez Lillo i Francisco Lloret Pastor

Juny de 2023

DECLARATION

Francisco José Martínez Lillo, Professor Titular del Departament de Química Inorgànica de la Universitat de València i **Francisco Lloret Pastor**, Catedràtic del Departament de Química Inorgànica de la Universitat de València

Certifiquen:
Que la present Tesi Doctoral titulada "Estudio magnetoestructural de nuevos sistemas moleculares basados en iones metálicos $5d$ y $4f$", en el marc del Programa de Doctorat en Química de la Universitat de València, ha sigut realitzada sota la nostra supervisió pel Graduat en Química i Màster en Química **Adrián Sanchis Perucho** a l'Institut de Ciència Molecular i al Departament de Química Inorgànica de la Universitat de València. Per a què així conste i per a què la seua presentació puga ser qualificada com a Tesi Doctoral amb Menció Internacional, signem el present document.

Paterna, Juny de 2023

FRANCISCO JOSE|MARTINEZ|LILLO
Firmado digitalmente por FRANCISCO JOSE|MARTINEZ|LILLO
Nombre de reconocimiento (DN): cn=FRANCISCO JOSE|MARTINEZ|LILLO, serialNumber=73565126V, givenName=FRANCISCO JOSE, sn=MARTINEZ LILLO, ou=CIUDADANOS, o=ACCV, c=ES
Fecha: 2023.06.05 19:40:12 +01'00'

Francisco José Martínez Lillo

FRANCISCO|LLORET|PASTOR
Firmado digitalmente por FRANCISCO|LLORET|PASTOR
Fecha: 2023.06.05 10:33:32 +02'00'

Francisco Lloret Pastor

AGRAÏMENTS

Per descomptat començar agraint als meus directors de Tesis. A Paco, perquè sempre esperava amb gran il·lusió a veure que ens ensenyava en les seues classes de Química Inorgànica III, i la raó per la qual vaig decidir dedicar-me a aquesta branca de la ciència. Recorde amb gust que era dels pocs en no emprar diapositives, i l'únic en utilitzar aquell estrany aparell que prou de nosaltres mai vam saber que era fins que va posar una d'eixes fetes a mà 'transparències'. També per la paciència per a explicar-me conceptes bàsics de magnetisme quan apareixia esporàdicament al seu despatx, que van ser unes quantes! Per altra banda, a José, el qual sempre que tenia un moment lliure es passava pel laboratori a vore que tal anaven les síntesis, i donar valuosos consells d'aspectes pràctics d'aquells que sols s'obtenen amb l'experiència. I sense oblidar també el fet que cada dia podia portar una nova idea per a una síntesi en una llista massa gran per a ser portada a cap per un sol home. Un minut de silenci per totes aquelles idees mortes.

Com no, agrair a la meua família, en especial al meu germà que em mantindrà en els subseqüents mesos de la nova temporada de la vida coneguda com '*el paro*'. I no mare, no és viable fer-te una *sortija* de reni o iridi.

També estic molt agraït a la resta dels integrants del grup: Rafa, Joan, Salah i Miquel, que en conjunt amb els meus directors, fan que siga un lloc molt agradable on treballar. I a Nico, que és probablement el millor tècnic de laboratori que es puga demanar.

També voldria agrair als bons amics que vaig fer tant en la facultat com en aquest laberint de rajola taronja conegut com l'ICMOL. A Camús, que probablement viu en el paradís de la gent celíaca i les baixes temperatures, aniré a vore't aquest estiu així que prepara la barana del moble. A Renato i Marta, amb els quals vaig compartir les penúries de la Tesi. Recorde quan Renato implorava el seu desig per la mort mentre escrivia la seua Tesi, jo per falta de temps vaig decidir deixar-me un *post-it* anotat per a fer-ho pròximament com es mostra en la Figura 1. Marta, una abraçada des d'ací i gràcies per introduir-me a la secta dels que prenen te. També vull agrair a Carlos, no hi ha moltes persones al món que sàpiguen de les penúries del Re(IV). El que em porta a agrair també als TFGs, que per sort o per desgràcia, van acabar treballant amb el reni i amb mi, Rafa, Ana i Irene.

Cal no oblidar tampoc el que per a mi és la secció dels reactius i les balances, on habiten els membres del '*otro lado*', actualment poblat per Cristina, Paula i Xavi, als quals desitge molta sort en les seues síntesis i inspiració per a escriure les Tesis. Així com una abraçada als seus antics membres ジョセミせんぱい i Fani. També desitjar molta sort i inspiració per a Nadia com a única membre predoctoral del grup de coordinació. A més a més, agrair a totes aquelles persones que sense la seua faena no farien que la meua fora tan fàcil, Maricarmen, José i Alex.

I would also like to express my sincere gratitude to Euan and his research group for allowing me to spend my PhD visit with them. It was a truly joyful experience, both in the lab and outside, thanks to the company of Emily, Dan, Lucy, Ellie, Ele, Marco, Mukesh, and Alvaro. The spicy chicken soup that I was treated to during the

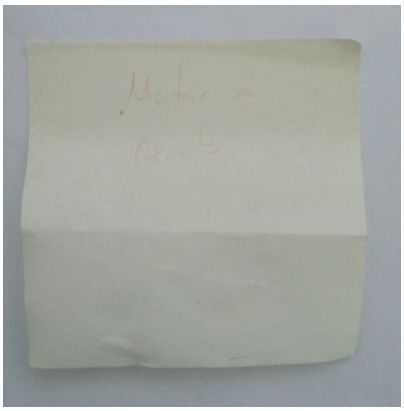

Figure 1: *Post-it* del període predoctoral de Renato en què estan plasmats els seus desitjos més obscurs. Sense dubte la tinta ja descolorida i paper desgastat mostra l'antiguitat de la peça i un període llarg d'escriptura.

group meeting at the beginning of my stay is still stinging inside me. Nevertheless, this was my first time ever travelling abroad, and I am grateful that it was to the rainy Edinburgh, a place that I remember fondly.

Com no, agrair també a la meua beca FPU referència 2017/02638, que en tants papers burocràtics ha estat.

Per últim, tot i que tinc una bona memòria a curt terme, la meua memòria a llarg termini és ja la d'un octogenari, la meua família pot acreditar-ho. Així doncs, en general agrair a qualsevol persona que haja influenciat per a què la Tesi arribe a bon port, d'aquesta manera si m'he deixat per agrair algú es pot incloure en l'anterior frase. Aquest és un truc que es va heretant de Tesi en Tesi.

TABLE OF CONTENTS

LIST OF ABBREVIATIONS

Abbreviations for units

K	Kelvin
Øe	Ørsted
A	Ampère
C	Coulomb
cm	Centimetre
emu	Electromagnetic unit
G	Gauss
g	Gram
H	Henry
Hz	Hertz
Kg	Kilogram
m	Metre
mol	Mole
s	Second
T	Tesla
V	Volt

General abbreviations and acronyms

$(AsPh_4)^+$	Tetraphenylarsonium cation
$(PPh_4)^+$	Tetraphenylphosphonium cation
$(NBu_4)^+$	Tetra-n-butylammonium cation
vs.	*versus*
ca.	*circa*
AC	Alternating current
bpym	2,2'-bipyrimidine
Buim	1-butylimidazole
cgs-emu	Centimetre-gram-second-electromagnetic unit
cip	Ciprofloxacin
DC	Direct current
DFT	Density functional theory
DMF	N,N-Dimethylformamide
dpa	2,2'-dipyridyl-amine
DPTA	Diethylenetriamine-N, N, N', N'', N''-pentaacetate
EPR	Electronic Paramagnetic Resonance
LF	Ligand field

MCE	Magneto-caloric effect
MeCN	Acetonitrile
Meim	1-methylimidazole
NMR	Nuclear Magnetic Resonance
ox	Oxalate
pba	1,3-propylenebis(oxamato)
pbaOH	2-hydroxy-1,3-propylenebis(oxamato)
PPMS	Physical Property Measurement System
PrOH	Propanol
QTM	Quantum Tunnelling of the Magnetisation
Ref.	Reference
SCM	Single-Chain Magnet
SI	*Système International*
SIM	Single-Ion Magnet
SMM	Single-Molecular Magnet
SOC	Spin-orbit coupling
SQUID	Superconducting Quantum Interference Device
TM-BEDT-TTF	Tetramethyl-bis(ethylenedithio)-tetrathiafulvalene
Viim	1-vinylimidazole
ZFS	Zero Field Splitting

List of main symbols

$10Dq$	D and q represent parameters regarding to the nature of the ligands and metals in the cubic crystal field
α, $\uparrow$	Spin function for $m_s = 1/2$ The α symbol is also used as a variable in the generalised Debye model or to indicate an angle degree
β, $\downarrow$	Spin function for m_s = -1/2
χ', χ''	In-phase or real, and out-of-phase or imaginary component of the magnetic susceptibility, respectively
χ	Magnetic susceptibility. DC or AC subindex will denote through which method the susceptibility was obtained, but if the contrary is not said χ is obtained by DC methods
χ_i^{Dia}	Pascal constant for diamagnetic contribution of atoms in a molecule
χ_S	Adiabatic susceptibility
χ_T	Isothermal susceptibility
χ_V, χ_M	Volume and molar magnetic susceptibilities, respectively
$\chi_\parallel$, $\chi_\perp$	Parallel and perpendicular to the principal axis magnetic susceptibility per mole, respectively
ΔT_{ad}	Difference of temperature under adiabatic conditions
Δ	Energy gap between states
$\hbar$	$\hbar = \frac{h}{2\pi}$. Reduced Plank constant

κ	Orbital reduction factor
λ	Spin-orbit coupling constant
λ_i^{Dia}	Pascal constant for diamagnetic contribution of bonds in a molecule
μ	Microscopic magnetic dipole moment
μ_0	Vacuum permeability
μ_B	$9.2740100783(28) \times 10^{-24}\,\mathrm{J{\cdot}T^{-1}}$. Bohr magneton
μ_N	$5.0507837461(15) \times 10^{-27}\,\mathrm{J{\cdot}T^{-1}}$. Nuclear magneton
μ_{eff}	Effective magnetic moment
ν	Lineal frequency Distortion parameter
Ω	Accessible and non-degenerate states
ω	Angular frequency. Related to the lineal frequency by $\omega = 2\pi\nu$
ϕ	Perturbed wave-function
π	3.14159... Irrational pi number Electron density from a π bond
ψ	Wave-function
τ	Relaxation time. τ_{av} is used for an average relaxation time
τ_0	Pre-exponential factor from the Orbach relaxation mechanism
θ	Weiss temperature
θ_k	Stevens coefficients
$\widehat{\mathcal{H}}$	Energy operator, also known as Hamiltonian
$\widehat{\mathcal{H}}_Z$	Zeeman operator. $\widehat{\mathcal{H}}_{Z,\parallel}$ and $\widehat{\mathcal{H}}_{Z,\perp}$ represent the parallel and perpendicular components, respectively
$\widehat{\mathcal{H}}_J$	Exchange interaction between neighbouring atoms Hamiltonian
$\widehat{\mathcal{H}}_{LF}$	Ligand field Hamiltonian
$\widehat{\mathcal{H}}_{SOC}$	Spin-orbit coupling Hamiltonian
$\widehat{O}_k^q$	Equivalent Stevens operators $\widehat{O}_k^q$
$\widehat{V}_{tetra}$	Tetragonal distortion operator
ξ	Free ion single-electron spin-orbit coupling constant
A	Constant for the Direct relaxation mechanism
$A_k^q\langle r^k\rangle$	Ligand field parameters
B	Measured magnetic field
$B(y)$	Brillouin function
C	Curie constant Constant in the Raman relaxation mechanism
C_{4v}, C_{2v}	Symmetry label
c_{ij}	Mixing coefficient
D	Axial parameter of magnetic anisotropy
D_{4h}, D_{3h}	Symmetry label
E	Energy Rhombic parameter of magnetic anisotropy

e	1.602176634(exact) $\times 10^{-19}$ C. Elementary charge Electron
E_i', E_i''	First- and second-order energies after applying the Zeeman operator without the field parameter, respectively
$E_i^{(n)}$	n being equal to 0, 1 and 2 for zero-, first- and second-order energies, respectively
$E_{1/2}$	Half-wave potential
g	2.00231930436256(35). Landé g-factor for the free electron
g_J	Landé g-factor for a free ion considering spin-orbit coupling effects
$g_\parallel$, $g_\perp$	Landé g-factor parallel and perpendicular to the principal axis, respectively
H	Externally applied magnetic field. DC or AC subindex will denote the static and amplitude of the oscillating field, respectively. If the contrary is not said the field is referred to DC methods.
h	6.62607015(exact) $\times 10^{-34}$ J·s. Plank constant
H_c	Coercivity or coercive field
I	Electric current
J	Total angular momentum of the system Magnetic exchange coupling constant
j	Total angular momentum quantum number
k_B	1.380649(exact) $\times 10^{-23}\mathrm{J}\cdot\mathrm{K}^{-1}$. Boltzmann constant
L	Total orbital angular momentum of the system
l	Orbital angular momentum quantum number, also known as azimuthal quantum number
M	Volume magnetisation, where M_{DC} and M_{AC} denote in which type of current where obtained, but if the contrary is not said M is normally obtained by DC methods
m_e	9.1093837015(28) $\times 10^{-31}$ Kg. Mass of the electron
M_J	z-component of the total angular momentum of the system
M_L	z-component of the total orbital angular momentum
m_l	Magnetic quantum number
M_r	Magnetic retentivity or remanence
M_S	z-component of the total spin angular momentum
M_s	Saturation magnetisation
m_s	Spin quantum number
N	Normalisation constant
n	Principal quantum number
N_A	6.02214076(exact) $\times 10^{23}$ mol^{-1}. Avogadro's number
O_h	Octahedral symmetry
R	Gas constant $R = k_B N_A$ Statistical least-square agreement factor
R_n	Radial function

S	Total spin angular momentum of the system
s	Spin angular momentum quantum number
S_E	Entropy
S_m	Magnetic entropy
T	Temperature
T_C	Curie temperature
T_N	Néel temperature
U	Energy barrier for the reversal of the magnetisation
$Y^l_{m_l}$	Spherical harmonic functions

ABSTRACT

In the present summary, it is described the scope and main goals of this Thesis work together with its methodology. At the same time, the reader is guided through the main results. To begin with, the full structure of this Thesis is basically divided into four Chapters, namely, an introduction which provides an overview where the general basic theoretical concepts about Molecular Magnetism are reviewed, followed by three subsequent Chapters. Two are dedicated to compounds based on $5d$ metal ions, specifically Re(IV), Ir(III) and Ir(IV), while the next focuses on the Ho(III), a $4f$ metal ion. Finally, there is a last remark Chapter that serves as a conclusion of the results that can be extracted from previous ones together with some perspectives for future works.

Chapter 1 delves into the fundamental knowledge related to the Molecular Magnetism field from a quantum view approach, where the orbital and spin angular momentum give rise to magnetic moments, whose relation with statistical thermodynamics leads to the magnetic behaviour of macroscopic samples. However, the deduced expression depends on the knowledge of the energy function of every thermally populated states. As they are most likely unknown for a specific system, it is rather common to rely on a few approximations. The Van Vleck formula is able to reproduce the magnetic susceptibility of a sample as long as the magnetic field can be considered a small perturbation of the initial system. Moreover, it is show how the approximation only holds at high temperature, where the externally applied magnetic field energy is lower than the thermal available energy. Besides, the deduced Van Vleck formula is only valid for paramagnetic systems, where $M = 0$ when $H = 0$. In this way, the paramagnetic behaviour of simple systems is explained.

In a second introductory part, it is presented the interaction between the orbital and spin angular momentum within an atom, and how it gives rise to the spin-orbit coupling of the magnetic moments, which is introduced through two different energies schemes. The first one known as L-S model for lighter elements and j-j model for heavier atoms. The so-called ZFS effect may arise by the combined effect of the spin-orbit coupling and the symmetry of the system, leading to the splitting of the different energy levels without the application of an external field. Those systems become then magnetically anisotropic. Another magnetic interaction appears relevant based on the distance between the different metallic centres and the temperature of the system. Those interactions can be mainly through ferromagnetic or antiferromagnetic arrangements, where at enough low temperature may not be neglected for any paramagnetic system. For weak interactions, they can be easily accounted by the Weiss parameter (θ). Besides, for systems where there is no orbital angular momentum associated to the ground state of the interacting metal ions, the interactions can be treated with an isotropic spin-spin exchange Hamiltonian, which includes the correlation between the chosen metallic centres by means of a magnetic exchange constant (J).

At the end of Chapter 1, it is considered the dynamic measurements of the magnetic susceptibility, and how the redistribution of the magnetic dipoles requires

of a certain amount of time that depends on the frequency of the externally applied magnetic field and the temperature. Systems with only one relaxation time or a distribution of them through the generalised Debye model, are briefly reviewed, along with the more common relaxation mechanisms that could take place. To this regard, the first system reported to have its spin dynamics studied is introduced, and how it leads to interesting magnetic hysteresis loops of a molecular level compared to the classic ferromagnetic ones.

The magnetic properties of species containing $4f$ and specially $5d$ metal ions have been relatively less explored compared to $3d$ based systems. This stems from the difficulty dealing with the stronger spin-orbit couplings that heavier atoms present, which becomes a direct influence factor on the magnetic anisotropy that characterises them. As consequence, while the knowledge of detailed exchange mechanisms related to $3d$ ions is considerably advanced, there is less understanding of the magnetic correlation in $4f$ and $5d$ systems. In this way, the following Chapters are mainly focused on the coordination chemistry and characterisation of systems based on Re(IV), Ir(III), Ir(IV) and Ho(III) metal ions. The scope of this research seeks to study either the magnetic behaviour of mononuclear complexes and enhance our comprehension of the magnetic exchange of species containing these metal ions, while exploring potential new applications for these systems. For achieving that goal, all these lines of work aim to share a methodology from a synthetic point of view within the Molecular Magnetism field, where the obtained compounds are mostly characterised by a preliminary infrared spectrum followed by an elemental analysis of C, N, and H percentages together with the heavy elements proportions. Afterwards, their structures are solved by means of single-crystal X-ray diffraction, and their pattern compared to the bulk by powder X-ray diffraction in order to confirm their homogeneity. In addition, for magnetically active samples the measurement of their magnetic properties on powder samples is conducted, and together with the structural data a correlation with the magnetic behaviour is performed.

Chapter 2 is dedicated to the study of systems based on Re(IV) metal ion, which is selected due to its high ZFS effects and effective spin value. Moreover, the lack of orbital contribution for octahedral Re(IV) complexes constitutes an advantage over other elements, where first and second spin-orbit effects take place. Thus, Re(IV) systems are relatively easier to fit through theoretical models. A lot of interesting results can be obtained from Re(IV) complexes. In the literature can be found compounds with remarkable properties, as SIM behaviour, expected to be exhibited for isolated Re(IV) entities, whilst polynuclear compounds contribute to a better knowledge of the magnetic exchange between different metal centres, where SMM phenomena may also arise. Besides, another singular magnetic phenomena, such as spin-canting, anti-, ferro-, ferri- or metamagnetism have been observed previously in systems containing the Re(IV) metal ion.

The published works within this Chapter can be divided into two parts. The first one is dedicated to study the magnetic properties of anionic mononuclear $[ReX_6]^{-2}$ species (X = F, Cl, Br, I), whilst a second part is dedicated to the neutral $[ReCl_4(bpym)]$ (bpym = 2,2'-bipyrimidine) compound.

As part of a collaboration with the University of Nevada (Las Vegas), the presented work, Article 1, describes the ammonium salt of the $[ReF_6]^{-2}$ anionic entity. This system exhibits two magnetic behaviours, metamagnetism and slow relaxation of the

magnetisation coexisting together, an attribute unusual in molecular systems based on 5*d* metal ions reported so far. It crystallises in the trigonal space group $P\bar{3}m1$. The hydrogen atoms from the ammonium cation are not considered during the refinement procedure, however, their most favourable positions are calculated by DFT methods, showing that oriental disorder can occur in ammonium salts. These distortions shorten some H···F distances emphasising hydrogen bonding. DFT bonding calculations of the $[ReF_6]^{-2}$ anion in its experimental geometry shows the presence of Re-F σ bonds, they being nearly ionic. Its comparison with the gas phase anion gives longer average Re-F bond lengths, so the difference is due to packing forces. The salt is also characterised by Raman spectroscopy, where the splitting of the Raman peaks are correlated with the site symmetries of the $[ReF_6]^{-2}$ anion.

On the other hand, the study of the magnetic properties by DC methods reveals an antiferromagnetic ordering of the spin carriers through weak intermolecular F···F (*via* Re-F···F-Re) and N···F interactions (*via* Re-F···N···F-Re) with a maximum in the χ_M *vs.* T plot. As the maximum wanes when higher magnetic fields are applied, it suggests the occurrence of a field-induced antiferromagnetic-to-paramagnetic ordering transition typical of metamagnetic systems. The magnetisation curve measured at 2 K support the occurrence of this behaviour, where the M values increase with the applied field and a smooth inflexion point is reached at a critical field. To study further the magnetic properties of the $(NH_4)_2[ReF_6]$ salt, AC magnetic susceptibility measurements have been performed, showing incipient out-of-phase signals at very low temperature, which is indicative of a system with slow relaxation of the magnetisation.

Regarding this particular work, which I am signing as the forth coauthor with an equal participation as the second and third ones, my personal contribution has focused mainly on the purification of the $(NH_4)_2[ReF_6]$ sample proportioned by our colleges and its characterisation by means of infrared spectroscopy, together with the preparation, measurement and treatment of the experimental data obtained through SQUID and PPMS devices.

The $(PPh_4)_2[ReX_6]$ [PPh_4^+ = tetraphenylphosphonium cation, X = Br or I] salts, fully described in Article 2 in a paper made in collaboration with the *Universidad de la República* (Uruguay), are one of the few examples of mononuclear compounds based on the Re(IV) metal ion that display field-induced slow magnetic relaxation described in the literature. The salts crystallise in the triclinic system with space group $P\bar{1}$, and their structures are made up of bulky $(PPh_4)^+$ cations that keep well separated the hexahalorhenate(IV) anions from each other.

Variable-temperature DC magnetic susceptibility measurements show a very similar behaviour for both compounds, typical of magnetically isolated Re(IV) systems. The decrease of the $\chi_M T$ values at low temperature mainly due to the high ZFS effects that the Re(IV) metal ion possess. On the other hand, AC magnetic measurements reveal the presence of out-of-phase signals for both compounds in the low temperature range, when an external magnetic field of 1000 or 5000 G is applied. However, the relaxation dynamics that the two compounds exhibit is not equally affected by the external fields, being 5000 G the optimal for the bromo derivative as suggested by the presence of more χ'' maxima that shifts towards higher frequencies, whilst its number decrease for the iodo derivative complex at that field. The obtained values of the α parameter by Cole-Cole representations suggest a narrow

distribution of the relaxation times for these mononuclear Re(IV) complexes. Thus, $\ln\tau$ *vs.* $1/T$ data are fitted considering that the relaxation of the magnetisation is driven by a sole Orbach mechanism. For a more accurate description of the whole curve in the bromo derivative case, a set of four spin-lattice relaxation mechanism of the magnetisation, namely, Orbach, Direct, Raman and QTM is considered. Remarkably, the bromo derivative complex exhibits the higher energy barrier of the $[ReX_6]^{-2}$ family.

My contribution to this work, where I appear as the second coauthor, has been centred on the practical aspects of synthesising, and properly crystallising the reported compounds in an appropriate manner for single-crystal X-ray diffraction studies. I have also been involved in the measurement and resolution of the structural data together with the X-ray powder characterization, as well as in the interpretation and processing of the experimental data obtained through the SQUID and PPMS magnetometers.

The last systems related to the hexahalorhenate(IV) species of this dissertation aim to keep the interesting magnetic properties displayed by Re(IV) metal ion, while adding new functionalities to the final material by the use of $[ReX_6]^{-2}$ (X = Cl, Br) anionic entities along with a cation with potentially biological interest. Thus, two novel Re(IV) compounds, of formula $[H_2cip][Hcip][ReCl_6]Cl \cdot H_2O$ and $[Hcip]_2[ReBr_6]$ (cip = ciprofloxacin) described in Article 3, constitute the first magnetoestructural study performed on salts based on protonated ciprofloxacin antibiotic containing a paramagnetic $5d$ ion.

The chloro derivative crystallises in the $P2_1/c$ space group, whilst the bromo derivative in the *Pbca*. Non-interacting Re(IV) mononuclear systems are possible to be obtained thanks to the bulky protonated ciprofloxacin cations. For a better understanding of the electrostatic forces that held together the crystal packing of both salts computed Hirshfeld surfaces are calculated and analysed, reflecting the variety of interactions that take place in their crystal lattices.

DC magnetic susceptibility measurements display a very similar behaviour for both compounds, typical of mononuclear systems containing a magnetically isolated Re(IV) ion. No maximum of the magnetic susceptibility is detected in the χ_M *vs.* T plot at low temperature, indicating the absence of significant antiferromagnetic interactions. Thus, the decrease detected in $\chi_M T$ *vs.* T plots would be mainly due to ZFS effects, which are very significant in mononuclear Re(IV) based systems. AC magnetic susceptibility measurements at low temperature reveal field-induced out-of-signals for both salts systems, where $\ln\tau$ *vs.* $1/T$ plots are obtained at an optimal 5000 G external field. The data can be firstly fitted considering that the magnetization relaxation only involves an Orbach process, but a more accurate fitting of the whole experimental data curve is possible considering Direct and Raman mechanisms.

In the next part, it is explored the direct substitution of two chloride ligands from the $[ReCl_6]^{-2}$ entity by a bpym ligand, as a different approach for synthesising new systems using the complex as a ligand. Nevertheless, in Article 4, it is reported the effect of the crystallization solvent on the $[ReCl_4(bpym)]$ compound, and how its magnetic properties change in contrast with the unsolvated system.

$[ReCl_4(bpym)] \cdot MeCN$ and $[ReCl_4(bpym)] \cdot CH_3COOH \cdot H_2O$ crystallise in the monoclinic system with space groups $P2_1/n$ and $P2_1/c$, respectively. Both sys-

tems present short Re-Cl···Cl-Re contacts displaying a corrugated crystal framework, which host the solvent molecules. Moreover, intermolecular interactions also occur between [$ReCl_4$(bpym)] entities and their crystallisation solvents. To assess all these contacts, Hirshfeld surfaces have been calculated and their fingerprint plots analysed.

Regarding the magnetic properties of both compounds, the significant antiferromagnetic through-space interactions between different Re(IV) entities preclude the occurrence of the slow relaxation of the magnetisation phenomenon. Both systems exhibit a similar magnetic behaviour with a reduction in the $\chi_M T$ values with the decreasing temperature, as a result of the antiferromagnetic interactions between Re(IV) ions as well of the ZFS effect. No maximum of the magnetic susceptibility is detected for either compound. In contrast, the magnetic properties of the unsolvated system are very different, exhibiting magnetic ordering through spin-canting. Thus, it is possible to tune the magnetic behaviour in this type of Re(IV) complexes by changing the crystallisation solvent.

The use of [$ReCl_4$(bpym)] metalloligand towards a paramagnetic metal ion as Cu(II) is reported in Article 5 with our collaborators from the *Università della Calabria* (Italy). The paper discusses two one-dimensional coordination polymers with the general formula $\{[ReCl_4(\mu\text{-bpym})CuX_2] \cdot Solv\}_n$, which exhibit different crystal structures depending on X and Solv. Specifically, when X = Cl and Solv = H_2O, the system crystallizes in the $P2_1/c$ space group, whereas when X = Br and Solv = $CHCl_3$, it crystallizes in the $P2_1/n$ space group. Both systems are made up of dinuclear [$ReCl_4(\mu$-bpym)CuX_2] units, which are linked together through double Cu-X-Cu halide bridges generating chains with solvent molecules present in their respective crystal lattices. In this way, these compounds constitute the first reported examples of doubly halogen-bridged and bipyrimidine-based Cu(II) chains including a paramagnetic $5d$ metal ion.

Intermolecular interactions of the type Re-Cl···Cl-Re and X···π are present for both compounds, together with hydrogen bonds that connect terminal chlorine atoms of the dinuclear units in the chloro derivative compound. Thus, several magnetic exchanges can occur through intermolecular interactions, but mainly *via* Re-Cl···Cl-Re contacts. Intramolecular interactions also take place between Re(IV) and Cu(II) ions through the bpym ligand and between Cu(II) ions mediated by halogen atoms. The magnetic susceptibility data obtained by DC measurements show how the $\chi_M T$ values decrease as the temperature is lowered, chiefly due to antiferromagnetic molecular interactions and ZFS effects. The presence of maxima in the χ_M *vs.* T plots unambiguously supports the occurrence of antiferromagnetic exchange between the involved metal ions.

Due to the complexity of the systems presenting a highly anisotropic metal ion as Re(IV) and different magnetic exchanges, there is a lack of an adequate theoretical model to fully evaluate the experimental magnetic susceptibility curve. Nevertheless, two types of treatments are made in the temperature range 20-300 K, where there is a good lineal behavior of the ${\chi_M}^{-1}$ *vs.* T plot. In the first one, the data is fitted to the Curie-Weiss expression, where the negative Weiss constant and magnitude supports the fact that significant antiferromagnetic interactions occurs in both systems. In the second one, an isotropic simulation of the experimental data with two different exchange coupling constants for the Cu(II)-Cu(II) and Re(IV)-Cu(II)

interaction is also performed. The computed value of the Cu(II)-Cu(II) exchange indicates a relatively strong antiferromagnetic coupling, whereas a much less intense antiferromagnetic coupling would take place between Re(IV) and Cu(II) ions in both compounds.

In this collaborative work, which I am signing as the second coauthor, my personal contribution has been the practical aspects of synthesising and appropriately crystallising the $\{[ReCl_4(\mu\text{-bpym})CuBr_2] \cdot CHCl_3\}_n$ compound for its structural resolution. I have also been involved in its characterisation through X-ray powder diffraction, infrared spectrum and elemental analysis of C, H, N percentages together with the preparation, measurement, interpretation, and processing of experimental data obtained through the SQUID magnetometer.

On the other hand, the works dealing with iridium-based compounds are collected in Chapter 3. While Ir(III) systems have been intensively researched because of their potential technological applications in areas such as catalysis, imaging and sensing, Ir(IV) complexes have remained largely unexplored. Thus, this Thesis work is focused on the developing of new Ir(IV) compounds in an aim of better understanding its chemistry and properties. In contrast to Ir(III) species, it is a paramagnetic metal ion under octahedral and distorted octahedral symmetry, with promising potential magnetic properties due to its high ZFS effects, that confers Ir(IV)-based compounds with magnetic anisotropy. Moreover, as a $5d$ metal ion with a significant delocalisation of its electronic density over the ligands, it causes an enhancement on the magnetic properties in polynuclear compounds when compared to its $3d$ analogues. Nevertheless, its $^2T_2$ fundamental term combined with its high spin-orbit coupling make these systems very difficult to be analysed.

In this dissertation, commercially available alkaline hexahaloiridate(IV) salts are employed as starting reagents for ligand and cation exchange. Bulky counter-cations as $(NBu_4)^+$ not only confer practical properties to the final compound, as solubility in a wide variety of solvents, they also lead to interesting systems that can display slow relaxation of the magnetisation. Moreover, this new formed salts are present in the preparation of novel polynuclear Ir(IV) systems, by employing $[IrX_6]^{2-}$ units (X = Cl, Br) as building blocks towards other $3d$ paramagnetic metal ions, as for instance, Cu(II), where imidazole derivatives are also used as auxiliary ligands to block its equatorial coordination positions.

On the other hand, ligand exchange in these systems become a challenge from a synthetic point of view, mainly due to the easy reduction that Ir(IV) species undergoes to their more stable Ir(III) analogues. To this regard, Article 6 deals with the substitution of two bromide ligands with a bpym and the study of three new crystal structures based on Ir(III) metal ion and bpym, where polymorphism is also observed when different crystallisation solvents are used. Just a few works deal with the crystal polymorphism phenomenon within Ir(III) chemistry. Moreover, only a few crystal structures of mononuclear bpym-based Ir(III) have been reported up to date. Thus, $NBu_4[IrBr_4(bpym)]$ crystallising in the $P2_1/c$, and $[IrBr_3(bpym)(MeCN)]$, in the $P2_1/n$ and $P2_12_12_1$ space group, have been investigated. Intermolecular interactions of the type C-H···N and weak C-H···Br are present in the salt system. In contrast, the polymorphs display π···Br, C-H···Br and Br···Br contacts for stabilising their 3D supramolecular framework. Further analysis of their crystal structure have also being performed through SHAPE and CrystalExplorer programs.

The oxidation of these new Ir(III) compounds to Ir(IV) through chemical procedures is preliminary studied with stoichiometric mixtures of different oxidants in acidic aqueous solution, but the Ir(III) complexes demonstrated to be stable against oxidation. Furthermore, the electrochemical properties of these compounds were carefully investigated. Cyclic voltammetry experiments performed on these systems show the reversible behaviour of the Ir(III)-Ir(IV) pair in the 10-500 $\mathrm{mV\,s^{-1}}$ scanned range for the $NBu_4[IrBr_4(bpym)]$ salt, whereas no reversible peaks are observed for the other systems.

A novel and rational strategy to prepare new and interesting mixed magnetic materials based on Ir(IV) and paramagnetic $3d$ metal ion has been followed, which explored the use of $[IrX_6]^{-2}$ units (X = Cl, Br) as metalloligands towards Cu(II). In Article 7, the results regarding the chloro species are presented, where the starting Ir(IV) reagent $(NBu_4)_2[IrCl_6]$ used in the synthesis of the Ir(IV)-Cu(II) chains is structurally and magnetically characterised together with the heterobimetallic chain of formula $\{IrCl_5(\mu\text{-}Cl)Cu(Viim)_4\}_n$ (Viim = 1-vinylimidazole), which constitutes the first reported system based on Ir(IV) and Cu(II). Both complexes crystallise in the $C2/c$ space group. However, due to the bulky counter-cations in the mononuclear salt, $[IrCl_6]^{-2}$ units are well isolated between them. On the other hand, the crystal packing of the one-dimensional compound connect the different chains to each other through $\pi\cdots\pi$ stacking interactions, adopting perpendicular arrangements between them.

The $\chi_M T$ *vs.* T plot for the mononuclear compound is fitted to Curie-Weiss equation down to *ca.* 50 K, and some more remarks are made outside the publication in the theoretical model proposed in this Thesis work, where the $\chi_M T$ curve is fitted for the whole temperature range. On the other hand, the same plot for the one-dimensional system is roughly fitted considering an isotropic effective spin chain of $S = 1/2$, exhibiting a ferromagnetic exchange coupling between Cu(II) and Ir(IV). In this way, it is the first time that an evaluation of the magnetic interaction between this $3d$-$5d$ couple of metal ions linked together through the chloride ligand has been performed. Besides, AC magnetic susceptibility measurements are carried on the mononuclear compound to assess its induced-field out-of-phase signals. Its relaxation process is fitted through an Orbach mechanism for the lineal part of the $\ln\tau$ *vs.* $1/T$ plot. However, a whole description of the curve is reproduced when a Direct and Raman mechanism are considered.

On the other hand, Article 8 compiles the results obtained with the $[IrBr_6]^{-2}$ unit, this Article being the last published work on Chapter 3. The $(NBu_4)_2[IrBr_6]$ crystal structure was previously published elsewhere, whereas its experimental $\chi_M T$ values are presented in this Thesis work and fitted with the magnetic treatment introduced in this dissertation. Slow relaxation of the magnetisation behaviour has been confirmed by means of AC magnetic susceptibility measurements for the isolated hexabromoiridate(IV) entities, becoming the fifth reported Ir(IV)-based SIM. As in the case of the mononuclear chloro derivative compound, the $\ln\tau$ *vs.* $1/T$ plot shows a lineal range well reproduced through an Orbach mechanism for a process with just one relaxation time, whilst the whole curve is better reproduced by means of a Direct and Raman mechanisms.

The use of the mononuclear entity towards Cu(II) together with auxiliary ligands is also explored with the bromo derivative compound. Thus, three novel one-

dimensional complexes of formula $\{IrBr_5(\mu\text{-}Br)Cu(L)_4\}_n$ (L = Meim, Viim or Buim, being Meim = 1-methylimidazole and Buim = 1-butylimidazole) have been also structurally and magnetically studied. They crystallise in the $P\bar{1}$, $C2/c$ and $Pccn$ space groups, respectively. In the Meim and Viim derivatives there are significant Ir-Br···Br-Ir contacts and π···Br interactions between chains. In contrast, the bulkiness of the butyl groups of the Buim ligands keep fully separated the chains from each other.

As in the case of the chloro species, DC magnetic susceptibility data are roughly treated considering an isotropic effective spin chain of $S = 1/2$. The $\chi_M T$ *vs.* T plots feature an antiferromagnetic exchange coupling between Cu(II) and Ir(IV) metal ions at low temperature for the Meim and Viim derivatives, whilst a dominant ferromagnetic coupling is observed for the Buiim derivative.

The rare-earth element series have garnered significant interest due to their unique electronic, magnetic, and optical properties. For example, mononuclear complexes of Ln(III) ions exhibiting slow relaxation of the magnetisation, the so-called lanthanide SIMs, have attracted much attention in diverse areas of nanoscience and nanotechnology. Moreover, due to their well-known magnetothermal and quantum coherence properties, mononuclear Gd(III), Dy(III) and Ho(III) derivatives are representative examples of promising applications of Ln SIMs as both molecular cryomagnetic coolants and quantum information processing technologies. Consequently, Chapter 4 explores the properties and potential applications of the Ho(III) metal ion from the lanthanides metal-block.

Moreover, when searching for molecular materials with diverse physical properties that can be utilised in different technological applications, a recommended approach is to select a starting molecule possessing one of them. For this reason, our attention has been directed towards the extensively researched group of mononuclear complexes containing Ln(III) ions (Ln = Gd, Dy, Ho) and linear or cyclic polyaminocarboxylate ligands, which are commonly employed as contrast agents in magnetic resonance imaging. In Article 9, our first results regarding the synthesis, structural and general physicochemical characterisation of a novel Ho(III) complex of formula $Na_2[Ho(DPTA)(H_2O)] \cdot 8H_2O$ (DPTA = Diethylenetriamine-N,N,N',N'',N''-pentaacetate) as well as a preliminary investigation of the magnetic field dependence through DC and AC magnetic measurements are presented. The compound crystallises in the $P2_1/n$ space group and consists of two crystallographic independent nine-coordinate Ho(III) metal ions with similar distorted geometries, between a tricapped trigonal prism and a monocapped square antiprism, according to the SHAPE program calculations. The diholmium entities are further connected through Na^+ ions to give a three-dimensional network, where in their small rectangular pores are most of the crystallisation water molecules.

DC magnetic measurements show how the $\chi_M T$ values continuously decrease upon cooling, being mainly attributed to LF effects that cause the splitting of the different M_J on the $^5I_8$ ground state. This fact is further supported by the no superposition of the isothermal magnetisation curves. On the other hand, the dynamic magnetic properties are also studied, revealing out-of-phase signals with and without an externally applied magnetic field. The analysis of χ' and χ'' *vs.* ν plots in a 1-10 kHz range of frequencies is performed through the generalised Debye equation, showing a wide relaxation times distribution. The $\ln \tau$ *vs.* $1/T$ curve is fitted to a sole

Orbach mechanism with values within the range of other few examples of Ho(III) SIMs. Besides, despite its limited cryogenic magnetic refrigeration performance, the magnetothermal results illustrate the potential of magnetically anisotropic Ho(III)-based SIMs as prototypes of molecular cryomagnetic coolants operating near the strategically relevant hydrogen liquefaction temperature.

My contribution to this work, which I am signing as the fourth coauthor, has been centred on a fundamentally crystallographic aspect, focusing on the development of a measurement strategy and the collection of X-ray diffraction data on a single-crystal of the holmium compound, as well as refining the crystallographic data for its structural resolution.

CHAPTER 1

INTRODUCTION

The fascinating attraction between two materials like iron and lodestone always have wondered humankind. Thus, magnetism became a topic of scientific study in order to unravel such a mystery. Nevertheless, the first investigations were mainly based on minerals and inorganic materials, but with time, it was found that more complex molecules could exhibit interesting magnetic properties as to be weakly attract or repelled by magnetic fields. More recently, the understanding, control, and design of magnetic molecules has driven to the development of a new field of research known as Molecular Magnetism.[1–10]

This field deals with the magnetic properties of isolated molecules and assemblies of paramagnetic molecules. These molecules may contain one or more magnetic centres, which are not only restricted to the coordination chemistry of metal ions, organic radicals represent another good example in this area. On the other hand, assemblies of molecules are most often found in crystalline solids with very weak interactions between these basic entities. However, they can also be found in extended systems, built in a way that maximizes the interactions between the different entities, which hopefully would yield to bulk magnetic properties.

The scope of Molecular Magnetism is broad as it is a discipline that involves different fields of knowledge. For instance, synthetic chemistry in order to develop procedures to design molecule-based systems that exhibit predictable magnetic properties based on the symmetry and orthogonality of the magnetic orbitals. In this regard, a lot of different compounds have been reported containing several kinds of metallic ions, organic radicals, and novel bridging ligands. It also uses ideas from theoretical chemistry, which derive directly from the basic concepts developed by quantum mechanics, bringing the theoretical models used in other fields to their limits. In particular, the molecular orbital model obtained by self-consistent field methods, where the real wave-function of a system is too complex to be found directly and is simplified assuming that electrons behave independently from each other. Thus, an approximated wave-function is found after an iterative process, but as a result, the interaction between magnetic centres cannot be properly understood within this framework level because it lacks the correlation. Consequently, there are different interpretations of how the interaction between magnetic centres occurs with several models that compete, each of them with their advantages and disadvantages. For this reason, Molecular Magnetism is far from being a closed field from a theoretical viewpoint.

This research field also plays an important role in the use of molecular systems in the engineering of electronic circuits and devices, where the spin transition phenomenon that occurs in some transition metal complexes represents one of the most spectacular examples of molecular bistability. Furthermore, the spin-based electronics using the quantum effects of the electron spin for information processing allowed the study towards quantum computing. On the other hand, the slow relaxation of the magnetisation that certain systems presents, opened the opportunity to store magnetic information in the size of a molecule.

Lastly, the Molecular Magnetism field also make scene in areas that would not seem close to the material science study, for example in the interaction between the magnetic centres of a metalloenzyme within the field of biological processes involving active sites that contain metal ions.

At this stage, the introduction within this Thesis, even sometimes too basic or simplistic within the rich and vast area of Molecular Magnetism, it is a small summary of the basic concepts that I learned and subjectively assumed were of enough importance to understand, at least, most of the articles that constitute this dissertation.

1.1 Basic concepts of Molecular Magnetism

In classical mechanics, Ampère or Biot-Savart laws describe how a magnetic field, $\vec{B}$, arises from the movement of charged particles through a conductor as depicted in Figure 1.1a. Often it is convenient to represent the magnitude and direction of a magnetic field vector by imaginary lines called magnetic field lines as shown in Figure 1.1b, whereas a small arrow points its direction in the vicinity of the field source, while its density (number of lines per unit of area) determine their magnitude.

On the other hand, ordinary matter is composed of atoms, which are made of subatomic particles ordered in a nucleus where protons and neutrons dwell, and orbiting around them are the electrons, being the latter negatively charge. Thus, if an electron of mass, m_e, with charge, $-e$, is rotating in a circle as in Figure 1.1c, this movement that can be described as an angular momentum, $\vec{L}$, has associated then a magnetic dipole moment, $\vec{\mu}$, as given by equation (1.1). Note that the direction of the angular momentum of the electron and its magnetic dipole moment have opposite directions due to the negative charge of the electron. From now on for short, the magnetic dipole moment will be just called magnetic moment, and to point its origin they will be referred as orbital angular momentum and orbital magnetic moment.

$$\vec{\mu} = \frac{-e}{2m_e}\vec{L} \tag{1.1}$$

Before proceeding any further, the classical mechanics developed through the centuries are not able to correctly predict the results from the experiments at a subatomic level. This is manly due to the wave-like nature of particles. As de Broglie suggested, every mass in movement has associated a wavelength, thus all matter exhibits properties of both particles and waves. In macroscopic bodies their mass is so greater in comparison to their speed, that its wavelengths are undetectably small, and the wave-like properties cannot be observed. This undetectability is why classical mechanics can be used to explain the behaviour of macroscopic bodies. On the other hand, at microscopic scale, in which masses are small and wave properties are noticeable, it is necessary to apply a different approach and quantum mechanics are used.

In quantum mechanics, the state of a system is describe by wave-functions, and the only way to measure a parameter of such system without changing its state is through certain mathematical operators. However, it is impossible to know two different parameters of a system simultaneously if their operators do not commute.

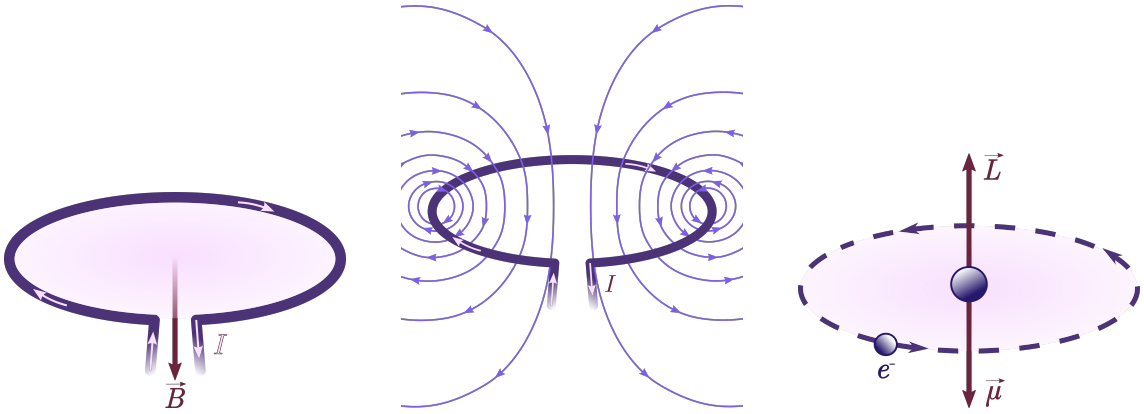

Figure 1.1: (a) A loop carrying a current of intensity I, which generates a magnetic field $\vec{B}$ (b) The magnetic field distribution as indicated by some field lines are shown for a current loop. (c) Simplified view of the orbit of an electron revolving around a nucleus. Note that the direction of I is by convention the opposite to the flow of electrons. The direction of the magnetic field is also known through the right-hand mnemonic rule.

In other words, when operators commute they have a set of functions in common. Therefore, before and after applying those operators the wave-function describing the state of the system is exactly the same. Moreover, the wave-functions found as a result of applying one or more operators have their values restricted to a set of discrete numbers (quantisation), instead of being able to present a continuous spectrum as in classical mechanics.

In the case of the angular momentum of any body in quantum mechanics, the operators that commute, and therefore are known simultaneously, are the square of the magnitude and one component of the angular momentum vector. Commonly the z-component is chosen by convention, because it leads to more simple expressions when polar coordinates are used. The result of applying those operators to a wave-function is described by equations (1.2) and (1.3), where the functions in common are known as spherical harmonics, $Y^l_{m_l}$. Furthermore, both the magnitude and the z-component of the angular momentum have restricted their values by the quantum numbers l and m_l. The allowed values of l are positive integers lying between 0 and ∞, while for m_l are integers between l and $-l$. A representation of the orbital angular momentum, $\vec{L}$, is shown in Figure 1.2.

$$\widehat{L}^2\, Y^l_{m_l} = L^2\, Y^l_{m_l}; \qquad L^2 = l(l+1)\hbar^2 \tag{1.2}$$

$$\widehat{L}_z\, Y^l_{m_l} = L_z\, Y^l_{m_l}; \qquad L_z = m_l\hbar \tag{1.3}$$

The magnitude of the magnetic moment of an electron due to the orbit can be calculated through the classical expression (1.1) and the quantum value of the angular momentum, leading to equation (1.4), where μ_B represents a fundamental quantity in Molecular Magnetism. It is the intrinsic magnetic moment of an electron called Bohr magneton.

$$|\vec{\mu}| = \frac{e}{2m_e}|\vec{L}| = \frac{e\hbar}{2m_e}\sqrt{l(l+1)} = \mu_B\sqrt{l(l+1)}; \qquad \mu_B = \frac{e\hbar}{2m_e} \tag{1.4}$$

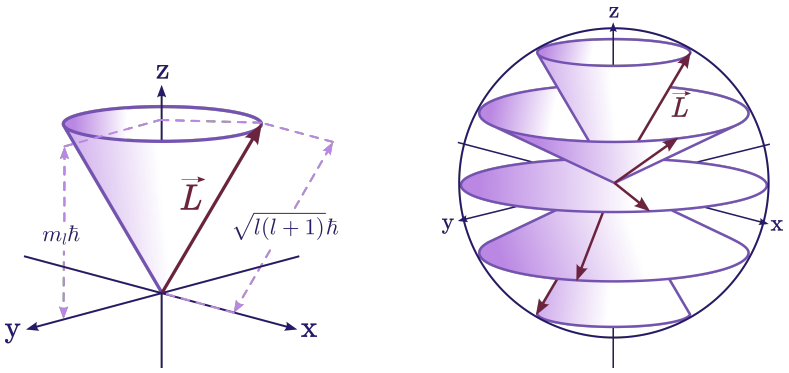

(a) **(b)**

Figure 1.2: (a) Magnitude and z-component of the orbital angular momentum, $\vec{L}$. Due to the uncertainty of the x- and y-component, an angular momentum is usually depicted as a vector precession around all possibilities which lead to a cone shape. (b) Representation of the different orientations of m_l for an orbital angular moment vector with $l = 2$.

Likewise, the z-component of the orbital magnetic moment is deduced from equation (1.1) and the value of L_z, as follows

$$\mu_z = \frac{-e}{2m_e} L_z = \frac{-e\hbar}{2m_e} m_l = -\mu_B m_l \tag{1.5}$$

Furthermore, all elemental particles have intrinsically associated to its existence a spin, $\vec{S}$, as if it was another fundamental property like its mass or charge. This spin can be treated as an angular momentum and it has associated a magnetic moment. For distinguishing from their orbital counterparts they are classically called spin angular momentum and spin magnetic moment. The quantification of this new angular momentum is analogous to the orbital already made. Thus, equations (1.2) and (1.3), can be written as (1.6) and (1.7).

$$\widehat{S}^2 \, \psi^s_{m_s} = S^2 \, \psi^s_{m_s}; \qquad S^2 = s(s+1)\hbar^2 \tag{1.6}$$

$$\widehat{S}_z \, \psi^s_{m_s} = S_z \, \psi^s_{m_s}; \qquad S_z = m_s\hbar \tag{1.7}$$

All known fermions, such as neutrons, protons and electrons, have quantify their spin angular momentum with the spin quantum number, s, to a unique value of $1/2$, hence the values of m_s are restricted to $1/2$ or $-1/2$ as depicted in Figure 1.3. Since the s value is the same in both cases they are usually referred only by their m_s number. Therefore, there are only two wave-function for describing the spin state of the electrons, $\psi_{\frac{1}{2}}$ and $\psi_{-\frac{1}{2}}$, for short they are commonly referred as α and β, respectively. Moreover, chemists often use the symbols $\uparrow$ and $\downarrow$ for representing them in energy diagrams. In contrast with the spherical harmonics where the functions are known, the spin functions α and β have not specified forms and can be considered to rely of some sort on hypothetical internal coordinate inside the particle.

Although the orbital and spin angular momenta are analogous, an important distinction between their magnetic moments should be made. It was demonstrated that fermions are relativistic and their magnetic moments are multiply by a dimensionless quantity, g, called Landé g-factor. In the case of the orbital magnetic moment

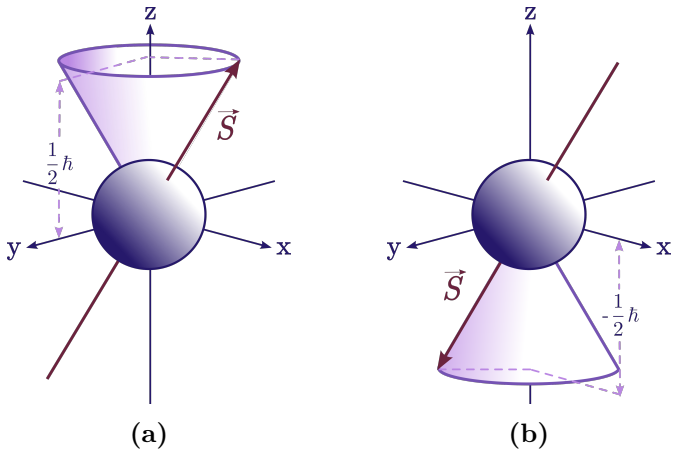

Figure 1.3: The z-component of the spin angular momentum of an electron for (a) $m_s = \frac{1}{2}$ and (b) $m_s = -\frac{1}{2}$.

of the electron the factor is equal to 1, but for their spin magnetic moment its value is *ca.* 2. Thus, equations (1.1) and (1.5), are written as (1.8) and (1.9).

$$\vec{\mu} = g\frac{-e}{2m_e}\vec{S} \tag{1.8}$$

$$\mu_z = -g\mu_B m_s \tag{1.9}$$

Indeed, in every neutral atom there is the exact same amount of protons and electrons with a wide variation of neutrons setting different isotopes, so the total magnetic moment of an atom should be the combination of the intrinsic magnetic moments due to the spin of all particles, plus the orbital contributions of the electrons. Nevertheless, the combination of all the magnetic moments of the particles at the nucleus, known as Nuclear magneton, μ_N is *ca.* 1800 times lower than the Bohr magneton. This high difference between values means that electrons are more strong magnets than protons and neutrons, and consequently, the magnetic properties of matter relies on their electronic configuration rather than their nuclear states. Nonetheless, the intrinsic magnetic moments of certain nuclei is a feature exploited in Nuclear Magnetic Resonance (NMR) experiments, but for most purposes nuclear-magnetic effects will be neglected.

The electronic configuration of an atom determines where is more probable to localise an electron. They are distributed throughout the atomic orbitals in a specific way by the *aufbau* principle used in conjunction with the Hund's rule and the Pauli exclusion principle. To begin with, an atomic orbital is a wave-function that appears as solution after applying the energy operator, also known as Hamiltonian denoted by $\widehat{\mathcal{H}}$, to a one-electron system. The equation (1.10) is known as the Schrödinger equation, where an atomic orbital is defined by a set of three quantum numbers, n, l, and m_l.

$$\widehat{\mathcal{H}}\,\psi_{n,l,m_l} = E\,\psi_{n,l,m_l} \tag{1.10}$$

The wave-function of an atomic orbital can be factorised between its radial and angular part as $\psi_{n,l,m_l} = R_n\,Y^l_{m_l}$, where $Y^l_{m_l}$, is the one discussed previously, but now the allowed values of l are positive integers lying between 0 and $n-1$, while n, is

a positive integer with values lying between limits 1 and ∞. Besides, m_l keeps its values as integers between $+l$ and $-l$.

In summary, n values determine the size of the orbit in which the electron is moving and defines its energy, while l values provide detailed information about the region of space in which an electron may move, describing the shape of the orbital, and last m_l relates to the directionality of that orbital.

As Pauli exclusion principle states, two electrons in an atom cannot have the same set of quantum numbers, so only two electrons can occupy the same orbital due to the only two possible values of m_s. This means that every electron in an atom is uniquely defined by its set of four quantum numbers, n, l, m_l and m_s, so the full wave-function that describes the state of an electron is that of equation (1.11). It is worth mentioning that the orientation of the electronic spin does not affect the energy of the system, because the Hamiltonian does not operate on the spin coordinates.

$$\psi_{n,l,m_l,m_s} = R_n \, Y^l_{m_l} \, \psi_{m_s} \tag{1.11}$$

Furthermore, the Hund's rule states that if an orbital presents degeneracy (same energy level), in its ground state, pairing of electrons cannot begin until each orbital in the set contains one electron, those electrons that remain unpaired have all parallel spins, in other words, they have all the same values of m_s. In conjunction with the other two rules, the *aufbau* principle organises the electrons into different orbitals in increasing energy order.

Going one step further, it is time to denote how magnetic moments of matter interact under an external magnetic field. In the first place, the externally applied magnetic field, that can be created by means of a current or a permanent magnet, will be indicated as $\vec{H}$, and distinguished from the measured magnetic field, $\vec{B}$, that appears in a region after applying a $\vec{H}$-field. The problem of notation and units used in magnetism deserves a few words, for being one of the few areas where the old cgs-emu system is still in use, and the SI system has not been universally applied.[11–13] Thus, the units of $\vec{H}$ are Ampère per metre ($\mathrm{A\,m^{-1}}$) in the SI and Ørsted (Øe) in the cgs-emu system, being 1 Øe $= 10^3/(4\pi)$ $\mathrm{A\,m^{-1}}$. Likewise, $\vec{B}$ is usually expressed as the derived unit Tesla (T) in the SI, while in the cgs-emu system Gauss (G) is preferred. They are related by 1 G $= 10^{-4}$ T.

The $\vec{H}$- and $\vec{B}$-field are related in vacuum by the permeability μ_0 constant through equation (1.12), where $\mu_0 = 4\pi \times 10^{-7}$ Henry per meter ($\mathrm{H\,m^{-1}}$) in the SI, but it is a dimensionless quantity equal to 1 in the cgs-emu system. The last statement implies that in the cgs-emu system, under vacuum conditions with no other object to interact with, the $\vec{H}$-field is equal to the $\vec{B}$-field, so the units of $\vec{B}$ and $\vec{H}$ have the same dimensions, although their units are given different names to help identify the field under discussion. Nevertheless, it is quite common to find both fields expressed in Gauss due to this treatment of units in the cgs-emu system. Both $\vec{H}$ and $\vec{B}$ are magnetic field vectors characterised by their magnitude and direction, as a result, they can be depicted by magnetic field lines (Figure 1.4a).

$$\vec{B} = \mu_0 \vec{H} \tag{1.12}$$

When an $\vec{H}$-field is applied to a sample, either of its individual magnetic moments, $\vec{L}$ or $\vec{S}$ of every atom, tend to align parallel to the direction of that $\vec{H}$-field.

If it is applied on the z-axis, because of the uncertainty on the x- and y-axis, those vectors never became fully align with the external field, and its movement should be seen as the precession of $\vec{L}$ and $\vec{S}$ vectors around the z-axis.

Indeed, as consequence of Pauli exclusion principle, two electrons in the same orbit will cancel completely their spin angular momenta and consequently, their spin magnetic moments. Therefore, the spin contribution to the total magnetic moment of an atom for paired electrons will be null. On the other hand, if the electrons of an atom became unpaired, and for now consider that its different spin magnetic moments cannot interact with each other, like if every electron was isolated one from the other, then, if such system is placed in vacuum conditions in the presence of a $\vec{H}$-field, their spin magnetic moments tend to be aligned with the field reinforcing it, and the result is an increase of the magnetic field in that area as depicted in Figure 1.4b. If the field is not homogeneous the result is an attraction to areas where the field is more intense. This phenomenon receives the name of paramagnetism. Certainly, the paramagnetism can also be due by orbital magnetic moments, but it only arises on electronic configurations when $M_L \neq 0$ (being M_L the sum of all m_l). On the other hand, the intrinsic magnetic moment of an electron due to the spin is always present, and it can only be cancelled out by electron pairing.

On the contrary to the spin cancellation, the cancellation of the orbital magnetic moments are not complete. In fact due to this factor, when the interaction with the $\vec{H}$-field results in repulsion, the $\vec{B}$-field becomes less intense as consequence of this *quasi* cancellation that appears and opposes the external magnetic field (Figure 1.4c). This phenomenon is called diamagnetism and is an underlying property of matter due to the interaction of the magnetic field with the motion of the electrons in their orbits. However, the magnetic moments that arises from this *quasi* cancellation are very small compared to the permanent magnetic moments. Thus, even when diamagnetism is always present, it is often masked by paramagnetism.

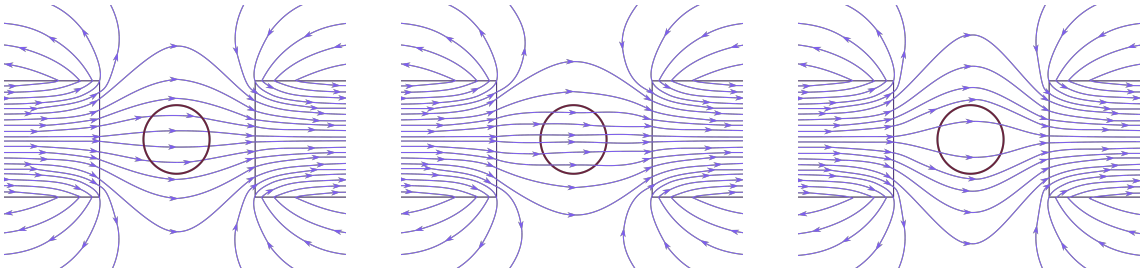

(a) **(b)** **(c)**

Figure 1.4: (a) Uniform magnetic field in vacuum created by means of two magnets and related by equation (1.12). (b) A paramagnetic system interacting with an external magnetic field, resulting in attraction. This is graphically depicted by a higher density of field lines inside the object. (c) A diamagnetic system interacting with an external magnetic field, resulting to be the opposite response of a paramagnetic system.

In order to quantify the degree in which a $\vec{B}$-field is different from a $\vec{H}$-field due to the total magnetic moment of a sample, another magnetic quantity will be introduced, $\vec{M}$, called the volume magnetisation of a substance. It has units of $\mathrm{A\,m^{-1}}$ in the SI. Alternatively, in the cgs-emu system is often expressed as $\mathrm{emu\,cm^{-3}}$. Although $\vec{B}$, $\vec{H}$, and $\vec{M}$ are vectors, they are usually parallel, hence from now on they will be written in scalar form. Both phenomenon, paramagnetism and diamagnetism,

are only observable when the H-field is present and all the magnetisation becomes zero when the field is removed. Undoubtedly, the magnetisation observed in a sample is due to the sum of both phenomenon, but if $M < 0$ the sample is said to be a diamagnetic substance. On the contrary, if $M > 0$ the sample should be referred as a paramagnetic substance.

In paramagnetism, the M value depends on the strength of the H-field, because increasing the field increases the amount of aligned magnetic moments. However, the magnetisation is not unlimited, it reaches a maximum value when all the magnetic moments are aligned with the field. At this point, the magnetization remains constant as the field increases, and it is said that the sample has reached its saturation value, M_s. Besides, M depends also on the temperature, because thermal energy opposes the ordering effect of the magnetic field. Thus, the magnetisation is a competition between the applied field and the temperature, where for lower temperatures the value of M_s is more easily reached. In diamagnetism, likewise paramagnetism, the value of M depends on the H intensity, but on the contrary, it never reaches a saturation limit because it arises from the change in the orbital motion of electrons that opposes the external field that created it. Moreover, random thermal motion of atoms does not affect those orbital magnetic moments, hence diamagnetism is temperature independent. Magnetisation curves can be seen in Figure 1.5 for both systems at different temperatures.

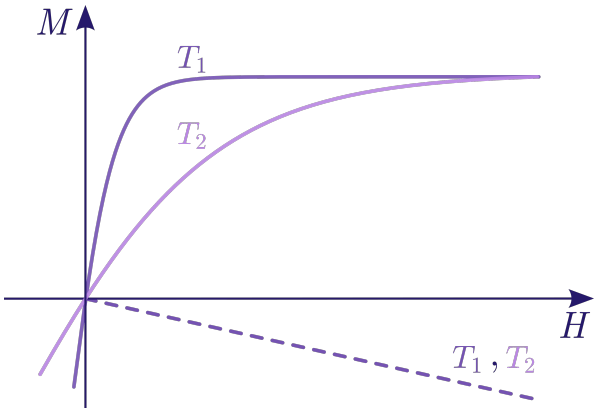

Figure 1.5: Magnetisation curve at two different temperatures, where $T_1 << T_2$. The saturation is reached sooner at low temperatures for a paramagnetic substance (solid line), while diamagnetism (dashed line) is independent of the temperature and never saturates.

In addition, the magnetisation being function of the applied field is not a convenient parameter, thus a new magnetic parameter is defined called the magnetic susceptibility, χ. Since M is a vector and H is an axial vector, the susceptibility should be treated as a second rank tensor. However, if the sample is not a single crystal, where the magnetisation may be different in different crystallographic directions, hence powder is used instead, M becomes independent of the orientation of the sample. Consequently, it becomes magnetically isotropic and the susceptibility is a scalar instead of a tensor. The value of the volume magnetic susceptibility, χ_V, is given in equation (1.13).

$$\chi_V = \frac{\delta M}{\delta H} \tag{1.13}$$

Furthermore, as long as the relationship between M and H remains lineal, a

situation that is usually accomplished when the H-field is low enough to not reach the M_s value of the sample, then equation (1.13) may be expressed as (1.14).

$$\chi_V = \frac{M}{H} \tag{1.14}$$

In this way, for a given temperature, the susceptibility indicates how responsive a material is to an applied magnetic field. Besides, as it is independent of the H-field intensity, this makes the susceptibility far more convenient than the magnetisation to compare data between researchers. The volume susceptibility is a dimensionless quantity in both unit systems. Nevertheless, it is rarely know the volume of a sample, being more common to know its weight, so the susceptibility per unit mass is more useful. It is obtained dividing it by the sample's density. For chemists, the susceptibility per mole is usually preferred, and it is obtained by multiplying the mass susceptibility by its atomic or molecular weight. As a result, the susceptibility depends now on the amount of the sample. They have units of $m^3\,Kg^{-1}$ and $m^3\,mol^{-1}$ in the SI, respectively. Likewise, in the cgs-emu system is expressed as $cm^3\,g^{-1}$ and $cm^3\,mol^{-1}$, respectively. Similarly to the magnetisation, if $\chi < 0$ the sample is referred as diamagnetic, and if $\chi > 0$ as paramagnetic.

In order to determine the paramagnetic susceptibility of a sample it is important to correct its intrinsic diamagnetism. Since the diamagnetism does not change its value with the temperature, and the diamagnetic susceptibility is independent of the field intensity, it may be treated as a constant. For this reason, Pascal proposed that the diamagnetism of a molecule could be calculated in an additive fashion as seen in equation (1.15), using values for the diamagnetic susceptibility of every atom, χ_i^{Dia}, and bond, λ_i^{Dia}, in the molecule. The empirical values of χ_i^{Dia} and λ_i^{Dia} became known as Pascal's constants.[14]

$$\chi^{Dia} = \sum_i \chi_i^{Dia} + \sum_i \lambda_i^{Dia} \tag{1.15}$$

Indeed, all the samples are placed inside some sort of sampler-holder as capsules to carry out the magnetic measurements, so the diamagnetism corrections due to the measuring system should also be made.

In general the cgs-emu system is preferred widely by most of the researchers because of its convenience relating B and H in vacuum, and also because Tesla is considered a large unit. The largest continuous field ever produced in a laboratory is ca. 40 T and the field at the Earth's surface is a few tens of μT.[15,16] For this dissertation, the cgs-emu system will be used following the common tendency.

1.2 Fundamental equations in Molecular Magnetism

From a thermodynamic point of view, the macroscopic magnetisation of a sample, M, is the variation of the internal energy of the system, E, with the applied magnetic field, H, as described in equation (1.16). The negative sign is placed for keeping the convention where a paramagnetic substance has a positive magnetisation, while

diamagnetism has negative values.

$$M = -\frac{\delta E}{\delta H} \tag{1.16}$$

In statistical thermodynamics, if it is considered a system sorted by i different energy levels, E_i, each one of them in presence of an external magnetic field will have a different magnetisation, due to their characteristic electronic configuration. The microscopic magnetic moment of a level, μ_i, has an analogous formulation as the macroscopic one. It is written as equation (1.17) presents.

$$\mu_i = -\frac{\delta E_i}{\delta H} \tag{1.17}$$

In order to know the macroscopic magnetisation through their microscopic magnetic moments, it is necessary to weigh the magnetisation of each moment by its contribution. The Maxwell-Boltzmann population, P_i, is able to describe the energy distribution for each level of a system based on the temperature parameter as the population medium, as expressed in equation (1.18), where k_B is Boltzmann constant and T is the absolute temperature.

$$P_i = \frac{\exp\left(-\frac{E_i}{k_B T}\right)}{\sum\limits_i \exp\left(-\frac{E_i}{k_B T}\right)} \tag{1.18}$$

Therefore, it is possible to know the macroscopic magnetisation of a system knowing the energy of every microscopic moment and its population. In addition, the macroscopic magnetisation can be defined per mole of a substance by multiplying through Avogadro's number, N_A, which leads to expression (1.19). Thus, it may be considered as the fundamental equation in Molecular Magnetism, and it does not lean on any approximation.

$$M = N_A \sum_i \mu_i P_i = N_A \frac{\sum\limits_i -\frac{\delta E_i}{\delta H} \exp\left(-\frac{E_i}{k_B T}\right)}{\sum\limits_i \exp\left(-\frac{E_i}{k_B T}\right)} \tag{1.19}$$

In order to know the energy of the different levels of a system, it is necessary the use of mathematical operators over their wave-functions. The orbital and spin magnetic moment operators and its z-component can be constructed from the classical expressions as described in equations (1.20) and (1.21). Furthermore, as $\widehat{L}$, $\widehat{L}_z$, $\widehat{S}$ and $\widehat{S}_z$, the $\hbar$ value is always returned, the constant will be omitted from now on for a more simple exposure and convenience.

$$\widehat{\mu} = -\mu_B \widehat{L}; \qquad \widehat{\mu} = -g\mu_B \widehat{S} \tag{1.20}$$

$$\widehat{\mu}_z = -\mu_B \widehat{L}_z; \qquad \widehat{\mu}_z = -g\mu_B \widehat{S}_z \tag{1.21}$$

Classically, the energy of a magnetic moment under a magnetic field is the scalar product of both magnitudes as written in equation (1.22), where the negative sign

indicates that the interaction decreases the energy of a system when the two magnitudes have the same direction, but increases when they have opposite directions.

$$E = -\vec{\mu} \cdot \vec{H} \tag{1.22}$$

Likewise, in quantum mechanics the operator of the energy associated to the magnetic interaction is called Zeeman, $\widehat{\mathcal{H}}_Z$, and it can be built from equation (1.22) as follows

$$\widehat{\mathcal{H}}_Z = -\widehat{\mu}\, H = \mu_B H \left(\widehat{L} + g\widehat{S}\right) \tag{1.23}$$

Moreover, if the system is considered isotropic ($x = y = z$) all directions are going to give the same results, hence, it is enough to apply the Hamiltonian in one direction for knowing the total magnetic moment. Thus, expression (1.23) becomes (1.24), z being for practical reasons the chosen axis.

$$\widehat{\mathcal{H}}_Z = \mu_B H \left(\widehat{L}_z + g\widehat{S}_z\right) \tag{1.24}$$

In order to illustrate how to use expression (1.19) and calculate the energy through the Zeeman Hamiltonian, it will be helpful to consider a simple system and study its characteristics. For example, a system made only of electrons without a nucleus and treated as isotropic. Therefore, the single magnetic moment is due to the spin, and also no diamagnetism is found. Consequently, expression (1.24) can be simplified to (1.25).

$$\widehat{\mathcal{H}}_Z = g\mu_B H \widehat{S}_z \tag{1.25}$$

Thus, the wave-functions that defined the states of a system composed only of electrons are α and β. In absence of a H-field the two states are equal in energy, but in presence of a field the degeneracy is broken. Expressions (1.26) and (1.27) indicates the energy and magnetic moment for a $m_s = \frac{1}{2}$, respectively, while (1.28) and (1.29) for $m_s = \text{-}\frac{1}{2}$. As α and β functions are normalised, the integrals $\langle\alpha|\alpha\rangle$ and $\langle\beta|\beta\rangle$ are equal to 1. The energy difference between levels is as state in equation (1.30).

$$\left\langle \alpha \middle| \widehat{\mathcal{H}}_Z \middle| \alpha \right\rangle = E_\alpha \langle\alpha|\alpha\rangle = \frac{1}{2} g\mu_B H \tag{1.26}$$

$$\langle\alpha|\widehat{\mu}_z|\alpha\rangle = \mu_{z,\alpha} \langle\alpha|\alpha\rangle = -\frac{1}{2} g\mu_B \tag{1.27}$$

$$\left\langle \beta \middle| \widehat{\mathcal{H}}_Z \middle| \beta \right\rangle = E_\beta \langle\beta|\beta\rangle = \frac{1}{2} g\mu_B H \tag{1.28}$$

$$\langle\beta|\widehat{\mu}_z|\beta\rangle = \mu_{z,\beta} \langle\beta|\beta\rangle = -\frac{1}{2} g\mu_B \tag{1.29}$$

$$\Delta E = g\mu_B H \tag{1.30}$$

In summary, the state with $m_s = \frac{1}{2}$ opposes the field and rises its energy, while the $m_s = \text{-}\frac{1}{2}$ becomes parallel and decreases its energy. In Figure 1.6a can be seen how is the interaction of both spin magnetic moments with an external field, whereas in Figure 1.6b the energy diagram of the system.

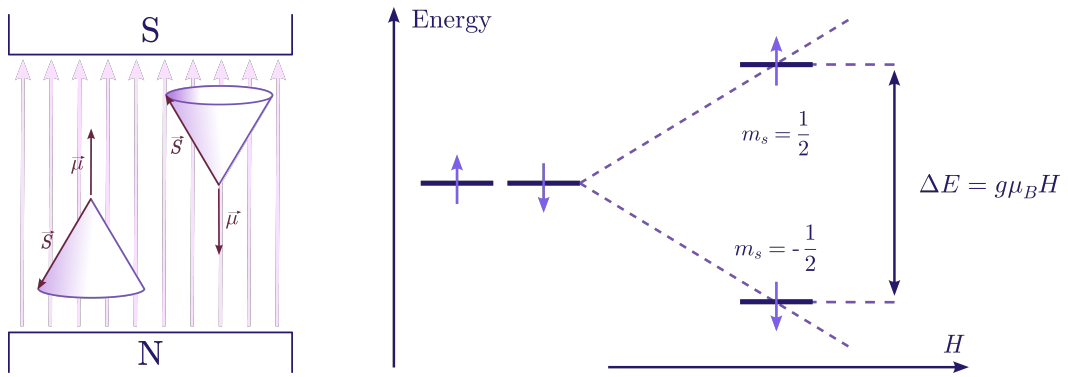

Figure 1.6: (a) Under a H-field, the spin magnetic moment experiences a force that tends to align it with the direction of that field. As the magnetic moment is spinning, the force causes the system to precess around the direction of the external field. Note how $m_s = -\frac{1}{2}$ is the one that become parallel with the field, while $m_s = \frac{1}{2}$ opposes to the field. (b) Before applying a magnetic field for an unpaired electron both values of m_s are possible and equal in energy. Under an external magnetic field, both energy levels are function of the H-field intensity.

Thus, the magnetisation of a mole of electrons can be deduced from equation (1.19) as expression (1.31), where the partial derivative of the energy respect to the field are trivial calculations for both energy levels.

$$M = \frac{N_A g \mu_B}{2} \tanh x; \quad x = \frac{g\mu_B H}{2k_B T}; \quad \tanh x = \frac{\exp(x) - \exp(-x)}{\exp(x) + \exp(-x)} \tag{1.31}$$

The expression (1.31) includes the hyperbolic tangent of x, whose values are compressed between $+1$ and -1 horizontal asymptotes (Figure 1.7a). Likewise, the magnetisation for a mole of electrons will be the tanh function multiplied by a constant. The value at M_s is reach at high H, where for a value of $g \approx 2$ the saturation will be equal to $N_A\mu_B$. Thus, M_s is the maximum value of the paramagnetic moment of a mole of electrons (Figure 1.7b). For this reason, it is very common to find the magnetisation of samples represented in $N_A\mu_B$ units.

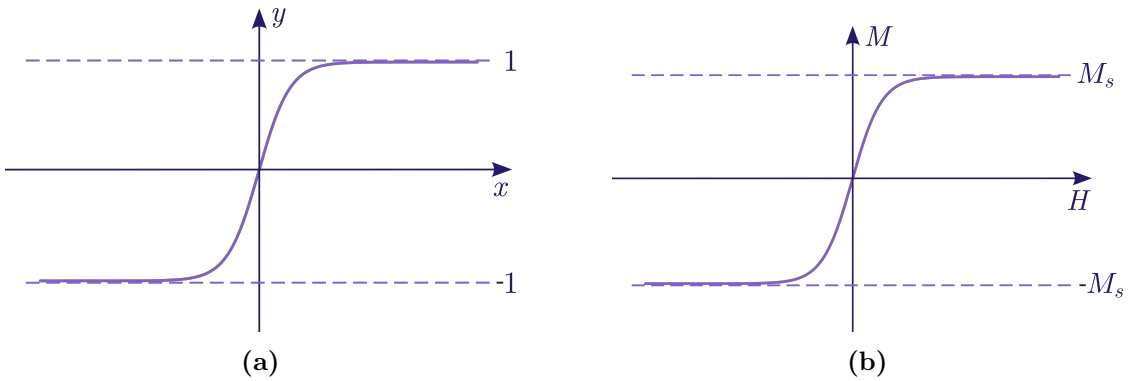

Figure 1.7: (a) Variation of the hyperbolic tangent function with x. (b) Variation of the magnetisation function with the field, where M_s represents the saturation value of a mole of electrons.

Classically for paramagnetic systems, the spin magnetic moment of an atom is represented by an arrow randomly oriented before applying an external field.

Thus, as the field increases more and more spins become align with it until the saturation point at a given temperature is reached (Figure 1.8). This representation, even though intuitive and simple, is not suitable in the quantum mechanics context, where the spin can only have two possible orientations. Therefore, a more accurate description should be made in terms of population. At $H = 0$ both states are equally in energy and find themselves equally populated and consequently $M = 0$. As the field increases the state that becomes more stable increases its population, whereas the opposite is depleted. Nevertheless, the thermal energy at room temperature will have a value of *ca.* 200 cm^{-1}, while the magnetic energy separation between levels will be no more than *ca.* 1 cm^{-1} for a 1 T field, as it can be deduced from equation (1.30). Indeed, it is possible to increase the field to increase the separation, but it is more suitable to decrease the temperature. At liquid Helium temperature the thermal energy will be *ca.* 3 cm^{-1}, being easier to highly populate the ground state to reach the saturation value.

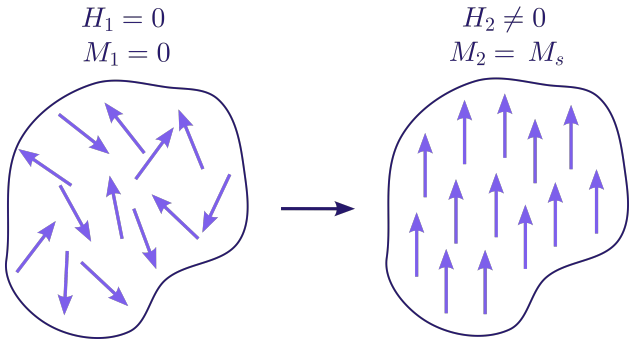

Figure 1.8: Classical representation of the spin magnetic moment for different paramagnetic centres. These are randomly oriented due to the thermal energy and overall the $M = 0$. After applying an external field strong enough to align all magnetic moments, the saturation value is reached.

In a more general case, equation (1.19) is often difficult to apply. Clearly, it requires knowledge on the energy function for all thermally populated states in order to calculate their derivatives. For this reason, Van Vleck proposed a simplification based on a few approximations.

First, in order to find expressions for the energy of every level, the perturbation theory was applied. In this method, the problem to solve is considered from the point of view of a problem which has already been solved. For example, a transition metal in an octahedral field would be treated as a perturbation of the free ion by the potential of the ligands. Thus, the treatment will start with the free ion determined wave-functions and energy levels, and then the changes on the energy and wave-functions due to the ligand field will be calculated. This theory works well as an approximation as long as the perturbation have not more energy than the initially possessed by the system. Actually, the magnetic interaction is no more energetic than *ca.* 1 cm^{-1} for a H-field of 1 T. On the other hand, the energy of a free atom in the first row transition metals are of *ca.* 10^4 cm^{-1}, while the ligand field have values of *ca.* 10^4 to 10^2 cm^{-1}. Therefore, the magnetic interaction can always be seen as a perturbation of the initial system under this conditions.

In the mathematical evaluation from the perturbation theory perspective, the Hamiltonian is divided into two parts. The first Hamiltonian is applied to the sys-

tem before the perturbation and determines for each level of the system the wave-functions, ψ_i, with their energies, $E_i^{(0)}$. They are called initial functions and energies of zero-order. Indeed, a set of ψ_i functions can be found per level if degeneracy is present. The second one is the perturbation Hamiltonian, $\widehat{\mathscr{H}}'$. All wave-functions that interact with it change their state to a new set of wave-functions, ϕ_i, with their respective energies, $E_i^{(1)}$. These are called perturbed functions and energies of first-order. Thus, it is possible to break the degeneracy of the initial system by first-order effects. Furthermore, the new calculated functions from one level may interact now with functions from other levels. In this way, second-order wave-functions and energies may develop, and so on and so forth. However, with the second-order interactions should be enough for most of the systems, after all if the problem is suitable for the perturbation theory, the quantities $E_i^{(0)}, E_i^{(1)}, E_i^{(2)}, \ldots$ decrease as the order of the perturbation correction increases.

The first-order energies corrections are calculated solving the system of equations (1.32), where H_{ii} and H_{ij} are integrals as presented in (1.33), i and j being different wave-functions of the system, and n the total number of them.

$$\begin{cases} \left(H_{11} - E^{(1)}\right) c_1 + H_{12}\, c_2 + \ldots + H_{1n}\, c_n = 0 \\ H_{21}\, c_1 + \left(H_{22} - E^{(1)}\right) c_2 + \ldots + H_{2n}\, c_n = 0 \\ \cdots \\ H_{n1}\, c_1 + H_{n2}\, c_2 + \ldots + \left(H_{nn} - E^{(1)}\right) c_n = 0 \end{cases} \tag{1.32}$$

$$H_{ii} = \left\langle \psi_i \middle| \widehat{\mathscr{H}}' \middle| \psi_i \right\rangle; \qquad H_{ij} = \left\langle \psi_i \middle| \widehat{\mathscr{H}}' \middle| \psi_j \right\rangle \tag{1.33}$$

This system of equations can be expressed as a matrix and solved through a determinant. One possible solution is the trivial one, where all the c_n coefficients are equal to zero. This is the only solution to the system unless the determinant of the factors of the c's is equal to zero. That determinant is known as the secular determinant and is presented in (1.34), where each element of the matrix is given by $H_{ii} - E^{(1)}$ for diagonal elements, and H_{ij} for off-diagonal elements. Moreover, after applying the perturbation Hamiltonian, due to the orthonormality between the functions all integrals of the type $\langle\psi_i|\psi_i\rangle$ will be equal to one and $\langle\psi_i|\psi_j\rangle$ will be equal to zero.

$$\begin{array}{c|cccc} & |\psi_1\rangle & |\psi_2\rangle & \cdots & |\psi_n\rangle \\ \hline \langle\psi_1| & H_{11} - E^{(1)} & H_{12} & \cdots & H_{1n} \\ \langle\psi_2| & H_{21} & H_{22} - E^{(1)} & \cdots & H_{2n} \\ \vdots & \vdots & \vdots & \vdots & \vdots \\ \langle\psi_n| & H_{n1} & H_{n2} & \cdots & H_{nn} - E^{(1)} \end{array} = 0 \tag{1.34}$$

Only when all off-diagonal elements of the determinant or sub-determinants are zero, the first-order energy is easily calculated as given by equation (1.35), and first-order wave-function coincides with the zero-order one, $\psi_i = \phi_i$.

$$E_i^{(1)} = H_{ii} \tag{1.35}$$

On the other hand, when the secular determinant (or sub-determinants) contains non-zero off-diagonal matrix elements, it means that the first-order perturbation mixes those wave-functions. As a result, new energy levels are developed and a new set of wave-functions must be calculated. In practice, it involves solving the secular determinant by a process known as diagonalization of the determinant, where all the elements are isolated in the diagonal by permuting rows and columns in order to separate the problem into smaller determinants. Thus, a $n \times n$ determinant will result in an equation of the nth degree in $E^{(1)}$, and therefore it has n roots, $E_1^{(1)}$, $E_2^{(1)}, \ldots, E_n^{(1)}$, some of them will be equal if degeneracy is present. Afterwards, with the obtained energy values it is possible to obtain the new wave-functions, which are a lineal combination of the zero-order ones with the form described by (1.36). This process involves the calculation of the different c_n coefficients from (1.32) equations, and the normalization constant, N, for accomplishing the $\langle \phi_i | \phi_i \rangle = 1$ condition.

$$\phi_j = N\left[c_1\psi_1 + c_2\psi_2 + \ldots + c_n\psi_n\right] = N\sum_{i=1}^{n} c_i\psi_i \tag{1.36}$$

In this way, if the perturbation is applied at the first-order over the new calculated set of wave-functions, it will produce a diagonalised matrix without non-zero off-diagonal elements, and therefore the first-order energy correction will be as given in (1.35).

Additionally, due to the interaction of the first-order functions with other ones from excited terms, second-order corrections to the energy and functions can be made as established in (1.37), and (1.38), respectively.

$$E_i^{(2)} = \sum_{i\neq j}^{n} \frac{H_{ij}H_{ji}}{E_i^{(0)} - E_j^{(0)}} \tag{1.37}$$

$$\phi_i = \psi_i + \sum_{i\neq j}^{n} c_{ij}\,\psi_j; \qquad c_{ij} = \frac{H_{ij}}{E_i^{(0)} - E_j^{(0)}} \tag{1.38}$$

In the magnetic interaction viewed from the perturbation theory perspective, the Zeeman Hamiltonian gives the first- and second-order energies as (1.39) and (1.40). It is useful to define both energies as function of H, as the integral is not defined for the magnetic field variables it can get out as a constant. Hence, it will be more clear to perform its derivatives in the future. Moreover, this expressions are more convenient because the external magnetic field is the only adjustable experimental parameter.

$$E_i^{(1)} = H\left\langle \psi_i \middle| \mu_B\left(\widehat{L} + g\widehat{S}\right)\middle| \psi_i \right\rangle = HE_i{}' \tag{1.39}$$

$$E_i^{(2)} = H^2 \sum_{i\neq j} \frac{\left\langle \psi_i \middle| \mu_B\left(\widehat{L} + g\widehat{S}\right)\middle| \psi_j \right\rangle^2}{E_i^{(0)} - E_j^{(0)}} = H^2 E_i{}'' \tag{1.40}$$

Then, the energy of an i level will be defined as $E_i = E_i^{(0)} + HE_i{}' + H^2E_i{}''$, where its magnetic moment can be deduced from expression (1.17) to $\mu_i = -E_i{}' - 2HE_i{}''$.

Thus, the first approximation of the general equation (1.19) is as follows:

$$M = N_A \frac{\sum_i \left(-E_i{}' - 2HE_i{}''\right) \exp\left(-\frac{E_i^{(0)}}{k_BT}\right) \exp\left(-\frac{HE_i{}'}{k_BT}\right) \exp\left(-\frac{H^2E_i{}''}{k_BT}\right)}{\sum_i \exp\left(-\frac{E_i^{(0)}}{k_BT}\right) \exp\left(-\frac{HE_i{}'}{k_BT}\right) \exp\left(-\frac{H^2E_i{}''}{k_BT}\right)} \tag{1.41}$$

Here is when Van Vleck made its second approximation. It is considered that $E_i{}'H << k_BT$ and $E_i{}''H <<< k_BT$, a sensible situation due to that in most cases H is certainly smaller than T. Thus, the second-order exponential term can be directly simplified to 1, and the first-order exponential term can be approximated by the limit of Taylor series, where $\exp(\pm x) = 1 \pm x$ when $x << 1$. Therefore, the equation (1.41) is simplified as

$$M = N_A \frac{\sum_i \left(-E_i{}' - 2HE_i{}''\right) \exp\left(-\frac{E_i^{(0)}}{k_BT}\right) \left(1 - \frac{HE_i{}'}{k_BT}\right)}{\sum_i \exp\left(-\frac{E_i^{(0)}}{k_BT}\right) \left(1 - \frac{HE_i{}'}{k_BT}\right)} \tag{1.42}$$

Furthermore, for a paramagnetic system $M = 0$ when $H = 0$, which leads to the requisite presented in equation (1.43).

$$\sum_i \left(-E_i{}'\right) \exp\left(-\frac{E_i^{(0)}}{k_BT}\right) = 0 \tag{1.43}$$

Thus, equation (1.42) is simplify to

$$M = N_A H \frac{\sum_i \left(\frac{E_i{}'^2}{k_BT} - 2E_i{}''\right) \exp\left(-\frac{E_i^{(0)}}{k_BT}\right)}{\sum_i \exp\left(-\frac{E_i^{(0)}}{k_BT}\right)} \tag{1.44}$$

Finally, the magnetic susceptibility can be calculated with the magnetisation as previously introduced by equation (1.14). Thus, the equation (1.45) is known as Van Vleck formula for paramagnetic systems.

$$\chi_M = N_A \frac{\sum_i \left(\frac{E_i{}'^2}{k_BT} - 2E_i{}''\right) \exp\left(-\frac{E_i^{(0)}}{k_BT}\right)}{\sum_i \exp\left(-\frac{E_i^{(0)}}{k_BT}\right)} \tag{1.45}$$

As a noteworthy remark, it is possible to construct a secular determinant with all the desired functions from the ground to excited states for diagonalization. Thus, the energy obtained will incorporate the energy corrections to the desired order. Nevertheless, the determinant will involve an equation of high order, which is normally difficult to solve algebraically, and numerical methods will be required to express the variation of the energy levels with the magnetic field. Moreover, even if there is an algebraic expression of the energy, it will require to be expressed as a power

series of H, because it needs to be in an appropriate form for its substitution into Van Vleck's formula.

It is convenient to define a couple of systems in order to understand the uses of the Van Vleck formula. Indeed, the magnetic susceptibility derived *via* Van Vleck's formula is the result of changes in the molecular energy levels of an atom with the magnetic field. However, the connection between this and the quantum numbers which define the energy terms is not so readily appreciated. For the next two cases, the zero of energy will begin at the ground state, so the zero-field energy will be defined as $E_i^{(0)} = 0$.

In the first case, for a system where the only thermally populated state have $S = 0$ and $L = 0$, where S and L represents the total spin and orbital angular momentum, respectively, the paramagnetic susceptibility is intuitively expected to be zero because of the lack of a magnetic moment to interact with. Thus, the sole component of the ground level denoted from now on with a 0 sub-index, has no first-order interaction with the field, ${E_0}' = 0$. In other words, the ground state does not change its energy when a magnetic field is applied. Nevertheless, this conclusion is only correct for the first-order interaction. If under a magnetic field this system has near excited states that can be populated, then the ground state becomes a mixture of itself with a little contribution of the other excited states, that may have a paramagnetic contribution, hence, second-order perturbations, ${E_0}'' < 0$, and the Van Vleck formula becomes as

$$\chi_M = -2N_A {E_0}'' \tag{1.46}$$

This paramagnetic contribution is called Temperature Independent Paramagnetism (TIP), because of its characteristic lack of dependence with the temperature parameter. The degree of TIP depends on how near in energy is the ground state from the excited states. In general this contribution is rather small, often of the same order of magnitude as the diamagnetism, but of opposite sign. Both contributions are corrected from the measurements in order to quantify correctly the temperature dependent paramagnetism.

In a more general second case, a system where $S \neq 0$ and $L \neq 0$ it consequently have after applying a magnetic field a first-order perturbation, so ${E_i}' \neq 0$. If second-order interactions are omitted, hence ${E_i}'' = 0$, the Van Vleck formula (1.45) can be demonstrated to be derived as (1.47). Furthermore, if there is no orbital contribution $L = 0$, the Van Vleck formula is simplified as (1.48). The last equation receives the name of Spin-only formula.

$$\chi_M = \frac{N_A {\mu_B}^2}{3k_B T} \left[L(L+1) + g^2 S(S+1) \right] \tag{1.47}$$

$$\chi_M = \frac{N_A {\mu_B}^2 g^2}{3k_B T} S(S+1) \tag{1.48}$$

As a noteworthy remark, some authors prefers to redefine the $\chi_M T$ product as a new parameter called effective magnetic moment, μ_{eff}, as shown in equation (1.49). Its description of the magnetic moment is the same as $\chi_M T$, and its units are denoted as Bohr magnetons even when it is a dimensionless quantity in the SI and cgs-emu

unit systems.[17]

$$\mu_{eff} = \left[\frac{3k_B}{N_A{\mu_B}^2}\right]^{1/2} [\chi_M T]^{1/2} \tag{1.49}$$

Similarly, before the Van Vleck formula, Pierre Curie deduced a phenomenological law to explain the paramagnetic behaviour of certain substances with the temperature (1.50), where C is known as the Curie constant and is characteristic of each system. Nowadays, the origin of the Curie constant can be seen from a quantum mechanics perspective deduced from the Van Vleck formula obtained above.

$$\chi_M = \frac{C}{T}; \qquad C = \frac{N_A{\mu_B}^2}{3k_B}\left[L(L+1) + g^2 S(S+1)\right] \tag{1.50}$$

Both, Curie and the obtained Van Vleck equation, rely on the approximation where ${E_i}'H << k_B T$ and ${E_i}'' = 0$, for this reason whenever this conditions are not met, the χ_M cannot be accurately obtained from those expressions. A representation of different χ_M plots obtained through this equations in shown in Figure 1.9.

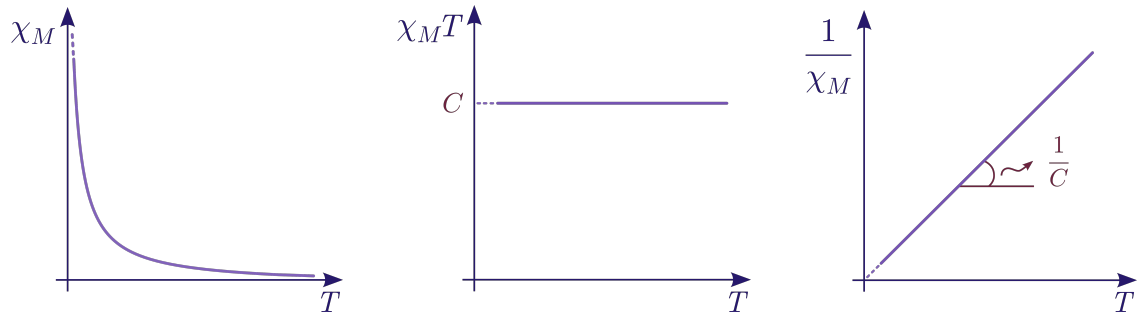

(a) **(b)** **(c)**

Figure 1.9: Different common representations of the molar magnetic susceptibility for a paramagnetic system (a) χ_M *vs.* T (b) $\chi_M T$ *vs.* T (c) ${\chi_M}^{-1}$ *vs.* T. Note how values of χ_M from Curie (1.50) or Van Vleck (1.47) equations are not known at low temperatures with high fields, where the approximation ${E_i}'H << k_B T$ cannot be met.

For systems with $L = 0$, hence, all the magnetisation is due to the spin, it is possible to assign a function for the energy that varies with the total spin value and the field known as the Brillouin function (1.51). Taking into account the molar magnetisation shown in expression (1.19) and the Brillouin function, after some mathematical treatment, the magnetisation can be expressed as equation (1.52) states. In Figure 1.10, it can be seen how when $\mu_B H < k_B T$ the Curie and Van Vleck formulas are a good approximation of the magnetisation, whilst at $\mu_B H > k_B T$ cannot effectively give its value where the saturation of the magnetisation occurs. In these conditions, the Brillouin function tends to the unit and the magnetisation to $M_s = N_A \mu_B g S$.

$$B(y) = \frac{2S+1}{2S}\coth\left(\frac{2S+1}{2S}y\right) - \frac{1}{2S}\coth\left(\frac{1}{2S}y\right); \qquad y = \frac{g\mu_B S}{k_B T}H \tag{1.51}$$

$$M = N_A g \mu_B S B(y) \tag{1.52}$$

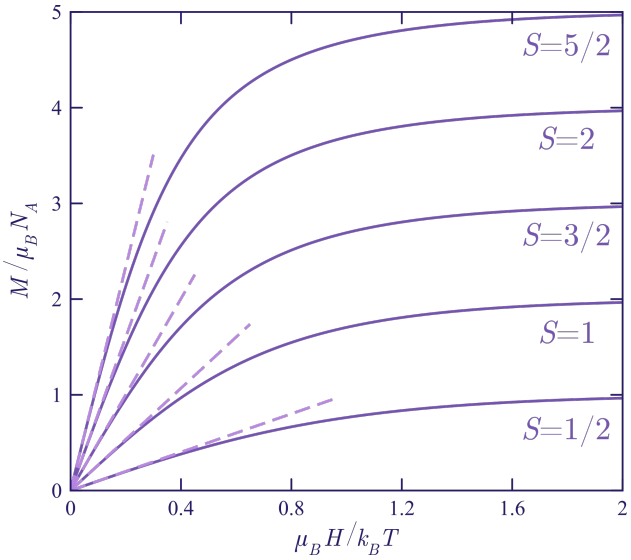

Figure 1.10: Magnetisation in $N_A\mu_B$ units *vs.* $\mu_B H/k_B T$ plots for systems with only spin contribution to paramagnetism. The g-factor is taken equal to 2.00. The solid line depicts the magnetisation by equation (1.52) whilst the dashed line by spin-only formula (1.48) multiply by H.

1.3 Spin-orbit coupling and ZFS effect

So far, it was considered that the magnetic moment due to the spin was independent of the magnetic moment of the orbit, and so they were treated separately. However, both magnetic moments interact with each other. The influence between moments is given the name of spin-orbit coupling. Nevertheless, there are two models for treating the interaction depending on how strong the spin-orbit coupling is.

The first one is for more lighter elements called L-S coupling, also known as Russell-Saunders. In this case, the main energy terms are determined chiefly by the electrostatic repulsion between electrons, and the spin-orbit coupling is considered small in comparison and treated from the perturbation theory perspective. In this way, the orbital and spin angular momenta of each electron are combined separately for the i electrons of the system, leading to total values of L and S as shown in equation (1.53). Then, they are mixed by the spin-orbit interaction and the combination leads to the total angular momentum of the system, J. This information is shown in Figure 1.11a. Nevertheless, the spin and orbital angular momenta can be arrange in a parallel or antiparallel fashion, so J presents a range of values compressed between $L+S$ and $|L-S|$ jumping in integer steps, as summarised in expression (1.54). Thus, the new energy terms are defined by their S, L and J values. Furthermore, each term presents $2J+1$ degenerate energy levels characterised by the different orientations of J on the z-axis, hence the different values of M_J, which are compressed between J and $-J$ jumping in integer steps.

$$S = \sum_i s_i; \qquad L = \sum_i l_i \tag{1.53}$$

$$J = L + S,\ L + S - 1,\ \ldots,\ |L - S| \tag{1.54}$$

Thus, following the Russell-Saunders scheme, the spin-orbit Hamiltonian will be treated as presented in equation (1.55), where $\widehat{L}$ and $\widehat{S}$ are the total orbital and spin angular momentum operators, and λ stands as the polyelectronic spin-orbit coupling parameter. For the transition metals block and lanthanides, it can be calculated from the free ion single-electron spin-orbit coupling constant, ξ, as equations (1.56) and (1.57) present for d^n and f^n systems. The ξ values become higher as heavier becomes the atom and further is its oxidation state.[8,10] Moreover, its value only depends on the radial part of the wave-function. Hence, ξ and λ are treated as a constant for the angular part operators in single-electron or polyelectronic systems, respectively. As the λ value is positive for d^n systems with $n < 5$, the lowest energy level is the one with the lowest J. On the other hand, when $n > 5$ the fundamental state is the one with the highest value of J. Same deduction is made for f^n systems. Indeed, under this conditions for values of n where the orbital is empty, half-full or full, no spin-orbit coupling can occur.

$$\widehat{\mathscr{H}}_{SOC} = \lambda \widehat{L}\widehat{S} = \left(\widehat{L}_x\widehat{S}_x + \widehat{L}_y\widehat{S}_y + \widehat{L}_z\widehat{S}_z\right) \tag{1.55}$$

$$d^n \begin{cases} n < 5; & \lambda = \dfrac{\xi}{2S}; \quad E_{|L-S|} < ... < E_{L+S} \\ n > 5; & \lambda = -\dfrac{\xi}{2S}; \quad E_{L+S} < ... < E_{|L-S|} \end{cases} \tag{1.56}$$

$$f^n \begin{cases} n < 7; & \lambda = \dfrac{\xi}{2S}; \quad E_{|L-S|} < ... < E_{L+S} \\ n > 7; & \lambda = -\dfrac{\xi}{2S}; \quad E_{L+S} < ... < E_{|L-S|} \end{cases} \tag{1.57}$$

Moreover, the spin-orbit coupling not necessarily needs to be applied only to the free ion. In octahedral transition metals coordination compounds, where the energy terms are obtained after the ligand field perturbation, e_g and t_{2g} define their electronic configurations. In the same way, when $n > 2$ in e_g^n, or $n > 3$ in t_{2g}^n electronic configurations, the polyelectronic spin-orbit constant becomes negative. Nevertheless, in those electronic configurations which give a T fundamental term as in d^1, d^2, low-spin d^4, low-spin d^5, high-spin d^6, and high-spin d^7 ions in octahedral surroundings, due to the isomorphism between a T and a P term both with $L = 1$ ($||\mathrm{T}|| = -||\mathrm{P}||$) the energy order is the opposite to the one expected considering their free ion configurations, that is when $\lambda > 0$, the lowest energy level is the one with the highest J (E_{L+S}), and when $\lambda < 0$, the ground level is the one with the lowest J $\left(E_{|L-S|}\right)$.

The spin-orbit coupling becomes more strong for atoms with a high value of the atomic number, and the spin-orbit coupling energies become more important than the bielectronic repulsion, and therefore it cannot be treated as a small perturbation for these atoms any more. A better scheme called j-j coupling is used. Here, the spin-orbit coupling is the most dominant energy of the system. Therefore, the orbital and spin angular momenta of each electron are combined separately as expressed in equation (1.58). Then, the weaker electrostatic repulsion effect may couple the total angular momentum from each electron, j_i, into the total angular momentum of the system, J, as (1.59) states. This information is summarised in Figure 1.11b. And at

last, if the atom is not isolated, the ligand field will split the energy terms according to the symmetry.

$$j_i = s_i + l_i \tag{1.58}$$

$$J = \sum_i j_i \tag{1.59}$$

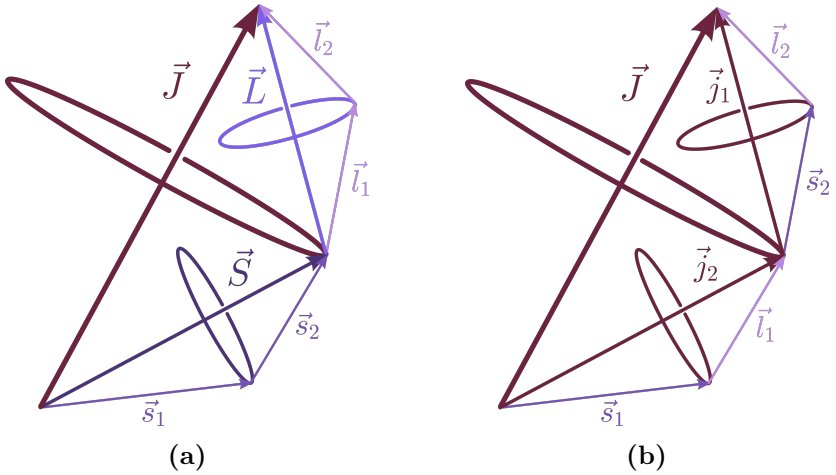

Figure 1.11: Classical vectorial representation of the spin and orbital angular momenta of two electrons labelled as 1 and 2. (a) They are combined separately to form the total spin and angular momenta. In this example S and L are added to form the total angular momentum J. (b) The orbital and spin angular momentum for each electron are combined by spin-orbit coupling, and then the total angular momentum of each electron combine to form the total angular momentum of the system.

Overall, in a metal complex there are three main energy contributions, the interelectronic repulsion, the ligand field splitting and the spin-orbit coupling. For the first-row transition metals the L-S model works acceptably well as the electrostatic repulsion is much greater than the ligand field, and this latter is greater than the spin-orbit coupling, so they are treated sequentially following the perturbation theory perspective. For the second-row transition metals, the ligand field and spin-orbit coupling start to catch up with the bielectronic repulsion, and for the three-row transition metals, the three energies may become of the same order of magnitude, and an intermediate coupling scheme would be more convenient. Besides, as the energy of the interactions are similar it could be necessary to treat them together and not sequentially. For lanthanides, the bielectronic repulsion and spin-orbit coupling are the most prominent energies with a weak ligand field interaction, whilst for actinides, the j-j coupling scheme is usually applied because the spin-orbit interaction for each electron is the dominant energy. It must be considered that both models, L-S and j-j, are extreme cases and its application may not always lead to reliable results with physical meaning. Nevertheless, in order to be able to compare the values for all transition metals and lanthanides between them, they will be treated within the context of the Russell-Saunders approach, even when the values are not really that equivalent and compatible.

In order to evaluate the spin-orbit coupling, only the L, S, M_L and M_S numbers will be necessary. Thus, the integrals of the functions ψ_{L,S,M_L,M_S} will be written with

Dirac notation, as $|L, M_L, S, M_S\rangle$, from now on for short. The $\widehat{L}\widehat{S}$ expression can be written in terms of raising and lowering operators, collectively known as ladder operators, as in expression (1.60). Thus, it is possible to avoid the use of x and y operators. Nevertheless, the ladder operators are no longer able to operate a function without changing their M_S and M_L values as given in equations (1.61) and (1.62), in contrast with the z operators found in expressions (1.3) and (1.7), adapted to Dirac notation in (1.63) and (1.64), respectively.

$$\widehat{\mathscr{H}}_{SOC} = \lambda\widehat{L}\widehat{S} = \lambda\widehat{L}_z\widehat{S}_z + \frac{\lambda}{2}\left(\widehat{L}_+\widehat{S}_- + \widehat{L}_-\widehat{S}_+\right) \tag{1.60}$$

$$\widehat{L}_\pm |L, M_L, S, M_S\rangle = \left[L(L+1) - M_L(M_L \pm 1)\right]^{1/2} |L, M_L \pm 1, S, M_S\rangle \tag{1.61}$$

$$\widehat{S}_\pm |L, M_L, S, M_S\rangle = \left[S(S+1) - M_S(M_S \pm 1)\right]^{1/2} |L, M_L, S, M_S \pm 1\rangle \tag{1.62}$$

$$\widehat{L}_z |L, M_L, S, M_S\rangle = M_L |L, M_L, S, M_S\rangle \tag{1.63}$$

$$\widehat{S}_z |L, M_L, S, M_S\rangle = M_S |L, M_L, S, M_S\rangle \tag{1.64}$$

The first- and second-order spin-coupling interactions may break the degeneracy of the ground state, and split it into different levels breaking the isotropy of the system. As a result, the magnetisation will no longer be independent of the direction of the field, and different grades of magnetisations will be achieved in different directions. This is an important phenomenon in Molecular Magnetism, because without the help of any field, *via* the spin-orbit coupling, several levels with different magnetic moments may rise. This phenomenon is known as Zero Field Splitting (ZFS). As the population medium of those levels is the temperature, and different levels may have different magnetic moments, the magnetisation of the system is strongly dependent on the temperature. Moreover, the measurements are usually carried on powder samples, so the total susceptibility can be approximated as an average made of the value for each component as expressed in equation (1.65).

$$\chi = \frac{\chi_x + \chi_y + \chi_z}{3} \tag{1.65}$$

Nevertheless, it is worth noting that the ZFS achieved when the metal center is located in a rigorously cubic ligand field environment is not too high. For instance, in the case of a high-spin d^5 ion, it has a $^6\mathrm{A}_{1\mathrm{g}}$ ground state under octahedral environment. In zero field, the first-order spin-orbit coupling will give two degenerate levels, a two-fold degenerate component, E', and a four-fold degenerate component, G' (considering the double group, O'). Second-order effects with components from another free ion terms, hence far from the ground state, will break their degeneracy splitting the two levels, at most of *ca.* 10^{-2} cm^{-1} for first-row transition metals. Thus, a very weak magnetic anisotropy will appear, but in principle as it is due to such low energy difference, it does not create any magnetic anisotropy in practise. For this reason, higher magnetic anisotropy usually appears by combination of the spin-orbit coupling and the distortion of the cubic symmetry, either axial ($z \neq x = y$) or rhombic ($z \neq x \neq y$). Consequently, if the symmetry of the system is not too high, the first- and second-order spin-orbit interactions can break the degeneracy of the ground state, and split it into different levels removing the isotropy of the system.

In the former example of a high-spin d^5 ion, any distortion will lower the symmetry and break the degeneracy of the G' into two two-fold degenerate states, and lead to a more noticeable anisotropy of the magnetic susceptibility. Thus, the energy separation between levels or anisotropy depends on the value of λ and a parameter of the symmetry distortion, where a noticeable ZFS will appear only when the symmetry of the system is not too high regardless the λ value.

Interestingly, when for an energy term there is an odd number of electrons, hence the total spin is a half-integer and the spin multiplicity calculated through $2S + 1$ is even, the combined effect of the spin-orbit coupling and a ligand field of any low symmetry, will always split as a result that energy multiplet at most into two-fold degenerate components. These two-fold degenerate components are called Kramers doublets. Thus, those systems with an even spin multiplicity energy term will always have a Kramer doublet which degeneracy cannot be completely eliminated by ZFS effects as a ground state.

On the other hand, for those energy terms with an even number of electrons, the splitting effect from the combination of the spin-orbit coupling and an axial distortion of the symmetry, results into one component with $m_j = 0$ and the rest of them will be Kramer doublets. Thus, the ground state could not always be a Kramer doublet as in the previous case. As the magnetic properties of the ground state become more relevant as the temperature is lowered, the fact of having a ground state with or without degeneracy has a drastic impact on the magnetic behaviour of a system. As there is a need of distinction between those two kind of systems, they are classified in two groups. In those cases where the degeneracy of the ground state multiplet cannot be completely removed by ZFS effects are known as Kramer systems, whereas those where it can be removed are called non-Kramer systems.

Alternatively, the ZFS within a ground state $L = 0$ and $S \neq 0$ can be treated with the phenomenological Hamiltonian presented in equation (1.66), where D represents the axial magnetic anisotropy parameter and E the rhombic parameter.

$$\widehat{H}_{ZFS} = D\left[\widehat{S}_z^2 - \frac{1}{3}S(S+1)\right] + E\left(\widehat{S}_x^2 - \widehat{S}_y^2\right) \tag{1.66}$$

1.4 Intermolecular magnetic interactions and magnetic orders

The phenomenon of diamagnetism and paramagnetism along with the interaction between the spin and orbital magnetic moments within an atom have been properly introduced. However, until now it was never considered the interaction between magnetic moments belonging to different atoms. So far, the magnetism was described for isolated paramagnetic centres, where each one was independent from the other without any contacts between them. In this way, all of them together constitute what is called a magnetically diluted system. Nonetheless, there is a large number of system which are said to be magnetically concentrated, where long range magnetic orders occur, being the different paramagnetic centres able to interact with each other in two different ways.

The intermolecular interaction with neighbouring members can line up parallel their magnetic moments or antiparallel in exactly opposite directions. They are

called ferromagnetic or antiferromagnetic, respectively. Moreover, if a compound is made up of paramagnetic centres with different effective magnetic moments, they cannot completely cancel when are arranged in a antiferromagnetic fashion, hence a net magnetic moment arises similar to ferromagnetic substances. These compounds are said to be ferrimagnetic. Lastly, it is possible that in an antiferromagnetic arrangement the magnetic moments are not completely align, and certain angle (α) remains among the paramagnetic centres, which could be of the same or different nature. This phenomenon is known as spin-canting and it leads to a small net magnetic moment, hence a very weak ferromagnetic-type behaviour. Indeed, in the same way, the spin-canting phenomenon can be present when the magnetic moments are arranged in parallel. A summary of these long range magnetic orders can be found in Figure 1.12.

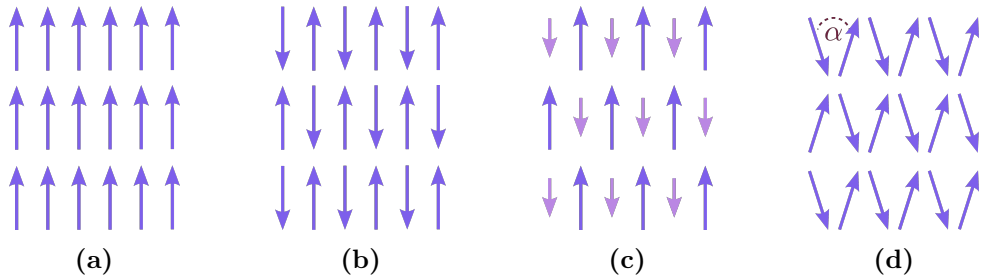

Figure 1.12: Cooperative phenomenon of paramagnetism substances with classical spin representation for a (a) Ferromagnetic interaction (b) Antiferromagnetic interaction (c) Non-compensated antiferromagnetic interactions also called ferrimagnetic behaviour (d) Antiferromagnetic spin-canting interaction. The angle of the canting is indicated by the α parameter.

These kinds of interactions can be mainly found in polinuclear compounds, where the different paramagnetic centres are bound by ligands acting as bridges with an essential role mediating the different interactions. Nevertheless, they can also be found in mononuclear entities with adjacent members in the crystal lattice. Every paramagnetic system at enough low temperature, where the intermolecular interactions may not be neglected, is expected to present long range magnetic order. That specific temperature is denoted as T_C (Curie temperature) or T_N (Néel temperature), for ferromagnetic or antiferromagnetic behaviour, respectively. The temperature at which the phenomenon arises depends on the intensity of the interactions. In general, for molecules with Van der Waals interactions it is the order of *ca.* 10^{-2} K. When the interactions are transmitted through hydrogen bonds the temperature can reach values of *ca.* 1 K. Moreover, when the interactions are carried out through the correct orbitals, it can be present at room temperature or even higher.

As a noteworthy remark, a classical magnet is characterised for having a high T_C well above room temperature. Thus, classical magnets exhibit strong long-range ferro- or ferrimagnetic interactions. Moreover, one characteristic of classical magnets is its ability to retain a certain amount of the magnetisation over long periods of time, contrary to paramagnets or diamagnets, it will not relax back to zero magnetisation when the imposed magnetising field is removed.

As a brief introduction, for ferro- and ferrimagnetic materials at a temperature below T_C, they are composed of small-volume regions in which there is a mutual alignment in the same direction of all magnetic dipole moments, as illustrated in

Figure 1.13a. Those regions are called domains, and each one is magnetised to its saturation. Different domains are separated by domain boundaries or walls, where the direction of magnetisation normally changes gradually from one to the other. In general, domains are microscopic in size and for polycrystalline materials each grain will consist of more than a single domain. Furthermore, for an unmagnetised sample each domain is randomly oriented, where the sum of the magnetisations of all domains equals zero. Under the application of an external field, it produces the breaking of the boundaries and the creation of bigger domains. If the field is strong enough it will produce a single domain where the saturation of the magnetisation is reached. A scheme of this process is presented in Figure 1.13b.

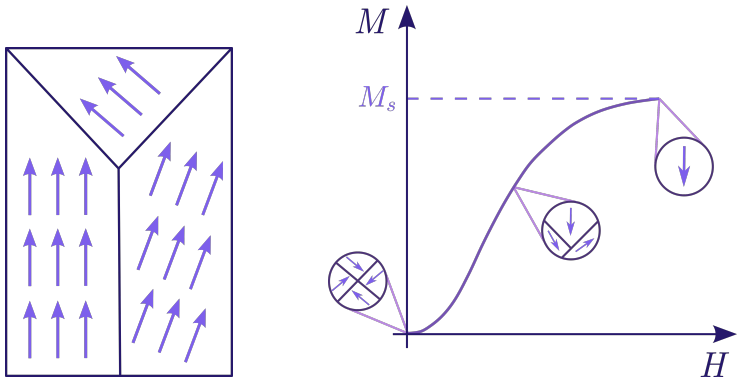

Figure 1.13: The arrows serves as classical spin representations (a) Schematic depiction of domains in a ferri- and ferromagnetic material. Within each domain all magnetic dipoles are aligned, whereas the direction of alignment varies from one domain to another. (b) Magnetisation curve of an initially unmagnetised ferri- or ferromagnetic system. Domain configurations during several stages of magnetisation are represented. The saturation of the magnetisation is also indicated.

In this type of magnetically ordered systems, they will remain partially ordered even after the removal of the external magnetic field. The parameter to measure the degree of this magnitude is known as magnetic retentivity or remanence, M_r. Additionally, the amount of reverse magnetic field that must be applied to the system to reduce its magnetisation to zero is called coercivity or coercive field, H_c. As a result of these two parameters, when a experiment is performed applying the field in one direction and then it is reversed, the magnetisation does not retrace its original path. This phenomenon is known as hysteresis effect and is represented by hysteresis loops or curves (Figure 1.14).

These parameters are of great importance in the rational design of new materials, where both ferri- and ferromagnetic materials can be classified as either soft or hard on the basis of their hysteresis characteristics (Figure 1.14b). For example, in data storage devices a weak coercive field will end on data corruption as is too easy to demagnetised. On the other side, if it is too big, the energy required for modifying the data (invert the magnetisation) will be of a large amount. For the retentivity, small values could end up with the reading system incapable of detecting the data. Thus, soft magnetic materials are generally used in devices that are subjected to alternating magnetic fields and in which energy losses must be low, like in the case of transformer cores, where a low coercivity for being easily magnetised and

demagnetised is searched.

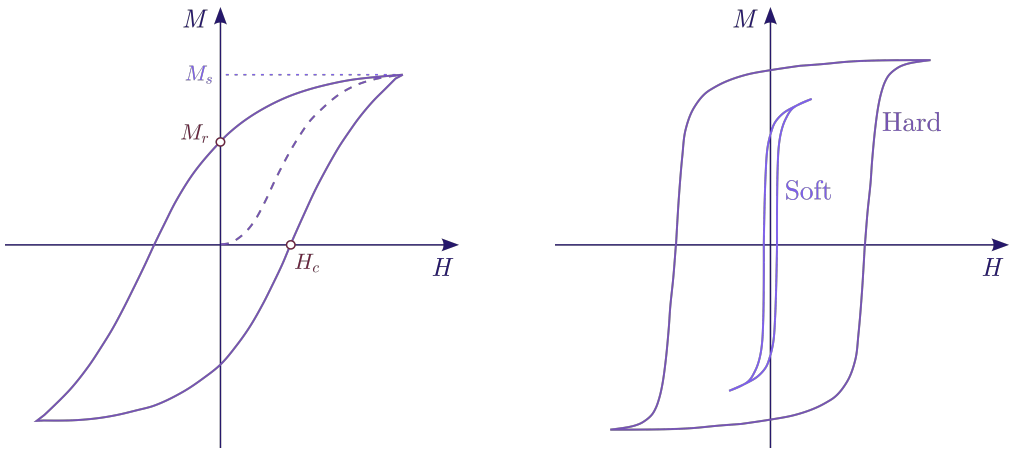

Figure 1.14: (a) The solid line represents the hysteresis loop, whereas the dashed line the initial magnetisation. Its singular points has been also indicated. (b) Types of hysteresis loops for hard or soft magnetic materials.

In order to treat the magnitude of the exchange interaction in a isotropic way, a simple approach can be done for temperatures above the T_C or T_N. Hence, in the paramagnetic state, where the effect of the intermolecular interactions is weak. The susceptibility data can be fitted modifying the Curie law adding a θ parameter called Weiss temperature. This new equation is called Curie-Weiss law (1.67). In Figure 1.15, it can be found the representation of different intermolecular interactions, where if $\theta = 0$, the material is a paramagnet. If $\theta < 0$ antiferromagnetic interactions dominate the magnetic behaviour, and if $\theta > 0$ ferromagnetic interactions prevail.

$$\chi_M = \frac{C}{T - \theta} \tag{1.67}$$

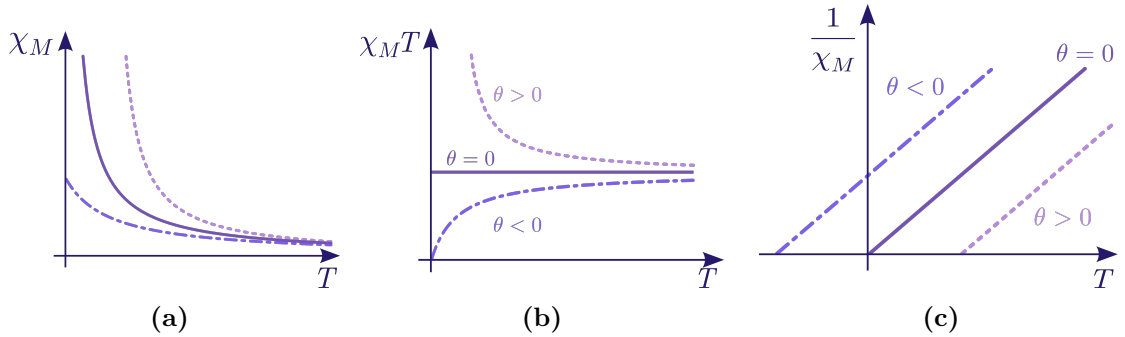

Figure 1.15: Different representations of the molar magnetic susceptibility obtained through the Curie-Weiss law for paramagnetic (solid line), ferromagnetic (dashed line) and antiferromagnetic (point and dashed line) systems (a) χ_M *vs.* T (b) $\chi_M T$ *vs.* T (c) ${\chi_M}^{-1}$ *vs.* T.

For systems where, to a first approximation, there is no orbital angular momentum associated with the ground states of the interacting metal ions, and where

the spin is treated under isotropic conditions, the magnitude of the spin-spin exchange interaction between an n number of neighbouring magnetic centres within a molecule can be treated with a Hamiltonian expressed as a sum of terms involving pairs of local spins as described in (1.68), where J_{ij} represents the exchange coupling constant between spins i and j. For $J < 0$ the interaction is said to be antiferromagnetic, and ferromagnetic when $J > 0$. Therefore, it is necessary to add a negative sign to the Hamiltonian expression for defining the ferromagnetic interactions as the less energetic and the antiferromagnetic as the higher ones. Moreover, equation (1.68) is written in a way that each interaction is counted only once, while in other notation is preferred to count J_{ij} and J_{ji} as equals and give J_{ij} twice the value expressed here.

$$\widehat{\mathcal{H}}_J = -\sum_{i>j}^{n} J_{ij}\widehat{S}_j \cdot \widehat{S}_i \tag{1.68}$$

Interestingly, the simplest case of a magnetic chain is provided by an array of equally spaced metal ions as schematised in Figure 1.16, with an effective isotropic spin of $S = 1/2$. Thus, the spin Hamiltonian in zero-field adapted to describe the isotropic interaction between nearest neighbouring ions, where the addition runs over the n sites of the chain is written as (1.69).

Figure 1.16: Scheme of a one-dimensional system with equally spaced metal centres and one magnetic exchange coupling constant, J.

$$\widehat{\mathcal{H}}_J = -J\sum_{i=1}^{n-1} \widehat{S}_{A_i} \cdot \widehat{S}_{A_{i+1}} \tag{1.69}$$

Nevertheless, when n tends to infinite, there is no analytical method that can be used to determine the energies of the low-lying states and the magnetic susceptibility. However, Bonner and Fisher solved the problem numerically by considering ring chains of increasing size and extrapolating for the case where n becomes infinite. The numerical expression result for $J < 0$ in presented in (1.70), where χ_M passes through a rounded maximum at a temperature, T_N, defined by (1.71).[18]

$$\chi_M = \frac{N_A g^2 {\mu_B}^2}{k_B T} \frac{0.25 + 0.074975x + 0.075235x^2}{1.0 + 0.9931x + 0.172135x^2 + 0.757825x^3}$$
$$x = \frac{|J|}{k_B T} \tag{1.70}$$

$$\frac{k_B T_N}{|J|} = 0.641 \tag{1.71}$$

On the other hand, a high-temperature series expansion has been proposed by Baker-Rushbrooke[19], for a ferromagnetically coupled ($J > 0$) uniform chain of spin

doublets as the following numerical expression

$$\chi_M = \frac{N_A g^2 {\mu_B}^2}{4k_B T}\left[\frac{1.0 + Ay + By^2 + Cy^3 + Dy^4 + Ey^5}{1.0 + A'y + B'y^2 + C'y^3 + D'y^4}\right]^{2/3}$$
$$y = \frac{J}{k_B T}; \quad A = 5.7979916; \quad B = 16.902653; \quad C = 29.376885; \tag{1.72}$$
$$D = 29.832959; \quad E = 14.036918; \quad A' = 2.7979916; \quad B' = 7.0086780;$$
$$C' = 8.6538644; \quad D' = 4.5743114$$

1.5 Spin dynamics and relaxation times

Until now, all magnetic properties were related to systems under a static magnetic field produced by means of a direct current, thus they are referred as DC or static magnetic properties. It was not yet covered the dynamic magnetic properties of systems obtained *via* an oscillating magnetic field. That field is produced by an alternating current (AC), so the magnetisation and susceptibility obtained are denoted as M_{AC} and χ_{AC}, respectively. With AC is possible to measure the sensitivity to change of the magnetisation with respect to a change in the applied field. In other words, it provides information about the slope of the magnetisation curve, its derivative. Indeed, in those parts where the relationship between M and H is lineal, the susceptibilities obtained by DC or AC methods coincide, while in the saturation χ_{AC} is equal to zero. This information is represented in Figure 1.17.

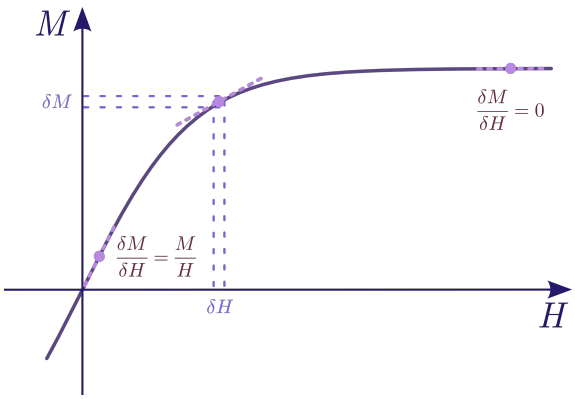

Figure 1.17: The derivative of the magnetisation curve at different points.

In AC measurements, the magnetic field varies with the time as indicated by equation (1.73), where the oscillating or alternating magnetic field, $H(t)$, it is a function of $\omega = 2\pi\nu$, ν being the frequency of the alternating current in Hertz units and typically in the range of 0.1 to 10^4 Hz (s^{-1}), t is in seconds, and H_{AC} is the amplitude of the field, which it is normally about 1 to 5 Øe, therefore $H_{\mathrm{AC}} << H_{\mathrm{DC}}$. Besides, the magnetisation due to the sample under this field follows a similar pattern, as it is given by equation (1.74). One characteristic of the AC measurements is that they can be performed in absence or presence of a DC magnetic field, so H_{DC} and M_{DC} may be null. Either way, all experiments in this dissertation are limited to the case where both magnetic fields are applied in parallel. Furthermore, the AC susceptibility is calculated as the DC, but using the amplitude of the AC

field as equation (1.75) states. As in the DC case, this equation assumes a lineal response between field and magnetisation, and non-lineal regimes will be avoided by performing experiments far from the saturation of the magnetisation.

$$H(t) = H_{\mathrm{DC}} + H_{\mathrm{AC}} \cos(\omega t) \tag{1.73}$$

$$M(t) = M_{\mathrm{DC}} + M_{\mathrm{AC}} \cos(\omega t) \tag{1.74}$$

$$\chi_{AC} = \frac{M_{\mathrm{AC}}}{H_{\mathrm{AC}}} \tag{1.75}$$

As an example, in a system formed by i paramagnetic ions with only two spin states, $M_S = +1/2$ and $M_S = -1/2$ without ZFS, under the presence of a H_{DC} the two levels will break their degeneracy, and they will be populated by the temperature as already explained in section 1.2. The presence of an oscillating field implies that the magnetic field surrounding the i paramagnetic ions changes over time. In an AC experiment it is possible to vary the frequency of the current, hence, the direction of the H_{AC} produced. In this way, it leads to transitions between the two levels as depicted in Figure 1.18. The redistribution of the magnetic dipoles of the sample over the two energy levels follows a relaxation process, which requires of a certain time called relaxation time, τ. Thus, a relevant feature of an AC experiment is that allows the possibility to ascertain the spin dynamics of the system under study by determining the relaxation time of its magnetic moment.

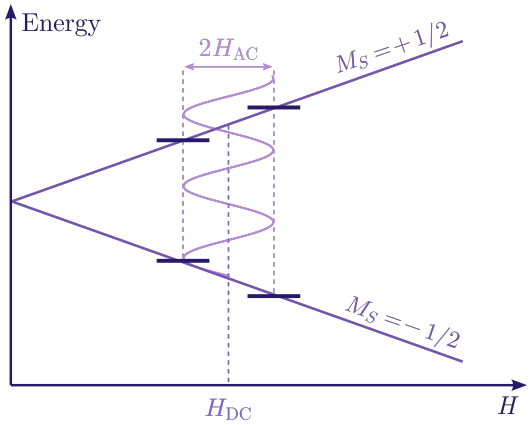

Figure 1.18: Spin relaxation of a system between only two levels under a H_{DC} in which an oscillating field is applied, being $H_{\mathrm{DC}} >> H_{\mathrm{AC}}$. The diagram is not at scale.

Three different regimes can be defined depending on the relaxation time of the magnetic moments of the sample. First, when the frequency of the alternating field is slower than the relaxation rate of the system ($\omega << \tau^{-1}$). In this case, the system responds instantaneously to the variations of the H_{AC} and the susceptibility obtained is comparable with the susceptibility measured by DC methods. In other words, the magnetic moments of the sample are always at equilibrium throughout the measurement, being able to align parallel to the oscillating magnetic field to the state of minimum energy. In these conditions, the AC susceptibility is also called isothermal susceptibility, χ_T, to indicate the thermal equilibrium of the spin system with its surroundings.

Secondly, when the variation of the AC field oscillates much faster than the relaxation rate of the system ($\omega >> \tau^{-1}$). In this condition, the system cannot respond quickly enough and is not able to achieve the minimum of energy aligning all the magnetic moments. The system has blocked their magnetic moments and they cannot be reoriented by H_{AC}, they being isolated from its surroundings. Under these circumstances, the susceptibility is usually called adiabatic susceptibility, χ_S, and it depends on the intensity of the magnetic field. In general, for very strong DC fields, $\chi_S << \chi_T$ and in some approximations χ_S is neglected. After all, if the magnetic moments are completely blocked and the oscillating field is not able to realign them, the magnetisation is not going to undergo a noticeable change, and a dynamic measure that asses its variation will have a low value.

Lastly, when both magnitudes are comparable ($\omega \approx \tau^{-1}$), the magnetic moments of the system are not able to response instantaneously with the oscillating field variation driven by the alternating current. The generated magnetisation delays after the driving field by a shift indicated by the variable φ, which carries the phase lag between the alternating current and the system. Thus, equation (1.74) is rewritten as (1.76), where it was not considered the DC term. This phenomenon is known in the Molecular Magnetism field as slow relaxation of the magnetisation.

$$\begin{aligned} M(t) &= M_{\mathrm{AC}} \cos(\omega t - \varphi) \\ &= M_{\mathrm{AC}} \cos\varphi \cos(\omega t) + M_{\mathrm{AC}} \sin\varphi \sin(\omega t) \end{aligned} \tag{1.76}$$

Moreover, the magnetisations can be rearranged in two parts, as in-phase or real, χ', and out-of-phase or imaginary component, χ'', as done in (1.77). The imaginary component is also known as absorption susceptibility because it is a measure of the energy absorbed or dissipated by the system under an AC field. On the other hand, the real component is also called the dispersion susceptibility.

$$\begin{aligned} M(t) &= \chi' M_{\mathrm{AC}} \cos(\omega t) + \chi'' M_{\mathrm{AC}} \sin(\omega t); \\ \chi' &= \frac{M_{\mathrm{AC}}}{H_{\mathrm{AC}}} \cos\varphi; \quad \chi'' = \frac{M_{\mathrm{AC}}}{H_{\mathrm{AC}}} \sin\varphi \end{aligned} \tag{1.77}$$

At a certain temperature and for a given H_{DC}, the AC susceptibility can be expressed as (1.78), which yields to real (χ') and imaginary (χ'') parts to the values given by equations (1.79) and (1.80), respectively. This model proposed by Casimir and du Pré to interpret the slow relaxation of the magnetisation, in ferric ammonium sulphate,[20] is analogous to the dielectric relaxation described by the Debye model.[21] Actually, many of the treatments of AC susceptibility take expressions used in dielectric relaxation.

In this case, the AC susceptibility may be written as a complex number as in (1.81), where the sign of the imaginary part is a matter of convention that depends on how the sign in the denominator of equation (1.78) is defined.[22] Either way, equations (1.79) and (1.80) remain independent of the sign convention chosen. It is worth mentioning, that at low and high frequencies φ equals zero. Therefore, the system is essentially fully in-phase and $\chi'' \approx 0$. Thus, the susceptibility is just the real component expressed as χ_T or χ_S.

$$\chi_{AC} = \chi_S + \frac{\chi_T - \chi_S}{1 + i\omega\tau} \tag{1.78}$$

$$\chi' = \chi_S + \frac{\chi_T - \chi_S}{1 + (\omega\tau)^2} \tag{1.79}$$

$$\chi'' = \frac{(\chi_T - \chi_S)\omega\tau}{1 + (\omega\tau)^2} \tag{1.80}$$

$$\chi_{AC} = \chi' - i\chi'' \tag{1.81}$$

As it can be deduced from equation (1.80) and it is shown in Figure 1.19a, the maximum value of χ'' is achieved when $\omega = \tau^{-1}$, and it corresponds to $\frac{\chi_T - \chi_S}{2}$. Moreover, for much higher or lower frequencies than the relaxation rate, the values of χ'' are negligible. In Figure 1.19b, it can be seen the effect of lower relaxation rates for a given temperature, in which for greater relaxation times the maximum is reached at lower frequencies.

In this way, a representation of χ'' *vs.* ν in a range of temperatures allows to characterise at which frequency the maximum is found, and therefore the relaxation time of the system at different temperatures by equation (1.82). Indeed, τ values will be determined with more exactitude fitting all the experimental data to the function from equation (1.80), determining $\Delta\chi = \chi_T - \chi_S$ along with τ rather than establish the relaxation time only with the value at the maximum frequency.

$$\tau(T) = \frac{1}{2\pi\nu_{max}} \tag{1.82}$$

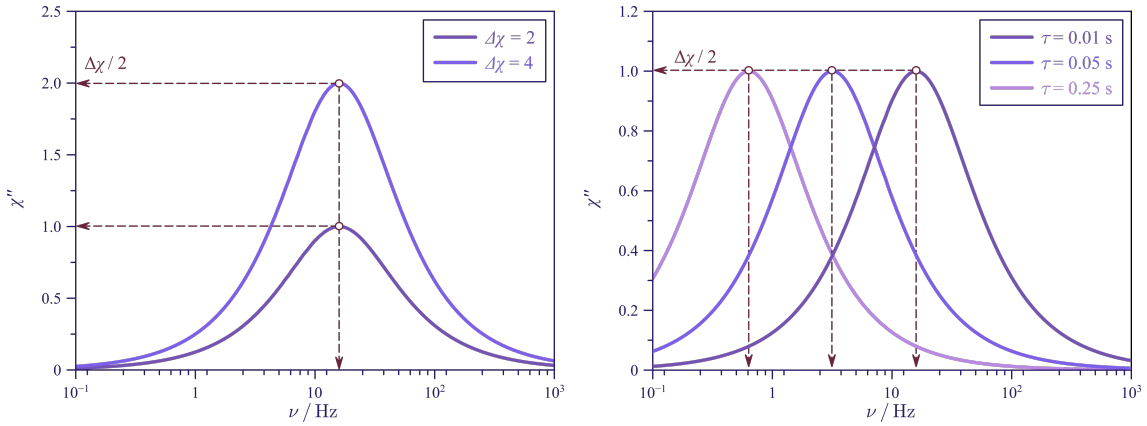

(a) **(b)**

Figure 1.19: Representation of χ'' *vs.* ν curves for a given temperature and (a) Different values of $\Delta\chi = \chi_T - \chi_S$ whilst the value of τ has been taken equal to 0.01 s (b) Different values of τ with $\Delta\chi$ constant to 2.00. The dashed lines represent the position of the different maxima on the horizontal and vertical axis. The frequencies are depicted in a logarithm scale.

On the other hand, it is also possible to determine the relaxation time from χ' *vs.* ν representations. In Figure 1.20a, it can be seen that the inflection point of the χ' function appears when $\omega = \tau^{-1}$ at $\frac{\chi_T + \chi_S}{2}$ which coincide with the maximum in χ''. Moreover, as it can be deduced from equation (1.79), when $\nu \to \infty$, $\chi' \to \chi_S$, whilst $\nu \to 0$, $\chi' \to \chi_T$. In Figure 1.20b, it is presented the χ' curves for several relaxation times, where for higher τ values the inflection point appears at lower frequencies. The same conclusion was made for χ''.

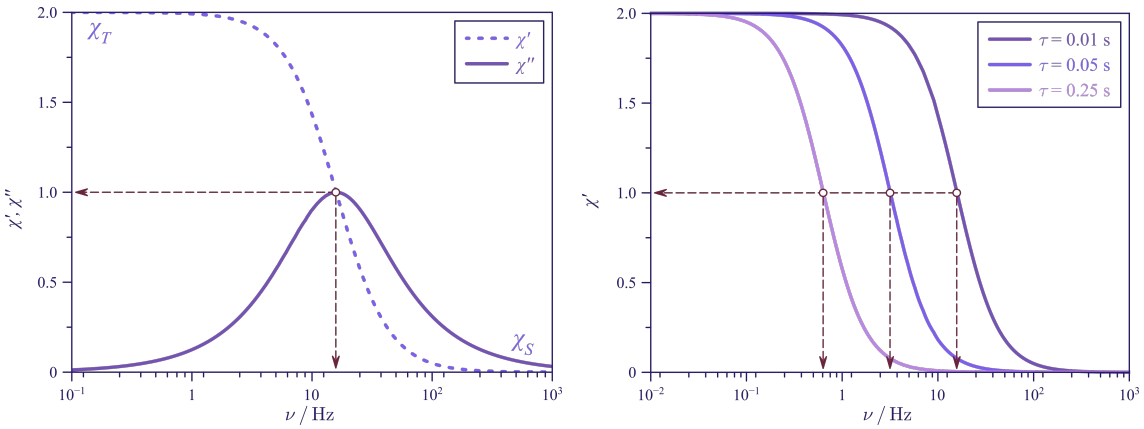

Figure 1.20: (a) Representation of χ_{AC} *vs.* ν curves at a constant temperature for a τ value of 0.01 s (b) Representation of χ' *vs.* ν curves for a given temperature for different relaxation times. The values of χ_T and χ_S of the in-phase susceptibility are taken as 2.00 and 0, respectively. The dashed lines represent the position of the different maxima on the horizontal and vertical axis. The frequencies are depicted in a logarithm scale.

Indeed, both equations (1.79) and (1.80) are really helpful in order to establish the relaxation time of a system. However, it is more convenient to use the expression (1.80) and χ'' representations since it is only necessary to determine two variables, $\Delta\chi$ and τ, whilst there are three, χ_S, χ_T and τ for expression (1.79).

On the other hand, it is possible to represent the measured data in χ'' *vs.* T plots at different constant frequencies. Thus, it will be seen how the relaxation time varies with the temperature at a given frequency. In this way, when $\omega = \tau^{-1}$, a maximum will appear in both the $\chi''(T)$ plot at different frequencies and in $\chi''(\nu)$ at different temperatures. Nevertheless, among the two types of curves, $\chi''(\nu)$ data can be fitted to the Debye model by equation (1.80).

Alternatively, it is possible to report χ'' *vs.* χ' resulting in a semicircle plot known as the Argand diagram. These plots are equivalent in the field of magnetism to the Cole–Cole plots for dielectrics.[23] From equation (1.79) and (1.80) is deduced expression (1.83), which resembles the equation of the circle (1.84), where the point (a, b) indicates its center and r its radius.

$$\left[\chi' - \left(\frac{\chi_T + \chi_S}{2}\right)\right]^2 + \chi''^2 = \frac{\chi_T + \chi_S}{2} \tag{1.83}$$

$$(x-a)^2 + (y-b)^2 = r^2 \tag{1.84}$$

A representation of the Argand diagram is shown in Figure 1.21, where the center is located at $\left(\frac{\chi_T+\chi_S}{2}, 0\right)$ and the radius corresponds to $\frac{\chi_T-\chi_S}{2}$. Furthermore, the top satisfies the condition $\omega = \tau^{-1}$. Hence, the relaxation time is deduced from the frequency that gives the maximum value of the semicircle. The result of a single perfect semicircle indicates the presence of only one relaxation time driven by a single relaxation process, besides, the intersection of the circle on the χ' axis gives the values for χ_T and χ_S. It is possible to perform experiments at different temperatures in order to verify the existence of a single relaxation time and, therefore, unique

values of χ_T and χ_S with the temperature. Indeed, if the consistency is maintained all diagrams should look the same regardless of the temperature.

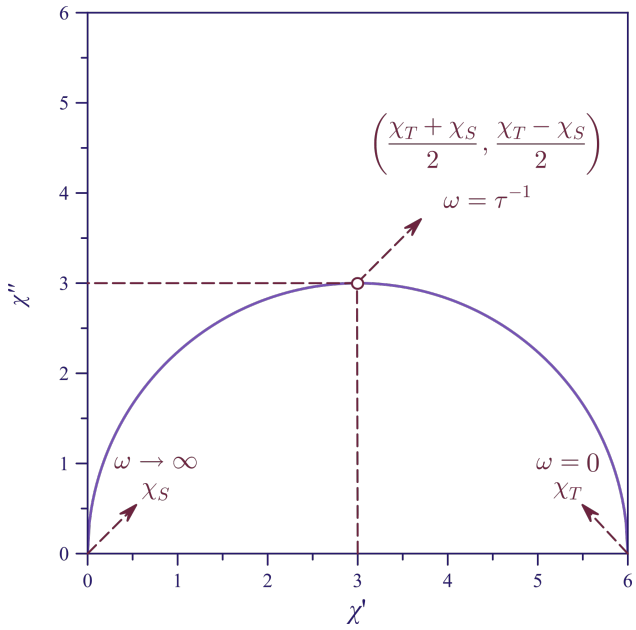

Figure 1.21: An Argand diagram at a constant temperature with a single relaxation time, showing their singular points. The values of χ_T and χ_S are taken as 6.00 and 0, respectively.

Nevertheless, different values of χ_T can be obtained from the analysis performed at different temperatures if the magnetisation has not reach its saturation, showing how the relaxation time depends on the temperature. For a system with only one relaxation time per temperature, and considering that τ varies with it following an exponential relation of the Arrhenius type presented in equation (1.85), it is possible to determine its energy barrier, U, and the pre-exponential factor, τ_0. These two parameters characterise the slow relaxation of the magnetisation in a compound. Moreover, equation (1.85) determines that as temperature ascends the relaxation time decreases.

$$\tau = \tau_0 \exp\left(\frac{U}{k_B T}\right) \tag{1.85}$$

In practice, natural logarithmic transformation is used on equation (1.85) to convert it into a linear relationship (1.86). In this way, the data is fitted by linear regression. A simulation of a system with different energy barriers and a fixed τ_0 is shown in Figure 1.22. It can be seen how it is necessary of high U values in order to increase the temperature at which the maxima in χ'' will appear. As an example, in order to detect out-of-phase signals at high temperature (T = 300 K) for a system with $\tau_0 = 10^{-8}$ s with a frequency of 1000 Hz, it will be necessary an U of *ca.* 2000 cm^{-1}. Moreover, it is important to take into account the limitations due to the measuring device. In general, a SQUID magnetometer is able to measure frequencies in the range from 0.1 to 1000 Hz, using values inferior to 0.1 Hz will make the experiments to long. In the case of a PPMS device, it may work in a

frequency range 100-10000 Hz.

$$\ln \tau = \ln (\tau_0) + \frac{U}{k_B} \frac{1}{T} \tag{1.86}$$

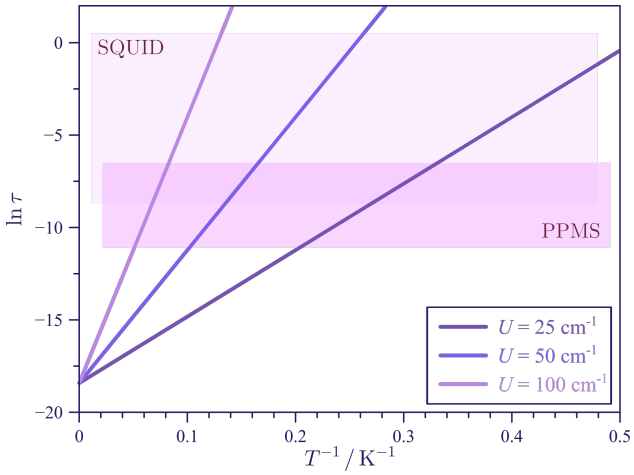

Figure 1.22: Ln τ *vs.* $1/T$ plots for systems with different energy barriers. The value of τ_0 is taken as 10^{-8} s. The range of frequencies for a SQUID and PPMS device is indicated.

Furthermore, deviations of the perfect semicircle from the Argand diagrams are commonly found. In practice, very few cases completely agrees with Debye equation (1.78). The model considers that the magnetisation decays or relax exponentially with time, and it assumes that the different entities have spherical shape and cannot interact with each other. Hence, all magnetic centres have the same relaxation time. The limit of completely non-interacting magnetic moments is unlikely to be encountered, due to the presence of cooperative effects that may raise neither at high or low temperatures. In order to take into account these deviations into the Debye model, for a given temperature a phenomenological parameter, α, is introduced for measuring the distribution of relaxation times.

Thus, equation (1.87) is known as the generalised Debye model, which yields to expressions (1.88) and (1.89) for χ' and χ'', respectively. The values of α are compressed between 0 and 1, where $\alpha = 0$ indicates that no distribution exist because it is a line, hence the generalised Debye model reduces to the ideal Debye model. For $\alpha = 1$, it becomes parallel to the axis showing infinite times. Thus, a distribution on the relaxation times lead to a distribution on the energy barriers.

$$\chi_{AC} = \chi_S + \frac{\chi_T - \chi_S}{1 + (i\omega\tau)^{1-\alpha}} \tag{1.87}$$

$$\begin{aligned} \chi' &= \chi_S + (\chi_T - \chi_S) \frac{1 + (\omega\tau)^{1-\alpha} \sin\left(\frac{\pi\alpha}{2}\right)}{1 + 2(\omega\tau)^{1-\alpha} \sin\left(\frac{\pi\alpha}{2}\right) + (\omega\tau)^{2(1-\alpha)}} \\ &= \chi_S + \frac{\chi_T - \chi_S}{2} \left[1 - \frac{\sinh\left[(1-\alpha)\ln(\omega\tau)\right]}{\cosh\left[(1-\alpha)\ln(\omega\tau)\right] + \sin\left(\frac{\pi\alpha}{2}\right)} \right] \end{aligned} \tag{1.88}$$

$$\begin{aligned}\chi'' &= (\chi_T - \chi_S)\frac{(\omega\tau)^{1-\alpha}\cos\left(\frac{\pi\alpha}{2}\right)}{1 + 2(\omega\tau)^{1-\alpha}\sin\left(\frac{\pi\alpha}{2}\right) + (\omega\tau)^{2(1-\alpha)}} \\ &= \frac{\chi_T - \chi_S}{2}\frac{\cos\left(\frac{\alpha\pi}{2}\right)}{\cosh\left[(1-\alpha)\ln(\omega\tau)\right] + \sin\left(\frac{\pi\alpha}{2}\right)}\end{aligned} \tag{1.89}$$

The relaxation times distribution for the generalised Debye model behaves symmetrically in a logarithmic scale around an average relaxation time, τ_{av}, following expression (1.90) and represented in Figure 1.23a for a constant temperature. As the temperature descends, intermolecular interactions may become more important and began to dominate incrementing the size of the entities along with the relaxation times, therefore a greater value of α would be expected. Moreover, the average relaxation time may also increase as the temperature descends, as discussed earlier. This information is shown in Figure 1.23b.

$$G(\ln\tau) = \frac{1}{2\pi}\left[\frac{\sin(\alpha\pi)}{\cosh\left[(1-\alpha)\ln\left(\frac{\tau}{\tau_{av}}\right)\right] - \cos(\alpha\pi)}\right] \tag{1.90}$$

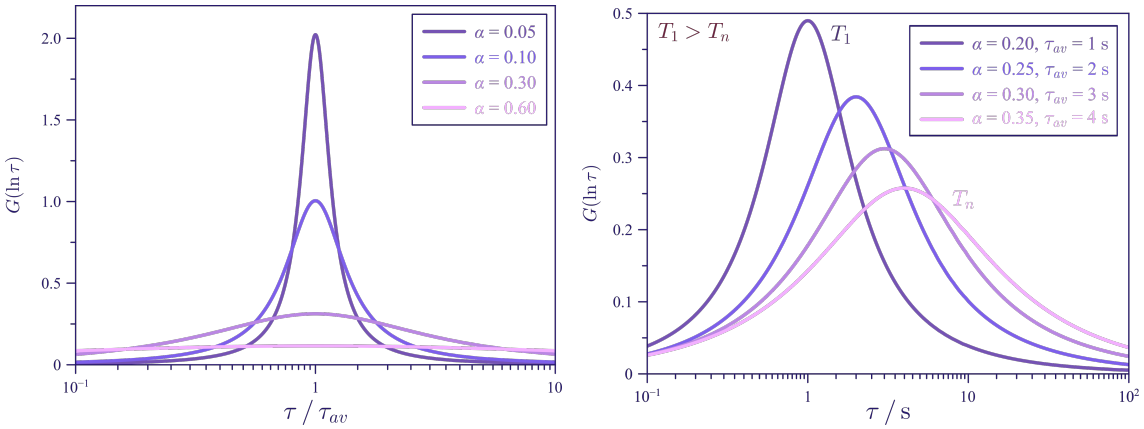

(a) **(b)**

Figure 1.23: Distribution of relaxation times following equation (1.90) for different α values (a) At a constant temperature (b) At different temperatures. The x-axis are depicted in a logarithm scale.

An alternative approach considering a logarithmically asymmetric distribution of relaxation times on the frequency axis is possible with Cole-Davison or Havriliak–Negami models,[22] among others.[24] Nevertheless, the published compounds within this dissertation are considered to have a symmetric distribution and the Debye generalised model will be the only one used.

It is possible to relate equation (1.88) and (1.89) to obtain expression (1.91), which it is useful for an Argand representation. In Figure 1.24 is shown the effect of α on different Argand diagrams, where for values different from zero, the semicircle becomes flattened and an arc is obtained. This indicates that the relaxation process is not characterised by a single relaxation time.

$$\chi'' = -F + \sqrt{F^2 + (\chi' - \chi_S)(\chi_T - \chi')}; \quad F = \frac{\chi_T - \chi_S}{2}\tan\left(\frac{\pi\alpha}{2}\right) \tag{1.91}$$

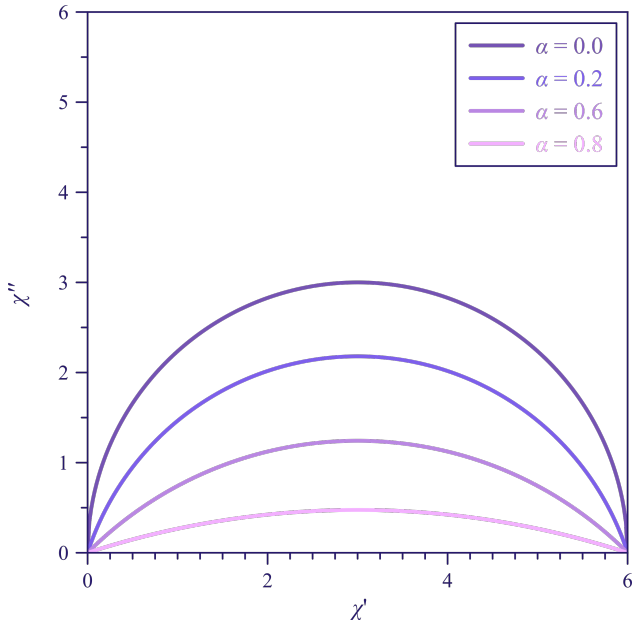

Figure 1.24: Argand diagrams at a constant temperature for different distributions of relaxation times. The value of τ_{av} is taken as 0.01 s, whilst χ_T and χ_S are 6.00 and 0, respectively.

In Figure 1.25, it can be seen the effect of the relaxation time distribution on χ' and χ''. It is interesting to note how the values of both susceptibilities decrease as greater becomes the distribution. Furthermore, at the same frequency and temperature, χ'' values can be very small compared to χ'.

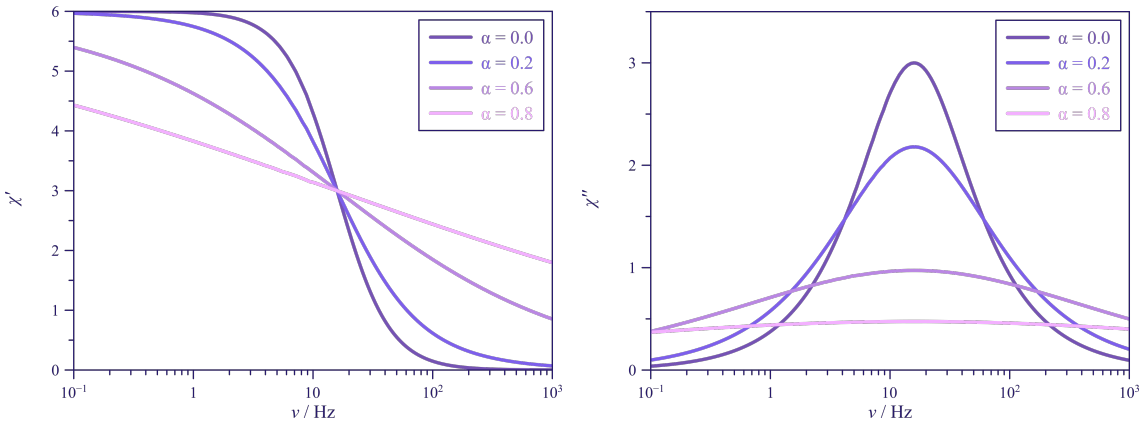

Figure 1.25: Representation of (a) χ' and (b) χ'' *vs.* ν at a constant temperature. Note how the inflection point in χ' or the maximum in χ'' match for all curves, due to the same τ_{av} at 0.01 s. These plots assume $\chi_S = 0$ and $\chi_T = 6$. The frequencies are depicted in a logarithm scale.

As a noteworthy remark, sometimes it is not possible to characterise the full relaxation curve, and only incipient signals without a well establish maximum are detected in the temperature and frequency window technically available, hence the fit of the data to the Debye model is not possible. In those cases, a rough evaluation

can be made assuming only one relaxation time and considering the system driven by only one energy barrier (1.85). Neglecting the χ_S term from expressions (1.79) and (1.80) the quotient χ''/χ' is equal to $\omega\tau$, thus U and τ_0 are estimated through equation (1.92).

$$\ln\left(\frac{\chi''}{\chi'}\right) = \ln(\omega\tau_0) + \frac{U}{k_B}\frac{1}{T} \tag{1.92}$$

Until now only one relaxation process was considered, but it is possible to encounter systems with more than one. The Debye equation (1.78) can be extended to a n-set Debye model (1.93), where each process may have its own relaxation time distribution. Consequently, depending on where the maxima of the different processes are located, it will be more or less easy to visualize them in χ'', and a sum of n-arcs will appear in the Cole-Cole plots.

$$\chi_{AC} = \chi_S + \frac{\chi_{T1} - \chi_S}{1 + (i\omega\tau_1)^{1-\alpha_1}} + \frac{\chi_{T2} - \chi_S}{1 + (i\omega\tau_2)^{1-\alpha_2}} + ... \tag{1.93}$$

Furthermore, each slow relaxation of the magnetisation process may take place driven by different mechanisms or a set of them. Due to the wide range of different spin relaxation interactions, several magnetic relaxations mechanisms are found in the literature, and the origin of those interactions has been a reason of study for years.[10,25–29]

As a brief introduction, the mechanisms considered relevant for the compounds described in this Thesis work are those involving the interactions of spins from the paramagnetic centres with the environment where they are place, which will be referred from now on as the lattice. The spin-lattice relaxation mechanisms involve transference of energy between the spin system and the vibrations of the lattice through phonons. Therefore, these mechanisms are dependent of the temperature, and it will be studied mainly three types, Orbach, Direct and Raman. On the other hand, there is another important temperature independent mechanism called Quantum Tunnelling of the Magnetisation abbreviated QTM. Thus, there is not a single mechanism determining the relaxation dynamics of a compound. Nevertheless, at the beginning of this research field, the relaxation process was only considered to be driven by an Orbach mechanism, and as consequence, a lot of the compounds magnetic behaviour is only related to it.

The main condition for a system to exhibit slow relaxation of the magnetisation is the existence of an energy barrier that separates the states with positive and negative magnetic moments with respect to a given axis or plane of magnetisation. This is achieved by means of the spin anisotropy, where the applied magnetic field will have different effects on the electronic spin depending of the chosen axis. A relaxation mechanism connect the different levels in order to invert the direction of the spin and regain the equilibrium. Thus, before applying any field both directions of the electronic spin are equally possible describing a symmetric double well with the same population. A potential energy diagram of the magnetic moment with an energy barrier separating the up and down orientations is shown in Figure 1.26a.

Furthermore, in the simplest case of a system with an easy axis of magnetisation with respect the other two coordinates, there are two kinds of energy barriers expressions according to the total spin of the system. For integer spins $U = |D|S^2$ and $U = |D|(S^2 - 1/4)$ for half-integer spins, calculated through equation (1.66)

neglecting the rhombic anisotropy. Nevertheless, in these systems after applying the alternating field, the levels are almost align between them and the QTM mechanism is the main pathway of relaxation. The QTM works shortening the relaxation path through two levels close in energy, so it is the more likely mechanism to happen in the vicinity of energy level crossings. Applying a static field, the double well becomes asymmetric and the QTM becomes less likely to happen as there is not a match between different energy levels (Figure 1.26b). If the sweep of the static field continues it can match again the two levels and the QTM becomes relevant again (Figure 1.26c). Thus, QTM is strongly dependent on the magnetic field.

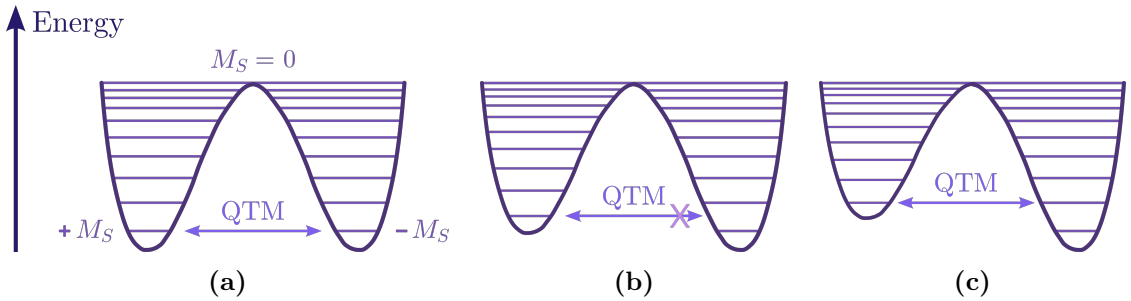

Figure 1.26: Drawing showing the potential energy of a integer spin system exhibiting slow relaxation of the magnetisation under (a) $H_{DC} = 0$ (b) $H_{DC,1} \neq 0$ (c) $H_{DC,2} > H_{DC,1}$.

On the other hand, in a Direct mechanism there is an exact match between the spin transition energy and a phonon from the lattice. Thus, it can be a direct transfer of energy from the spin system to the lattice. For Orbach and Raman mechanisms, they use a two-phonon process, where the first phonon from the lattice is absorbed to promote the spin system to an excited state for the Orbach, and through a virtual state for the Raman mechanism. Lately, the second phonon is released returning the system to the ground state but with the spin inverted. An schematic representation of the different mechanism is depicted in Figure 1.27.

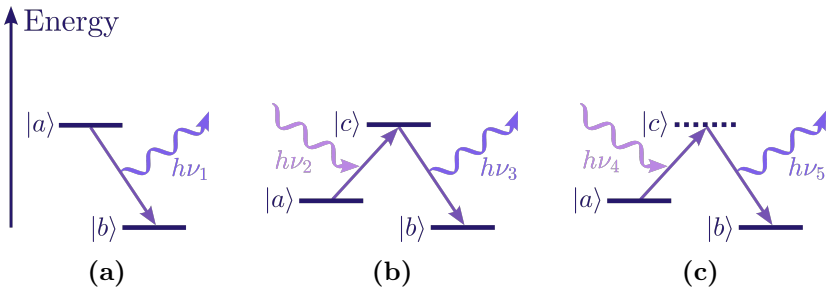

Figure 1.27: Schematic representation of the spin-lattice mechanism that can occur in a system (a) Direct (b) Orbach (c) Raman. The $|c\rangle$ represents a real excited state in the Orbach mechanism and a virtual state in the Raman diagram.

As there is a low density of low-energy phonons that match exactly the energy for the transition, the Direct mechanism is not too efficient at high temperatures. In contrast, the Orbach and Raman mechanisms involve the abortion of high-energy phonons which are more abundant at higher temperatures, and therefore more efficient. Nevertheless, as the temperature decreases the availability of high-energy phonons is severed and the Orbach and Raman mechanisms become less relevant, whilst the Direct mechanism turns into the main pathway.

In this way, the overall relaxation rate (τ^{-1}) is normally fitted to a mixture of the different mechanisms that may be available for a system as expressed in equation (1.94)

$$\tau^{-1} = \tau_{Orbach}^{-1} + \tau_{Raman}^{-1} + \tau_{Direct}^{-1} + \tau_{QTM}^{-1} \tag{1.94}$$

The Orbach term has already been introduced, $\tau_{Orbach}^{-1} = \tau_0^{-1} \exp\left(-\frac{U}{k_B T}\right)$, showing its exponential dependence with the temperature. The Raman term has the form of $\tau_{Raman}^{-1} = CT^n$, where n is treated as an adjustable parameter that can strongly deviate from its theoretical temperature dependence, which is $n = 7$ for non-Kramer (integer total spin) and $n = 9$ for Kramer systems (half-integer total spin). This is mainly due to the availably of the phonons. The Direct term $\tau_{Direct}^{-1} = AT$ depends on the temperature and its constant on the applied magnetic field. Lastly, the QTM is treated as a constant that is independent on the temperature, and strongly dependent on the field. The terms on equation (1.94) have been ordered to adopt significance on cooling from left to right. Each mechanism has different dependence with the temperature or none, and the different availability windows may make them coexist all together. In general, the QTM and Direct mechanisms normally operate at low temperatures, Orbach at highest and Raman has been seen in the whole temperature range.

As a noteworthy remark, if a relaxation process is only driven by a QTM mechanism, it being the only one which is temperature independent, the maxima in $\chi''(T)$ will be located at the same temperature. This could also be detected in the $\chi''(\nu)$ representations where the position of the maxima do not shift when increasing the temperature.

Although relaxation times are generally fitted to several mechanisms, and the inclusion of many of them within a model could lead to a better representation of the experimental data, it could also lead to an overparametrization situation where the values obtained for each mechanism may probably lose their physical meaning. In those cases, it may be recommended to fit the available data to less mechanisms in order to allow more reliable parameters for each one.

1.6 From classical magnets to molecular magnets

The strength of ferro- or ferrimagnetic interactions in a compound defines its T_C. Above that temperature, the material will lose its property of being capable to retain the magnetisation when the field is removed. Nevertheless, classical magnets have a T_C well above the room temperature. Thus, magnetism was a property traditionally associated with metallic and ionic lattices. For example, magnets were exclusively metals such as Fe, Co, Ni, Gd, some alloys or oxides like magnetite (Fe_3O_4), Fe_2O_3 or CrO_2. One of the most common uses of magnetic materials is indeed its characteristic to partially retain the applied magnetic field, which has been used to store information. However, because of the need to allocate larger amounts of data in the same space size, a challenge in the design of new magnets is their miniaturisation. To attain this purpose there are two different approaches. The first one is known as top-down, and consists on reducing the size of the material with physical procedures. The second approach is known as bottom-up, which begins with small entities and

ends with larger systems with the use of metal ions and ligands bond by chemical processes.

As a brief summary on the historical background of the bottom-up perspective, it is characterised by the rational synthesis of new polynuclear coordination compounds. In this approach, it is necessary to choose the nature, size, shape, reactivity, magnetic properties, and connectivity of the different building blocks. The problem at hand is to succeed choosing the conditions to favouring the ferromagnetic ordering, which is not a trivial matter. Achieving an intramolecular ferromagnetic interaction can be problematic, but achieving an intermolecular long-range ferromagnetic interaction is even more problematic, mainly due to the factors that governs the crystal packing, which are extremely subtle and hard to control.

For example, one of the first molecular-based ferromagnets driven by this rational design was the compound $\{MnCu(pbaOH)(H_2O)_3\}_n$ shown in Figure 1.28. It is made up of an alternating arrangement of Mn(II) and Cu(II) metal ions connected through the pbaOH ligand [pbaOH = 2-hydroxy-1,3-propylenebis(oxamato)] to constitute a ferrimagnetic chain. This is possible due to the antiferromagnetic interactions between the $S = 5/2$ and $S = 1/2$ spins from Mn(II) and Cu(II), respectively. This chains are assembled within the crystal lattice in a way that ferromagnetic fashion is favoured at $T_C = 4.1$ K and thus a soft hysteresis loop can be measured. However, it is remarkable how a similar compound, $\{MnCu(pba)(H_2O)_3 \cdot 2H_2O\}_n$ [pba = 1,3-propylenebis(oxamato)], undergoes antiferromagnetic interactions between chains with such small modification on the starting material (Figure 1.28). The contrast between the magnetic behaviours is explained with the differences in the crystal packing that both compounds present.[30]

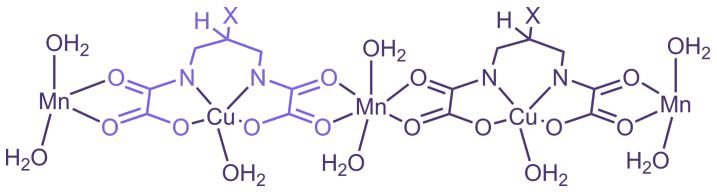

Figure 1.28: Schematic structural representation of $\{MnCu(pbaX)(H_2O)_3\}_n$ (X = H in pba and X = OH in pbaOH) chain. The pbaX structure has been highlighted.

With time, this area of new magnets design from its molecular perspective became relevant, and thus this new field of research named Molecular Magnetism was born, where the structural and magnetic properties of a great number of magnetically ordered molecular systems were described. All this research lead to a better comprehension of the mechanisms involved in the magnetic exchange between metal centres, together with the origins of the magnetism from the chemical nature of molecules. Nonetheless, the data was mainly related to the use of $3d$ metal ions.[1,7] Nowadays, the use of $4d$, $5d$ and specially $4f$ metal ions are being more explored.[10]

Nevertheless, the size reduction of a system to a molecular point may have important consequences on the hysteresis loop. In general terms, the size of the domains are at a nanoscale, therefore molecules below that size will not form domain walls and the magnetisation in each particle will become of a single magnetic domain. These types of systems are called superparamagnets. Furthermore, if the supermagnetic entities are isolated no hysteresis effect is possible by long-range interactions. However, in those supermagnets that present a slow enough relaxation of the magnetisation

an hysteresis effect emerges. This is reminiscent of the ferro- and ferrimagnetic behaviour, but this time without long-range interactions between the spin carriers, this hysteresis is purely at a molecular level. Nonetheless, the magnetic hysteresis exhibited by those systems have a particular characteristic, in those critical values of the field where the quantum tunnelling mechanism is favoured, the relaxation of the magnetisation is faster, and as consequence, the hysteresis loop presents a distinct staircase shape instead of being a smooth curve. A graphic example of an hysteresis loop of this type of systems is shown in Figure 1.29a.

As a result, those molecules that present a slow enough relaxation of the magnetisation to behave as magnets are called Single-Molecular Magnets (SMMs). The first SMM reported was the $[Mn_{12}O_{12}(O_2CCH_3)_{16}(H_2O)_4] \cdot 4H_2O \cdot 2CH_3COOH$ shown in Figure 1.29b. It consists of an inner centre made up of four Mn^{IV} ions with $S = 3/2$, arranged in antiparallel fashion to the external eight Mn^{III} ions with $S = 2$. The ferrimagnetic exchange results in a ground state of collective spins with $S = 10$.[31–33]

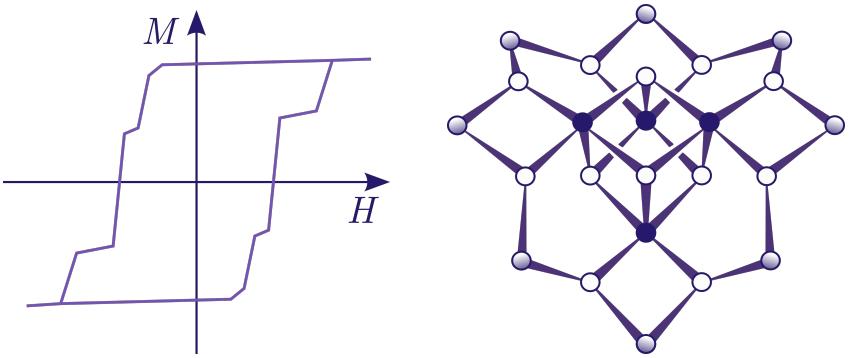

(a) **(b)**

Figure 1.29: (a) Magnetisation *vs.* applied magnetic field of a superparamagnet exhibiting an hysteresis effect. The vertical parts between the 'steps' correspond to the values of the field where the QTM is favoured and the relaxation faster than the measuring time. (b) Schematic drawing of the $\left[Mn_4^{IV}Mn_8^{III}(\mu\text{-}O)_{12}\right]^{16+}$ entity within the $[Mn_{12}O_{12}(O_2CCH_3)_{16}(H_2O)_4] \cdot 4H_2O \cdot 2CH_3COOH$ complex. The relative positions of Mn^{IV} are indicated by solid coloured circles, Mn^{III} by shade coloured circles, and μ_3-O^{2-} bridges by white circles.

Nevertheless, the slow relaxation of the magnetisation is not a behaviour exclusively exhibited by SMMs, systems that consist only of one paramagnetic centre or one-dimensional systems may also present this characteristic behaviour, hence they are called Single-Ion Magnets (SIMs) and Single-Chain Magnets (SCMs), respectively.

1.7 References

(1) Kahn, O. *Molecular magnetism*; VCH Publishers, Inc.: New York, USA: 1993.

(2) Ferrando-Soria, J.; Vallejo, J.; Castellano, M.; Martínez-Lillo, J.; Pardo, E.; Cano, J.; Castro, I.; Lloret, F.; Ruiz-García, R.; Julve, M. *Coord. Chem. Rev.* **2017**, *339*, 17–103.

(3) Carlin, R. L. *Magnetochemistry*; Springer-Verlag: Berlin, Germany: 1986.

(4) Blundell, S. *Magnetism in condensed matter*; Oxford University Press: New York, USA: 2001.

(5) Mabbs, F.; Machin, D. *Magnetism and transition metal complexes*; Chapman and Hall: London, UK: 1973.

(6) Earnshaw, A. *Introduction to magnetochemistry*; Academic Press INC.; New York, USA: 1968.

(7) Gatteschi, D. *Molecular nanomagnets*; Oxford University Press: Oxford, UK: 2008.

(8) Figgis, B. N.; Hitchman, M. A. *Ligand field theory and its applications*; Wiley-VCH: New York, USA: 2000.

(9) Griffith, J. S. *The theory of transition-metal ions*; University Press: Cambridge,UK: 1964.

(10) Benelli, C.; Gatteschi, D. *Introduction to Molecular Magnetism: From Transition Metals to Lanthanides*; Wiley-VCH Verlag GmbH & Co. KGaA: Weinheim, Germany: 2015.

(11) Trabesinger, A. *Nat. Phys.* **2017**, *13*, 716.

(12) Landee, C. P.; Turnbull, M. M.; Landee, C. P.; Turnbull, M. M. *J. Coord. Chem.* **2014**, *67*, 375–439.

(13) Quickenden, T. I.; Marshall, R. C. *J. Chem. Educ.* **1972**, *49*, 114.

(14) Bain, G. A.; Berry, J. F. *J. Chem. Educ.* **2008**, *85*, 532.

(15) Toth, J.; Bole, S. T. *IEEE TAS* **2018**, *28*, 1–4.

(16) Finlay, C. C. et al. *Geophys. J. Int.* **2010**, *183*, 1216–1230.

(17) Hoppeé, J. I. *J. Chem. Educ.* **1972**, *49*, 505.

(18) Bonner, J. C.; Fisher, M. E. *Phys. Rev.* **1964**, *135*, A640–A658.

(19) Baker, G. A.; Rushbrooke, G. S.; Gilbert, H. E. *Phys. Rev.* **1964**, *135*, A1272–A1277.

(20) Casimir, H.; du Pré, F. *Physica* **1938**, *5*, 507–511.

(21) Debye, P. *Polar Molecules*; Dover: New York, USA: 1929.

(22) Topping, C. V.; Blundell, S. J. *J. Condens. Matter Phys.* **2018**, *31*, 013001.

(23) Cole, K. S.; Cole, R. H. *J. Chem. Phys.* **1941**, *9*, 341–351.

(24) Zorn, R. *J. Chem. Phys.* **2002**, *116*, 3204–3209.

(25) Zabala-Lekuona, A.; Seco, J. M.; Colacio, E. *Coord. Chem. Rev.* **2021**, *441*, 213984.

(26) Aravena, D.; Ruiz, E. *Dalton Trans.* **2020**, *49*, 9916–9928.

(27) Boča, R.; Rajnák, C. *Coord. Chem. Rev.* **2021**, *430*, 213657.

(28) Castro-Alvarez, A.; Gil, Y.; Llanos, L.; Aravena, D. *Inorg. Chem. Front.* **2020**, *7*, 2478–2486.

(29) Orbach, R. : Bleaney, B. *Proc. R. Soc. A* **1961**, *264*, 458–484.

(30) Kahn, O.; Pei, Y.; Verdaguer, M.; Renard, J. P.; Sletten, J. *J. Am. Chem. Soc.* **1988**, *110*, 782–789.

(31) Caneschi, A.; Gatteschi, D.; Sessoli, R.; Barra, A. L.; Brunel, L. C.; Guillot, M. *J. Am. Chem. Soc.* **1991**, *113*, 5873–5874.

(32) Sessoli, R.; Gatteschi, D.; Caneschi, A.; Novak, M. A. *Nature* **1993**, *365*, 141–143.

(33) Thomas, L.; Lionti, F.; Ballou, R.; Gatteschi, D.; Sessoli, R.; Barbara, B. *Nature* **1996**, *383*, 145–147.

CHAPTER 2

RHENIUM

2.1 Theoretical magnetic model for a d^3 ion system

A free transition metal ion completely isolated in space presents five degenerate d orbitals. The first Hund's rule states that the lowest energy level has the maximum spin multiplicity. Following the second Hund's rule, the term with the largest value of L has the lowest energy, for a given spin multiplicity. Therefore, the energy term for the ground state of an atom is defined first by the highest values of S and secondly by the highest value of L. For a d^3 system as Re(IV), three unpaired electrons will give rise to a $M_S = 3/2$, hence, a $S = 3/2$ and spin multiplicity of 4. On the other hand, the highest value of L for this spin multiplicity is achieved when the electrons are distributed as shown in Figure 2.1, where a value of M_L equal to 3 implies the existence of a total angular momentum of 3. Therefore, the fundamental term defined as ${}^{2S+1}L$, for a d^3 free ion must be ^{4}F from a Russell-Saunders perspective.

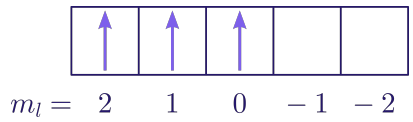

Figure 2.1: Ground state for a d^3 electronic configuration following the Hund's rules. As the total value of the z-component of the angular momentum for all atoms is $M_L = 3$, it must exist a $L = 3$ with $M_L = 3, 2, 1, 0, -1, -2, -3$ components. Same reasoning for the total spin value. Note how the notation in lowercase letters, m_l, is used for single-electrons and capital letters for polyelectronic terms, M_L.

To this model of a free metal ion absolutely isolated, the perturbation due to the ligands will be the next energy to consider, and after it, the effect of the spin-orbit coupling will be evaluated. Under an octahedral (O_h) symmetry as depicted in Figure 2.2a, the group theory suggests that the ^{4}F term will split as presented in Figure 2.2b.

Nevertheless, in order to know the energy order between the different levels it is necessary to conduct theoretical calculations. To this regard, the energy calculation over the d orbitals under an O_h symmetry can be demonstrated to result into two levels, t_{2g} and e_g, separated by an energy gap of $10Dq$ as shown in Figure 2.3a. In this way, it is possible to relate the energy of each strong ligand field electronic configuration (Figure 2.3b to 2.3d) with its corresponding energy level in weaker ligand fields.

The ground term ^{4}F has associated 28 wave-functions, but in order to evaluate the spin-orbit coupling and later the Zeeman, only the L, S, M_L and M_S numbers will be necessary. Nevertheless, the values of L and S remain constant for every wave-function inside a term, thus they can be abbreviated as $|M_L, M_S\rangle$. The only wave-functions to consider are the corresponding to the ground state ${}^4\mathrm{A}_{2\mathrm{g}}$ and the

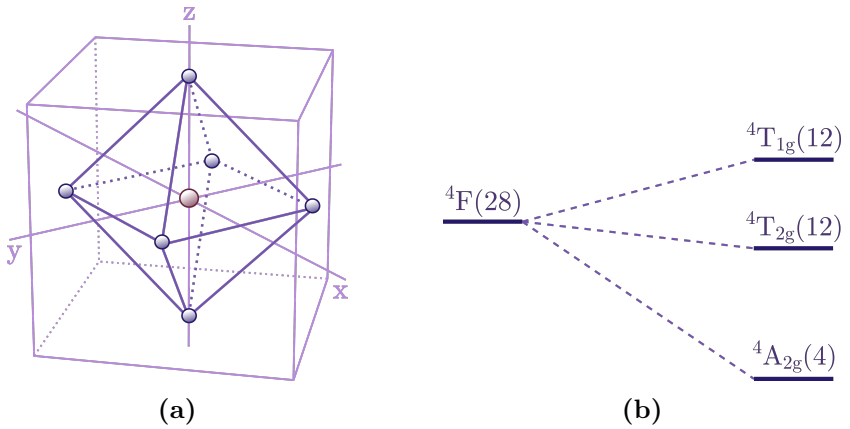

Figure 2.2: (a) Octahedral environment with the transition metal placed at the centre and the ligands at the vertex of the octahedron that they form. (b) Energy diagram for a ^{4}F term in a O_h symmetry. The numbers in parenthesis indicate the total degeneracy.

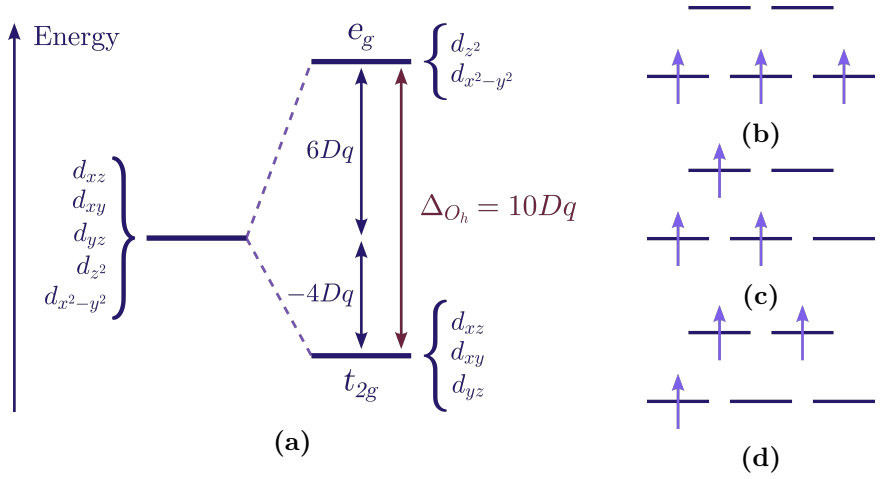

Figure 2.3: (a) Energy diagram of the d orbitals under an O_h symmetry. Δ_{O_h} stands for energy value between the two levels. Different electronic configurations for a d^3 under an O_h symmetry for (b) ground state with a ^{4}A$_{2g}$ term, (c) first exited with a ^{4}T$_{2g}$ and ^{4}T$_{1g}$ term, and (d) Second exited state with a ^{4}T$_{1g}$ term.

most near exited state ^{4}T$_{2g}$, summarised in Table 2.1. The other exited states are considered to be too high in energy and their levels immensely depopulated, thus their contribution will be neglected. All wave-functions have been calculated to be linear combinations adapted to the symmetry of the system, hence they are orthogonal between them. Furthermore, the functions are also normalised.

The next step is to calculate the first-order spin-orbit coupling energies for the ground state. From the perturbation theory perspective, all the elements belonging to the secular determinant must be evaluated with the spin-orbit operator introduced previously in (1.60). The resulting secular determinant is presented in (2.1). As all the elements outside the diagonal are zero, the first-order energies for each level are easily match by (1.35). However, the first-order energy corrections for all the components of the level are equal to zero. As an example, the evaluation of one of the elements of the matrix for ψ_1 is shown in (2.2), being the result zero. This was the expected outcome because the ^{4}A$_{2g}$ term has no orbit contribution, $L = 0$, and therefore there is nothing to coupling the spin with. The same conclusion is made

Table 2.1: O_h symmetry adapted wave-functions for $^4A_{2g}$ and $^4T_{2g}$ terms from a d^3 system.

Term	ψ_i	
$^4A_{2g}$	1	$\frac{1}{\sqrt{2}}\{\|2,3/2\rangle - \|-2,3/2\rangle\}$
	2	$\frac{1}{\sqrt{2}}\{\|2,1/2\rangle - \|-2,1/2\rangle\}$
	3	$\frac{1}{\sqrt{2}}\{\|2,-1/2\rangle - \|-2,-1/2\rangle\}$
	4	$\frac{1}{\sqrt{2}}\{\|2,-3/2\rangle - \|-2,-3/2\rangle\}$
$^4T_{2g}$	5	$-\frac{1}{\sqrt{8}}\left\{\sqrt{3}\,\|-3,3/2\rangle - \sqrt{5}\,\|1,3/2\rangle\right\}$
	6	$-\frac{1}{\sqrt{8}}\left\{\sqrt{3}\,\|-3,1/2\rangle - \sqrt{5}\,\|1,1/2\rangle\right\}$
	7	$-\frac{1}{\sqrt{8}}\left\{\sqrt{3}\,\|-3,-1/2\rangle - \sqrt{5}\,\|1,-1/2\rangle\right\}$
	8	$-\frac{1}{\sqrt{8}}\left\{\sqrt{3}\,\|-3,-3/2\rangle - \sqrt{5}\,\|1,-3/2\rangle\right\}$
	9	$-\frac{1}{\sqrt{8}}\left\{\sqrt{3}\,\|3,3/2\rangle - \sqrt{5}\,\|-1,3/2\rangle\right\}$
	10	$-\frac{1}{\sqrt{8}}\left\{\sqrt{3}\,\|3,1/2\rangle - \sqrt{5}\,\|-1,1/2\rangle\right\}$
	11	$-\frac{1}{\sqrt{8}}\left\{\sqrt{3}\,\|3,-1/2\rangle - \sqrt{5}\,\|-1,-1/2\rangle\right\}$
	12	$-\frac{1}{\sqrt{8}}\left\{\sqrt{3}\,\|3,-3/2\rangle - \sqrt{5}\,\|-1,-3/2\rangle\right\}$
	13	$\frac{1}{\sqrt{2}}\{\|2,3/2\rangle + \|-2,3/2\rangle\}$
	14	$\frac{1}{\sqrt{2}}\{\|2,1/2\rangle + \|-2,1/2\rangle\}$
	15	$\frac{1}{\sqrt{2}}\{\|2,-1/2\rangle + \|-2,-1/2\rangle\}$
	16	$\frac{1}{\sqrt{2}}\{\|2,-3/2\rangle + \|-2,-3/2\rangle\}$

for the diagonal elements from ψ_2, ψ_3 and ψ_4 wave-functions. This fact proves that a d^3 ion placed in an octahedral environment has not first-order spin-orbit coupling.

$$\begin{vmatrix} \widehat{\mathcal{H}}_{SOC} & |\psi_1\rangle & |\psi_2\rangle & |\psi_3\rangle & |\psi_4\rangle \\ \langle\psi_1| & 0-E & 0 & 0 & 0 \\ \langle\psi_2| & 0 & 0-E & 0 & 0 \\ \langle\psi_3| & 0 & 0 & 0-E & 0 \\ \langle\psi_4| & 0 & 0 & 0 & 0-E \end{vmatrix} = 0 \tag{2.1}$$

$$E_1^{(1)} = H_{11} = \left\langle \psi_1 \middle| \lambda \widehat{L}\widehat{S} \middle| \psi_1 \right\rangle = 3\lambda \langle \psi_1 | \psi_{13} \rangle - \lambda\sqrt{6} \langle \psi_1 | \psi_{10} \rangle = 0 \tag{2.2}$$

Nevertheless, the first-order spin-orbit calculation for ψ_1 revealed two functions belonging to the first exited $^4T_{2g}$ term (ψ_{13} and ψ_{10}), which means that there must exist a little percentage of mixing of these functions with ψ_1 by second-order spin-orbit coupling. The second-order energy is calculated through expression (1.37).

Following the former example, the energy of second-order perturbation for ψ_1 is

$$E_1^{(2)} = \frac{\left\langle \psi_{13} \middle| \lambda \widehat{L}\widehat{S} \middle| \psi_1 \right\rangle^2}{0 - 10Dq} + \frac{\left\langle \psi_{10} \middle| \lambda \widehat{L}\widehat{S} \middle| \psi_1 \right\rangle^2}{0 - 10Dq} = \frac{-15\lambda^2}{10Dq} \tag{2.3}$$

Similarly, the calculations for ψ_2, ψ_3 and ψ_4 lend to the same results. Thus, after mixing with the functions of the excited term, the ground state keeps degenerated and there is no ZFS as is expected for a regular octahedron considered an isotropic system. The effect of the spin-orbit coupling is as shown in Figure 2.4.

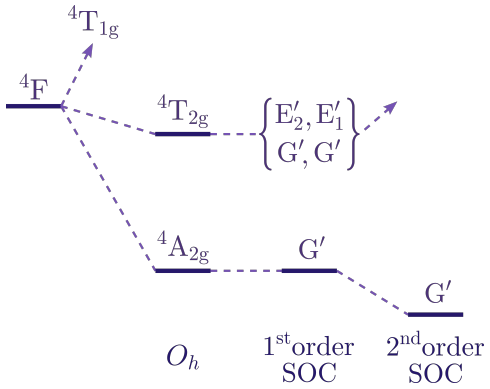

Figure 2.4: First- and second-order spin-orbit coupling for a d^3 system under O_h symmetry. In order to simplify, only the ground state is properly indicated.

To conclude, the new wave-functions are calculated as linear combinations like the perturbation theory suggest in equation (1.38). The functions corresponding to the $^4A_{2g}$ term are presented in (2.4).

$$\begin{cases} \phi_1 = \psi_1 - \dfrac{3\lambda}{10Dq}\psi_{13} + \dfrac{\sqrt{6}\lambda}{10Dq}\psi_{10} \\ \phi_2 = \psi_2 - \dfrac{\lambda}{10Dq}\psi_{14} + \dfrac{\sqrt{8}\lambda}{10Dq}\psi_{11} - \dfrac{\sqrt{6}\lambda}{10Dq}\psi_5 \\ \phi_3 = \psi_3 + \dfrac{\lambda}{10Dq}\psi_{15} + \dfrac{\sqrt{6}\lambda}{10Dq}\psi_{12} - \dfrac{\sqrt{8}\lambda}{10Dq}\psi_6 \\ \phi_4 = \psi_4 + \dfrac{3\lambda}{10Dq}\psi_{16} - \dfrac{\sqrt{6}\lambda}{10Dq}\psi_7 \end{cases} \tag{2.4}$$

In order to study the magnetic properties, the Zeeman operator for isotropic systems described in equation (1.24) must be applied to the new determined system, where the g value was taken as 2 for simplifying the calculations. This is always possible as long as the next perturbation is smaller than the previous one. As there are only non-zero members in the diagonal of the secular determinant (2.5), the first-order energy for each level is easy related by (1.35). As an example, the first-order correction energy for ϕ_1 can be found in (2.6), where as the ligand field is greater than the spin-orbit coupling in this model, the a^2 terms are approximated to 0. Moreover, it is convenient to define a new g as $g = 2\left(1 - \frac{4\lambda}{10Dq}\right)$. In this way, the energy levels are defined by the possible M_S spin states of the metal ion, multiply by

the magnetic moment of the electron, a constant g particular for each system, and the applied magnetic field. These results clearly show how in presence of a magnetic field, the ground state splits into four different energy levels by first-order Zeeman effects.

$$\begin{array}{c|cccc|} \widehat{\mathcal{H}}_Z & |\phi_1\rangle & |\phi_2\rangle & |\phi_3\rangle & |\phi_4\rangle \\ \hline \langle\phi_1| & \frac{3}{2}g\mu_B H - E & 0 & 0 & 0 \\ \langle\phi_2| & 0 & \frac{1}{2}g\mu_B H - E & 0 & 0 \\ \langle\phi_3| & 0 & 0 & -\frac{1}{2}g\mu_B H - E & 0 \\ \langle\phi_4| & 0 & 0 & 0 & -\frac{3}{2}g\mu_B H - E \\ \hline \end{array} = 0 \tag{2.5}$$

$$\begin{aligned} E_1^{(1)} &= H_{11} = \left\langle \phi_1 \middle| \widehat{\mathcal{H}}_Z \middle| \phi_1 \right\rangle = \\ &= \mu_B H \left[3 - 2a \langle\psi_1|\psi_1\rangle - 2a + 3a^2 \langle\psi_{13}|\psi_{13}\rangle + a^2 \langle\psi_{10}|\psi_{10}\rangle\right] \approx \\ &\approx \frac{3}{2} g\mu_B H; \qquad a = \frac{3\lambda}{10Dq}; \qquad g = 2\left(1 - \frac{4\lambda}{10Dq}\right) \end{aligned} \tag{2.6}$$

In addition, in order to calculate the TIP, it is possible to determine the second-order Zeeman energies as a result of the interaction between the components from the ground state with the components from excited terms. Nevertheless, an approximation will be made for simplification. Considering that the spin-orbit interaction is much less energetic than the ligand field, the difference between the ground state and the first exited term can be approximated to $10Dq$. Moreover, the new set of wavefunctions of the ground state obtained after the second-order spin-orbit coupling will be approximated to the zero-order ones, that is $\phi_i \approx \psi_i$. Thus, the second-order Zeeman interaction will easily lead to (2.7) for ψ_1, with same results for ψ_2, ψ_3 and ψ_4.

$$E_1^{(2)} = \frac{\left\langle \psi_{13} \middle| \mu_B H \left(\widehat{L}_z + g\widehat{S}_z\right) \middle| \psi_1 \right\rangle^2}{0 - 10Dq} = \frac{-4{\mu_B}^2 H^2}{10Dq} \tag{2.7}$$

A summary of the magnetic energy corrections is found in Table 2.2, where the zero was chosen for the previously determined second-order spin-orbit energy, which it is shared by all the functions belonging to the ground state. Besides, the magnetic interaction has been incorporated to the energy diagram in Figure 2.5.

Table 2.2: First and second Zeeman coefficients for a d^3 ion under an octahedral symmetry.

ϕ_i	$E_i^{(0)}$	$E_i{}'/\mu_B$	$E_i{}''/{\mu_B}^2$
1	0	$\frac{3}{2}g$	$-\frac{4}{10Dq}$
2	0	$\frac{1}{2}g$	$-\frac{4}{10Dq}$
3	0	$-\frac{1}{2}g$	$-\frac{4}{10Dq}$
4	0	$-\frac{3}{2}g$	$-\frac{4}{10Dq}$

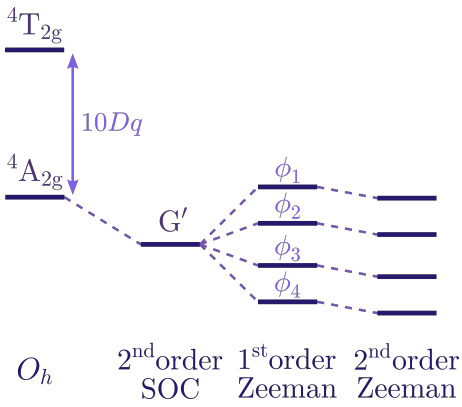

Figure 2.5: The splitting diagram for a $^4A_{2g}$ ground term under the action of spin-orbit coupling and a magnetic field. The first-order spin-orbit coupling was omitted as it has no effect. The energy diagram is not at scale.

Finally, introducing the values from Table 2.2 into the Van Vleck formula (1.45), it is found that the molar susceptibility is as expressed in equation (2.8). The susceptibility will be correct for either crystal or powder samples, due to the isotropy of the system.

$$\chi_M = \frac{5N_A{\mu_B}^2g^2}{4k_BT} + \text{TIP}; \qquad \text{TIP} = \frac{8N_A{\mu_B}^2}{10Dq} \tag{2.8}$$

Nevertheless, real systems often present distortions from the regular octahedral geometry. Therefore, the former model has very restricted applications. In general, the most common distortion involve tetragonal distortion in Re(IV) complexes. As consequence, the symmetry is lowered from O_h to D_{4h} if both axial ligands are of the same nature, if not the C_{4v} symmetry will be used instead. This change leads to a new energy diagram represented in Figure 2.6. The wave-functions are redistributed in the new terms, those belonging to the $^4A_{2g}$ are now under the $^4B_{1g}$ label. On the other hand, ψ_5 to ψ_{12} and ψ_{13} to ψ_{16} from Table 2.1 are now under the ^4E_g and $^4B_{2g}$ terms, respectively.

When the spin-orbit Hamiltonian is applied over the four wave-functions belonging to the ground state, the first-order coupling energies are still zero. In fact, as the four wave-functions for $^4B_{1g}$ are the same as for $^4A_{2g}$ term, the calculations are identical to the previously performed, and the constructed secular determinant is as in (2.1). Therefore, there is no effect by first-order coupling in a tetragonally distorted octahedron either. Nonetheless, as the symmetry is now lowered, the second-order coupling results in the splitting of the ground level of the system. Furthermore, as the ground and exited terms have an even number of spin multiplicity, the axial distortion combined with the spin-orbit effect will split all the levels into Kramer doublets. The calculation of the second-order energies are found in equations (2.9) and (2.10), for ψ_1 and ψ_2, respectively. Besides, this information is represented in Figure 2.6.

$$E_1^{(2)} = \frac{\left\langle \psi_{13} \middle| \lambda\widehat{L}\widehat{S} \middle| \psi_1 \right\rangle^2}{0-\Delta_1} + \frac{\left\langle \psi_{10} \middle| \lambda\widehat{L}\widehat{S} \middle| \psi_1 \right\rangle^2}{0-\Delta_2} = -\frac{9\lambda^2}{\Delta_1} - \frac{6\lambda^2}{\Delta_2} \tag{2.9}$$

$$E_2^{(2)} = \frac{\left\langle \psi_{14} \middle| \lambda \widehat{L}\widehat{S} \middle| \psi_2 \right\rangle^2}{0-\Delta_1} + \frac{\left\langle \psi_{11} \middle| \lambda \widehat{L}\widehat{S} \middle| \psi_2 \right\rangle^2}{0-\Delta_2} + \frac{\left\langle \psi_5 \middle| \lambda \widehat{L}\widehat{S} \middle| \psi_2 \right\rangle^2}{0-\Delta_2} = -\frac{\lambda^2}{\Delta_1} - \frac{14\lambda^2}{\Delta_2} \tag{2.10}$$

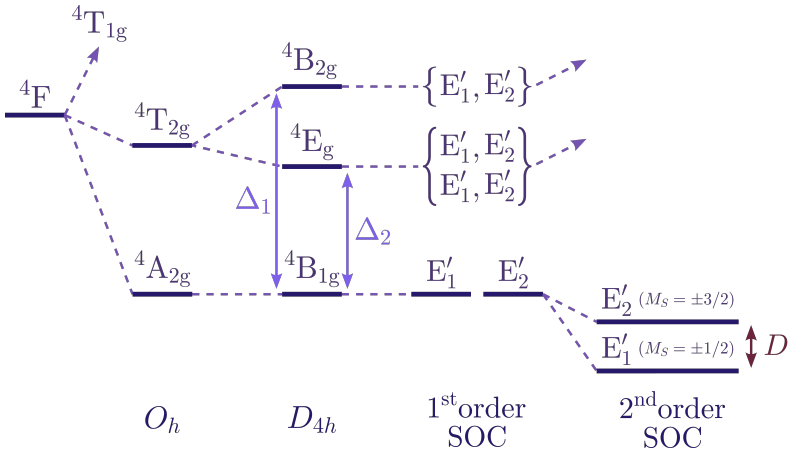

Figure 2.6: Energy diagram for a ^{4}F term under O_h and D_{4h} symmetries. The symbol of parity 'g' will drop for the C_{4v} symmetry.[1] The first- and second-order spin-orbit couplings are also depicted, and the ZFS confirmed for the second-order interaction.

The new wave-functions obtained for the ground state after applying the spin-orbit Hamiltonian are calculated through (1.38) and are summarised in (2.11).

$$\begin{cases} \phi_1 = \psi_1 - \dfrac{3\lambda}{\Delta_1}\psi_{13} + \dfrac{\sqrt{6}\lambda}{\Delta_2}\psi_{10} \\ \phi_2 = \psi_2 - \dfrac{\lambda}{\Delta_1}\psi_{14} + \dfrac{\sqrt{8}\lambda}{\Delta_2}\psi_{11} - \dfrac{\sqrt{6}\lambda}{\Delta_2}\psi_5 \\ \phi_3 = \psi_3 + \dfrac{\lambda}{\Delta_1}\psi_{15} + \dfrac{\sqrt{6}\lambda}{\Delta_2}\psi_{12} - \dfrac{\sqrt{8}\lambda}{\Delta_2}\psi_6 \\ \phi_4 = \psi_4 + \dfrac{3\lambda}{\Delta_1}\psi_{16} - \dfrac{\sqrt{6}\lambda}{\Delta_2}\psi_7 \end{cases} \tag{2.11}$$

The Kramer doublets are formed by ϕ_1 with ϕ_4, and ϕ_2 with ϕ_3. Hence, $E_1^{(2)} = E_4^{(2)}$ and $E_2^{(2)} = E_3^{(2)}$. The energy difference between Kramer doublets gives the value of the ZFS to be $D = 8\lambda^2\left(\frac{1}{\Delta_2} - \frac{1}{\Delta_1}\right)$. From this result it can be deduced that if $\Delta_1 = \Delta_2$, there is no splitting and the system behave isotropically. Moreover, a higher value of λ translates as a higher splitting between levels. In the present notation, positive D values stabilize the $\pm 1/2$ states, whereas a negative value stabilizes the $\pm 3/2$ states.

The next step will be to apply the Zeeman operator. However, this time the system is anisotropic with $x = y \neq z$, which means that expression (1.23) is split between the z-direction, from now on also called the 'parallel component' presented in equation (2.12), and the x- and y-directions, from now on also named as the 'perpendicular component'. As $\widehat{L}_x$ and $\widehat{L}_y$ are not defined, it is necessary to use

again the ladders operators modifying the Zeeman operator as shown in equation (2.13). To simplify the calculations the g values will be taken as 2.

$$\widehat{\mathcal{H}}_{Z,\parallel} = \mu_B H_\parallel \left(\widehat{L}_z + g\widehat{S}_z\right) \tag{2.12}$$

$$\begin{aligned}\widehat{\mathcal{H}}_{Z,\perp} &= \mu_B H_\perp \left(\widehat{L}_x + g\widehat{S}_x + \widehat{L}_y + g\widehat{S}_y\right) \\ &= \frac{\mu_B H_\perp}{2}\left(\widehat{L}_+ + \widehat{L}_- + g\widehat{S}_- + g\widehat{S}_+\right)\end{aligned} \tag{2.13}$$

The secular determinants for the parallel component are presented in (2.14) and (2.15) for the two Kramer doublets. As in the octahedral case, the terms with λ^2/Δ^2 are approximated to 0, and a new g is defined as $g_\parallel = 2\left(1 - \frac{4\lambda}{\Delta_1}\right)$. It can be seen how both doublets break their degeneracy under a magnetic field in the z-direction, but they do not mix between them. The first-order energy for ϕ_1 is shown in (2.16) as an example of calculation for the parallel component.

$$\begin{vmatrix} \widehat{\mathcal{H}}_{Z,\parallel} & |\phi_1\rangle & |\phi_4\rangle \\ \hline \langle\phi_1| & \frac{3}{2}g_\parallel\mu_B H_\parallel - E & 0 \\ \langle\phi_4| & 0 & -\frac{3}{2}g_\parallel\mu_B H_\parallel - E \end{vmatrix} = 0 \tag{2.14}$$

$$\begin{vmatrix} \widehat{\mathcal{H}}_{Z,\parallel} & |\phi_2\rangle & |\phi_3\rangle \\ \hline \langle\phi_2| & \frac{1}{2}g_\parallel\mu_B H_\parallel - E & 0 \\ \langle\phi_3| & 0 & -\frac{1}{2}g_\parallel\mu_B H_\parallel - E \end{vmatrix} = 0 \tag{2.15}$$

$$\begin{aligned} E_1^{(1)} = H_{11} &= \left\langle \phi_1 \middle| \widehat{\mathcal{H}}_{Z,\parallel} \middle| \phi_1 \right\rangle = \\ &= \mu_B H_\parallel \left[3 - 2a\langle\psi_1|\psi_1\rangle - 2a + 3a^2\langle\psi_{13}|\psi_{13}\rangle + b^2\langle\psi_{10}|\psi_{10}\rangle\right] \approx \\ &\approx \frac{3}{2}g_\parallel\mu_B H_\parallel; \qquad a = \frac{3\lambda}{\Delta_1}; \qquad b = \frac{3\lambda}{\Delta_2}; \qquad g_\parallel = 2\left(1 - \frac{4\lambda}{\Delta_1}\right) \end{aligned} \tag{2.16}$$

Second-order energy corrections between doublets are in order since they are just separated by an energy gap of D. Nevertheless, they can be easily predicted as zero because after the application of the parallel Zeeman operator over the ψ_i functions belonging to the ϕ_1 and ϕ_4 Kramer doublet, all wave-functions will remain the same, and as any of them form part of ϕ_2 and ϕ_3, the calculated energies will result to be zero in the case of the parallel component.

Further second-order corrections with components from excited terms can be made. As in the octahedral case, some approximations will take place. This time, the energy separation between the ground and excited state for the parallel component will be Δ_1, neglecting the second-order spin-orbit energy correction. Likewise, $\phi_i \approx \psi_i$. Thus, calculations reveal that second-order Zeeman effects on the parallel component of the magnetic field will have the same result on the four wave-functions of the ground state, being $E_i^{(2)} = \frac{-4{\mu_B}^2 H_\parallel^2}{\Delta_1}$.

In order to determine the susceptibility, it is necessary to take into account the previous energy values of the spin-orbit coupling. The zero of energy before applying

the magnetic field is taken for the $M_S = \pm 1/2$ Kramer doublet state ($E_{2,3}^{(0)} = 0$), while the $M_S = \pm 3/2$ will be at a initial distance of D ($E_{1,4}^{(0)} = D$). This information along with the first- and second-order magnetic energy corrections is summarised in Table 2.3.

Table 2.3: First and second Zeeman coefficients for a d^3 ion under a tetragonal distorted octahedral symmetry in the parallel component.

ϕ_i	$E_i^{(0)}$	E_i'/μ_B	[a] $E_i''/{\mu_B}^2$
1	D	$\frac{3}{2}g_\parallel$	$-\frac{4}{\Delta_1}$
2	0	$\frac{1}{2}g_\parallel$	$-\frac{4}{\Delta_1}$
3	0	$-\frac{1}{2}g_\parallel$	$-\frac{4}{\Delta_1}$
4	D	$-\frac{3}{2}g_\parallel$	$-\frac{4}{\Delta_1}$

[a] Approximated second-order magnetic interactions arising from functions belonging to excited terms (see text).

Thus, the parallel component of the susceptibility calculated by Van Vleck formula leads to (2.17).

$$\begin{gathered}\chi_z = \chi_\parallel = \frac{N_A {g_\parallel}^2 {\mu_B}^2}{4k_BT}\,\frac{1+9\exp(-x)}{1+\exp(-x)} + \mathrm{TIP}_\parallel;\\ x = \frac{D}{k_BT};\quad g_\parallel = 2\left(1-\frac{4\lambda}{\Delta_1}\right);\qquad \mathrm{TIP}_\parallel = \frac{8N_A{\mu_B}^2}{\Delta_1}\end{gathered} \tag{2.17}$$

Similarly, the first- and second-order Zeeman interactions can be calculated for the perpendicular component. This time, the first-order magnetic interaction has no effect on $M_S = \pm 1/2$ components, thus $E_1^{(1)} = E_4^{(1)} = 0$, whilst it mixes the functions belonging to the $M_S = \pm 3/2$ Kramer doublet. Their respective secular determinants are found in (2.18). The new g is defined as $g_\perp = 2\left(1-\frac{4\lambda}{\Delta_2}\right)$. On the other hand, after solving the determinant, $E_2^{(1)}$ and $E_3^{(1)}$ are easily calculated as $g_\perp\mu_B H_\perp$ and $-g_\perp\mu_B H_\perp$, respectively.

$$\begin{array}{c|cc} \widehat{\mathcal{H}}_{Z,\perp} & |\phi_1\rangle & |\phi_4\rangle \\ \hline \langle\phi_1| & 0-E & 0 \\ \langle\phi_4| & 0 & 0-E \end{array} = 0\,; \qquad \begin{array}{c|cc} \widehat{\mathcal{H}}_{Z,\perp} & |\phi_2\rangle & |\phi_3\rangle \\ \hline \langle\phi_2| & 0-E & g_\perp\mu_B H_\perp \\ \langle\phi_3| & g_\perp\mu_B H_\perp & 0-E \end{array} = 0 \tag{2.18}$$

The second-order corrections due to the interaction between the Kramer doublets are found in (2.19) and (2.20) for ϕ_1 and ϕ_2, respectively. For ϕ_3 and ϕ_4 their second-order energies are the same as $E_2^{(2)}$ and $E_1^{(2)}$, respectively.

$$E_1^{(2)} = \frac{\left\langle\phi_2\middle|\widehat{\mathcal{H}}_{Z,\perp}\middle|\phi_1\right\rangle^2}{0-D} = -\frac{3g_\perp^2{\mu_B}^2}{4D}H_\perp^2 \tag{2.19}$$

$$E_2^{(2)} = \frac{\left\langle \phi_1 \middle| \widehat{\mathcal{H}}_{Z,\perp} \middle| \phi_2 \right\rangle^2}{D - 0} = \frac{3g_\perp^2 {\mu_B}^2}{4D} H_\perp^2 \tag{2.20}$$

Further second-order corrections with excited terms can also be made with the same criteria used before. The energy results for the wave-functions belonging to the two Kramer doublets is the same and equal to $E_i^{(2)} = \frac{-4{\mu_B}^2 H_\perp^2}{\Delta_2}$. All the energy corrections are summarised in Table 2.4. If these values are introduced into the Van Vleck formula, it leads to the susceptibility expressed in (2.21).

Table 2.4: First and second Zeeman coefficients for a d^3 ion under a tetragonal distorted octahedral symmetry in the perpendicular component.

ϕ_i	$E_i^{(0)}$	$E_i{}'/\mu_B$	$E_i{}''/{\mu_B}^2$	[a] $E_i{}''/{\mu_B}^2$
1	D	0	$\frac{3g_\perp^2}{4D}$	$-\frac{4}{\Delta_2}$
2	0	$g_\perp$	$-\frac{3g_\perp^2}{4D}$	$-\frac{4}{\Delta_2}$
3	0	$-g_\perp$	$-\frac{3g_\perp^2}{4D}$	$-\frac{4}{\Delta_2}$
4	D	0	$\frac{3g_\perp^2}{4D}$	$-\frac{4}{\Delta_2}$

[a] Approximated second-order magnetic interactions arising from functions belonging to excited terms (see text).

$$\begin{gathered} \chi_x = \chi_y = \chi_\perp = \frac{N_A {g_\perp}^2 {\mu_B}^2}{k_B T} \frac{1 + \frac{3}{2x}\left[1 - \exp\left(-x\right)\right]}{1 + \exp\left(-x\right)} + \mathrm{TIP}_\perp; \\ x = \frac{D}{k_B T}; \quad g_\perp = 2\left(1 - \frac{4\lambda}{\Delta_2}\right); \quad \mathrm{TIP}_\perp = \frac{8 N_A {\mu_B}^2}{\Delta_2} \end{gathered} \tag{2.21}$$

The magnetic susceptibility of a powder sample must be calculated as an average from the parallel and perpendicular components as described in (2.22). A representation of both components with the average susceptibility is shown in Figure 2.7, where the TIP was removed. It is important to note that the variations of χT are not very sensitive to the sign of D. Therefore, it is difficult, if not impossible, to determine unambiguously the correct sign of D from a powder magnetic susceptibility measurement.

$$\chi = \frac{\chi_\parallel + 2\chi_\perp}{3} \tag{2.22}$$

At low temperatures, where $k_B T << |D|$, the average powder magnetic susceptibility can be approximated through (2.23), where it was considered $g = g_\parallel = g_\perp$, and the TIP removed. In this way, for $g = 1.88$, which is a common value for magnetically isolated mononuclear rhenium(IV) compounds with axial distortion, the value of $\chi_M T$ will be of *ca.* 1.0 $\mathrm{cm^3\,mol^{-1}\,K}$ at very low temperatures.

$$\chi_M \approx \frac{3 N_A {\mu_B}^2 g^2}{4 k_B T} \tag{2.23}$$

Alternatively, the ZFS can be treated through the Hamiltonian described in equation (1.66), where the value of E is taken as zero, given that the D_{4h} symmetry

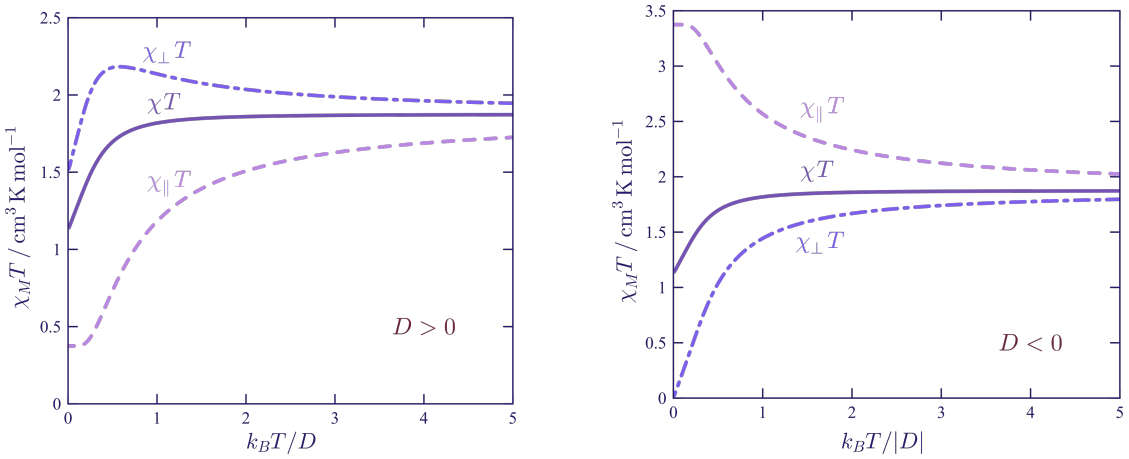

Figure 2.7: χT *vs.* $k_B T/|D|$ representations for a spin quartet term with an axial anisotropy for (a) $D > 0$ (b) $D < 0$. Both $g_\parallel$ and $g_\perp$ are taken equal to 2.00, and the TIP have been removed.

system keeps $x = y$. This calculation of the susceptibility through spin Hamiltonians do not take into account the orbital part, hence, no spin-orbit coupling is considered. Thus, the g parameter is the one modifying its value to adapt to the model. An important remark when using the phenomenological spin Hamiltonian compared to the treatment done herein is in order. Following the energy scheme as depicted in Figure 2.6, the energy difference between Kramer doublets was considered D, whilst is considered $2D$ when equation (1.66) is applied, as shown in (2.24).

$$D\left[\left(\frac{3}{2}\right)^2 - \frac{15}{12}\right] - D\left[\left(\frac{1}{2}\right)^2 - \frac{15}{12}\right] = 2D \tag{2.24}$$

On the other hand, to fit the magnetisation curves of Re(IV) compounds with tetragonal distortion through the Brillouin function presented in (1.52), it is necessary to modify the expression to accommodate the new axial anisotropic factor D.[2] Furthermore, as a noteworthy remark the [$ReCl_4$(bpym)] complex presented on Article 4 exhibits an actual symmetry C_{2v}, which is lower than D_{4h}. For this point group the orbital doublet ^4E_g will split into two orbital singlets $^4B_1$ and $^4B_2$ at energies Δ_x and Δ_y from the ground state $^4B_1$, respectively. This will introduce the rhombic parameter of anisotropy, E, to the system followed by a modification on the energy diagram due to the interaction between $^4B_1$ singlets. Nevertheless, due to the strict equivalence between the x and y axes in the six-coordinated entity, both singlets remain mostly degenerated, that is, $\Delta_x \approx \Delta_y \approx \Delta_2$ and the value of E is considered to have a low value compared to the axial anisotropy.[3]

2.2 Re(IV) coordination chemistry

Rhenium compounds can be present in a wide variety of oxidation states from I to VII. Nevertheless, most of the works found in the literature deals with Re(III), Re(V) or Re(VII) complexes. In comparison, Re(IV) has been more scarcely explored.[4,5] This is manly due to the tendency of Re(IV) against redox processes. The

principal side reaction is the hydrolysis that it undergoes in presence of water on neutral or basic media, which leads the rhenium ion to further oxidation states. As a result, this solvent is normally avoided in the preparation of Re(IV) compounds or metalloligands, which are stable in acidulated aqueous solutions.

One of the advantages of using Re(IV) includes the lack of orbital angular momentum on the ground state, as it was introduced in the previous section. Thus, no first spin-orbit coupling is possible and the magnetic behaviour of Re(IV) species can be fitted with relative ease compared to other elements or oxidation states with first and second spin-orbit effects, like Co(II) systems for instance. Furthermore, the high value of λ, which is *ca.* 1000 cm^{-1}, confers a large magnetic anisotropy by second-order spin-orbit coupling (ZFS) compared to isoelectronic first-row transition metal ions like Cr(III) with λ *ca.* 90 cm^{-1}.[6] Moreover, the magnetic coupling between different paramagnetic centres in polynuclear compounds can be understood due to the larger diffuseness of the 5*d* orbitals, which would increase the overlap between the ligand orbitals increasing the chance of finding the magnetic electron on the ligand atoms. Hence, strengthening the magnetic interactions between different paramagnetic centres compared with analogous first-row systems with more contracted 3*d* orbitals. Thus, the Re(IV) species may have remarkable magnetic properties in both mononuclear and polynuclear systems.

From a structural and synthetic point of view, the hexahalide derivatives $[ReX_6]^{2-}$ (X = Cl and Br) are the simplest Re(IV) species. They are normally prepared by reduction of the perrhenic acid by hypophosphorous acid in concentrated HX media, illustrated by reaction (2.25), the yields being in a 85-90% range.[7] Another analogous synthesis can be carried away with ammonium or potassium $[ReO_4]^{2-}$ salts, but the use of perrhenic acid allows to isolate the hexachloro- or hexabromorhenate(IV) with the cation from the chosen (AX) salt.

$$4HReO_4 + 8AX + 3H_3PO_2 + 16HX \leftrightharpoons 4A_2[ReX_6] + 3H_3PO_4 + 10H_2O \qquad A = NH_4 \text{ or K and X = Cl or Br} \tag{2.25}$$

In contrast, the hexafluoro and hexaiodo derivatives present more complicated procedures. In the case of the hexafluorhenate(IV), it is required the use of strong fluorinating agents as molten bifluoride salts, AHF_2 (A = NH_4 or K) over the previously prepared hexahalohenate(IV) derivatives, where the isolation of the $A_2[ReF_6]$ salt in water demonstrated to be challenging.[8–10] On the other hand, the hexaiodo derivative is prepared by direct reduction of perrhenic acid in concentrated HI media (2.26).[11,12] Nevertheless, hexaiodorhenate(IV) compounds tend to decomposition. Violet vapours can be seen in closed containers where these salts are stored. As a result, only K_2ReI_6 and $(NH_4)_2[ReI_6]$ structures have been determined by single-crystal X-ray diffraction.[11]

$$2HReO_4 + 4KI + 14HI \leftrightharpoons 2K_2ReI_6 + 3I_2 + 8H_2O \tag{2.26}$$

From a magnetism point of view, the behaviours of mononuclear hexahalorhenate(IV) complexes with different diamagnetic cations have been studied since the 60's and it still is an active research field nowadays.[6,10,11,13–21] As a general tendency, the intermolecular interactions between different rhenium entities lead to antiferromagnetic couplings transmitted by contacts between halogen ligands orbitals.

Therefore, its intensity depends on the nature of the halogen ligand and the halogen-halogen distance. However, ferromagnetic interactions can also be found.[14,15] Thus, the use of bulky countercations will increase the Re-X···X-Re distance and decrease the degree of interaction to a point where the different $[ReX_6]^{2-}$ entities are isolated. In this way, the system may display slow relaxation of the magnetisation which is characteristic of the SIM behaviour.

As a representative example of how intermolecular halogen-halogen interactions can change the magnetic properties of hexahalorhenate(IV) salts, $(AsPh_4)_2[ReI_6]$ and $(NH_4)_2[ReI_6]$ are presented in Figures 2.8a and 2.8b, respectively. For $(AsPh_4)_2[ReI_6]$ the $\chi_M T$ values remain nearly constant in a wide range of temperatures and only decrease at low temperatures. In principle, this decrease could be attributed to ZFS effects. On the other hand, $(NH_4)_2[ReI_6]$ exhibits a decrease on the $\chi_M T$ values from room temperature, which is most likely caused by the antiferromagnetic intermolecular interactions as confirmed by the maximum in the χ_M *vs.* T plot at low temperature. Besides, this compound exhibits ZFS effects.

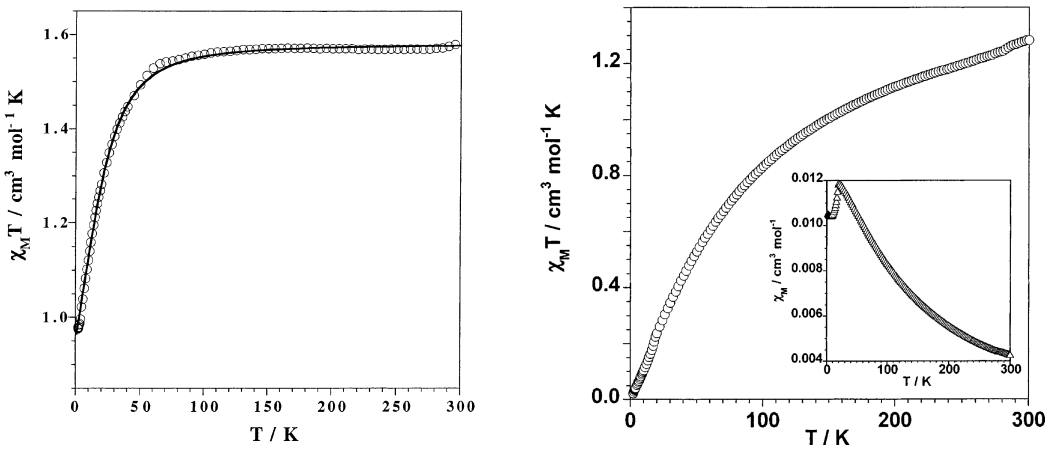

Figure 2.8: $\chi_M T$ *vs.* T curves for (a) $(AsPh_4)_2[ReI_6]$, where (∘) shows the experimental data and (−) the best fit through equation (2.22). (b) $(NH_4)_2[ReI_6]$. The inset shows χ_M *vs.* T plot. Adapted from Ref.[11]

Indeed, it is also possible to prepare salts with paramagnetic cations.[22–27] Furthermore, the use of certain diamagnetic or paramagnetic cations may incorporate to the system new interesting physical properties like electric conductivity[28–30] or luminescence,[31] while conserving the intrinsic magnetic properties associated to Re(IV) compounds. Thus, it can lead to a final product with multifunctional properties. Moreover, the $[ReX_6]^{2-}$ units have also been used as metalloligands towards diamagnetic or paramagnetic transition metal ions. In this regard, only a few one-dimensional and one two-dimensional polymeric structure (Figure 2.9) with their magnetic behaviours described, have been reported.[32–35]

Lastly, hexahalorhenate(IV) species are often used as precursors to synthesise new mononuclear complexes.[5] Nonetheless, the low liability of a $5d^3$ metal ion towards substitution due to the normally high crystal field stabilization energy, makes it necessary to heat at high temperatures to favour the ligands exchange. Besides, because of the easy oxidation of Re(IV), the presence of even small amounts of water in non-aqueous solvents at high temperatures will lead to rhenium species with higher

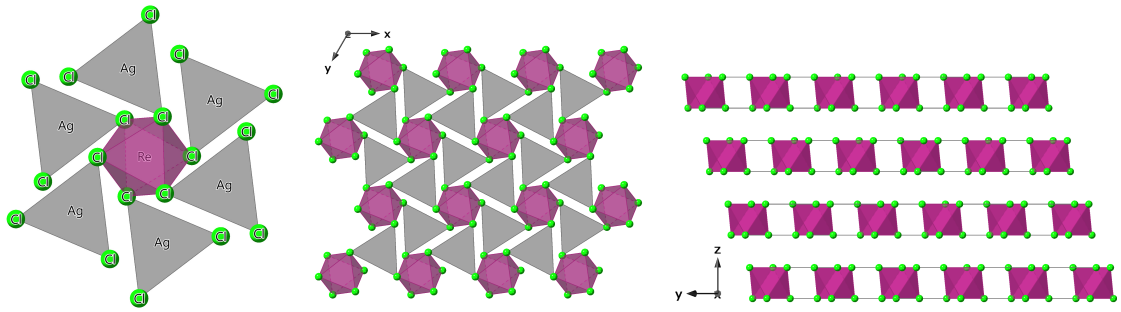

Figure 2.9: Polyhedral views of the coordination polymer of formula $[Ag_2ReCl_6]_n$ (a) Coordination mode of the $[AgCl_3]^{2-}$ units towards the rhenium atom (b) View along the crystallographic z-axis and (c) x-axis of the two-dimensional motifs of $[Ag_2ReCl_6]_n$.

oxidation states. In this respect, dioxygen-free non-aqueous previously dry solvents such as DMF, MeCN, 1- or 2-PrOH are often used together with stoichiometric excess of the incoming ligand to favour the substitutions.

These new compounds normally incorporate ligands with free coordination positions that serve as bridging points towards another metallic centres. Thus, the complex can be used as a ligand to either diamagnetic or paramagnetic ions from the *d*- or *f*-block. The nature of the chosen ligands that act as bridges connecting the metallic centres becomes of great importance, as they are responsible to mediate the magnetic interactions and modify the coordination spheres of the centres, which connects. This new metalloligands often involve the substitution of two halogen ions with ligands such as oxalate,[13,36] 2,2'-bipyrimidine,[37] malonate,[38] cyanide[39] or 2-(2'-pyridyl)imidazole,[40] among others, making them good building-blocks for the preparation of new homo- or heteronuclear molecular-based materials. For example, compound $(NBu_4)_5[Gd^{III}\{Re^{IV}Br_4(\mu\text{-ox})\}_4(H_2O)] \cdot H_2O$ stands as the first Re(IV) system incorporating a $4f$ ion.[41] On the other hand, it is also possible to achieve slow relaxation of the magnetisation in one-dimensional systems. For instance, compounds prepared with the $[ReCl_4(CN)_2]^{2-}$ entity prove to be useful tools for building SCM together with first-row transition metals (Figure 2.10).[42]

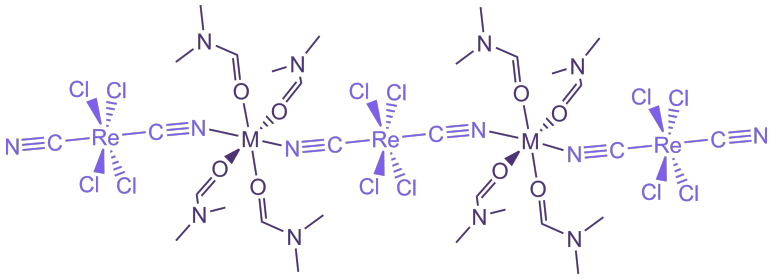

Figure 2.10: Schematic structural representation of the $[ReCl_4(\mu\text{-}CN)_2M(DMF)_4]$ one-dimensional compounds (M = Mn, Fe, Co, Ni). The $[ReCl_4(CN)_2]^{2-}$ anionic unit has been highlighted.

2.3 References

(1) P. W. Atkins, M. S. C.; Phillips, C. S. G. *Tables for group theory*; Oxford University Press: Oxford, UK: 2006, p 27.

(2) Boča, R. *Coord. Chem. Rev.* **2004**, *248*, 757–815.

(3) Martínez-Lillo, J.; Mastropietro, T. F.; Lhotel, E.; Paulsen, C.; Cano, J.; De Munno, G.; Faus, J.; Lloret, F.; Julve, M.; Nellutla, S.; Krzystek, J. *J. Am. Chem. Soc.* **2013**, *135*, 13737–13748.

(4) Dilworth, J. R. *Coord. Chem. Rev.* **2021**, *436*, 213822.

(5) Martínez-Lillo, J.; Faus, J.; Lloret, F.; Julve, M. *Coord. Chem. Rev.* **2015**, *289-290*, 215–237.

(6) Figgis, B. N.; Lewis, J.; Mabbs, F. E. *J. Chem. Soc.* **1961**, 3138–3145.

(7) Watt, G. W.; Thompson, R. J.; Gibbons, J. M. *Inorganic Syntheses Vol. 7*; John Wiley and Sons Ltd.: New York, USA: 1963, pp 189–192.

(8) Peacock, R. D. *J. Chem. Soc.* **1956**, 1291–1293.

(9) Weise, E. *Z. Anorg. Allg. Chem.* **1956**, *283*, 377–389.

(10) Pedersen, K. S.; Sigrist, M.; Sørensen, M. A.; Barra, A.-L.; Weyhermüller, T.; Piligkos, S.; Thuesen, C. A.; Vinum, M. G.; Mutka, H.; Weihe, H.; Clérac, R.; Bendix, J. *Angew. Chem. Int.* **2014**, *53*, 1351–1354.

(11) González, R.; Chiozzone, R.; Kremer, C.; De Munno, G.; Nicolò, F.; Lloret, F.; Julve, M.; Faus, J. *Inorg. Chem.* **2003**, *42*, 2512–2518.

(12) Chakravorti, M. C.; Gangopadhyay, T.; Angelici, R. J.; Choi, M. G. *Inorganic Syntheses Vol. 27*; John Wiley and Sons Ltd.: New York, USA: 1990, pp 294–295.

(13) Chiozzone, R.; González, R.; Kremer, C.; De Munno, G.; Cano, J.; Lloret, F.; Julve, M.; Faus, J. *Inorg. Chem.* **1999**, *38*, 4745–4752.

(14) Martínez-Lillo, J.; Armentano, D.; De Munno, G.; Marino, N.; Lloret, F.; Julve, M.; Faus, J. *CrystEngComm* **2008**, *10*, 1284–1287.

(15) Martínez-Lillo, J.; Pedersen, A. H.; Faus, J.; Julve, M.; Brechin, E. K. *Cryst. Growth Des.* **2015**, *15*, 2598–2601.

(16) Armentano, D.; Barquero, M. A.; Rojas-Dotti, C.; Moliner, N.; De Munno, G.; Brechin, E. K.; Martínez-Lillo, J. *Cryst. Growth Des.* **2017**, *17*, 5342–5348.

(17) Piccinelli, F.; Bettinelli, M.; Cano, J.; Lloret, F.; Julve, M.; Dolmella, A. *Eur. J. Inorg. Chem.* **2020**, *2020*, 2246–2252.

(18) Malecka, J.; Mrozinski, J.; Jaeger, L.; Wagner, C. *Pol. J. Chem.* **1998**, *72*, 1879–1885.

(19) Nelson, C. M.; Boyd, G. E.; Smith, W. T. J. *J. Am. Chem. Soc.* **1954**, *76*, 348–352.

(20) Busey, R. H.; Sonder, E. *J. Chem. Phys.* **1962**, *36*, 93–97.

(21) Minkiewicz, V.; Shirane, G.; Frazer, B.; Wheeler, R.; Dorain, P. *J. Phys. Chem. Solids* **1968**, *29*, 881–884.

(22) Singh, M. K.; Etcheverry-Berríos, A.; Vallejo, J.; Sanz, S.; Martínez-Lillo, J.; Nichol, G. S.; Lusby, P. J.; Brechin, E. K. *Dalton Trans.* **2022**, *51*, 8377–8381.

(23) González, R.; Chiozzone, R.; Kremer, C.; Guerra, F.; De Munno, G.; Lloret, F.; Julve, M.; Faus, J. *Inorg. Chem.* **2004**, *43*, 3013–3019.

(24) González, R.; Romero, F.; Luneau, D.; Armentano, D.; Munno, G. D.; Kremer, C.; Lloret, F.; Julve, M.; Faus, J. *Inorg. Chim. Acta* **2005**, *358*, 3995–4002.

(25) Pedersen, A. H.; Geoghegan, B. L.; Nichol, G. S.; Lupton, D. W.; Murray, K. S.; Martínez-Lillo, J.; Gass, I. A.; Brechin, E. K. *Dalton Trans.* **2017**, *46*, 5250–5259.

(26) Zhang, Y.; Fanna, D. J.; Shepherd, N. D.; Karatchevtseva, I.; Lu, K.; Kong, L.; Price, J. R. *RSC Adv.* **2016**, *6*, 75045–75053.

(27) Martínez-Lillo, J.; Cano, J.; Wernsdorfer, W.; Brechin, E. K. *Chem. – Eur. J* **2015**, *21*, 8790–8798.

(28) Pop, F.; Allain, M.; Auban-Senzier, P.; Martínez-Lillo, J.; Lloret, F.; Julve, M.; Canadell, E.; Avarvari, N. *Eur. J. Inorg. Chem.* **2014**, *2014*, 3855–3862.

(29) Kushch, N. D.; Buravov, L. I.; Kushch, P. P.; Shilov, G. V.; Yamochi, H.; Ishikawa, M.; Otsuka, A.; Shakin, A. A.; Maximova, O. V.; Volkova, O. S.; Vasiliev, A. N.; Yagubskii, E. B. *Inorg. Chem.* **2018**, *57*, 2386–2389.

(30) Kepert, C. J.; Kurmoo, M.; Day, P. *J. Mater. Chem.* **1997**, *7*, 221–228.

(31) Gong, D.-P.; Chen, J.-F.; Zhao, Y.; Cao, D.-K. *Dalton Trans.* **2016**, *45*, 3443–3449.

(32) Martínez-Lillo, J.; Kong, J.; Barros, W. P.; Faus, J.; Julve, M.; Brechin, E. K. *Chem. Commun.* **2014**, *50*, 5840–5842.

(33) Bulicanu, V.; Pedersen, K. S.; Rouzières, M.; Bendix, J.; Dechambenoit, P.; Clérac, R.; Hillard, E. A. *Chem. Commun.* **2015**, *51*, 17748–17751.

(34) Pedersen, A. H.; Julve, M.; Martínez-Lillo, J.; Cano, J.; Brechin, E. K. *Dalton Trans.* **2017**, *46*, 16025–16033.

(35) Martínez-Lillo, J.; Armentano, D.; De Munno, G.; Lloret, F.; Julve, M.; Faus, J. *Cryst. Growth Des.* **2006**, *6*, 2204–2206.

(36) Chiozzone, R.; Cuevas, A.; González, R.; Kremer, C.; Armentano, D.; De Munno, G.; Faus, J. *Inorg. Chim. Acta* **2006**, *359*, 2194–2200.

(37) Chiozzone, R.; González, R.; Kremer, C.; Cerdá, M. F.; Armentano, D.; De Munno, G.; Martínez-Lillo, J.; Faus, J. *Dalton Trans.* **2007**, 653–660.

(38) Cuevas, A.; Chiozzone, R.; Kremer, C.; Suescun, L.; Mombrú, A.; Armentano, D.; De Munno, G.; Lloret, F.; Cano, J.; Faus, J. *Inorg. Chem.* **2004**, *43*, 7823–7831.

(39) Harris, T. D.; Bennett, M. V.; Clérac, R.; Long, J. R. *J. Am. Chem. Soc.* **2010**, *132*, 3980–3988.

(40) Martínez-Lillo, J.; Armentano, D.; De Munno, G.; Faus, J. *Polyhedron* **2008**, *27*, 1447–1454.

(41) Martínez-Lillo, J.; Cañadillas-Delgado, L.; Cano, J.; Lloret, F.; Julve, M.; Faus, J. *Chem. Commun.* **2012**, *48*, 9242–9244.

(42) Harris, T. D.; Bennett, M. V.; Clérac, R.; Long, J. R. *J. Am. Chem. Soc.* **2010**, *132*, 3980–3988.

Article 1

RSC Adv., **2021**, *11*, 6353-6360

DECLARATION

Francisco José Martínez Lillo, Professor Titular del Departament de Química Inorgànica de la Universitat de València i **Francisco Lloret Pastor**, Catedràtic del Departament de Química Inorgànica de la Universitat de València

Certifiquen que:

En el treball titulat *Coexistence of metamagnetism and slow relaxation of magnetisation in ammonium hexafluoridorhenate*, els autors i el seu ordre és 'James Louis-Jean,* Samundeeswari M. Balasekaran,‡ Keith V. Lawler,‡ **Adrián Sanchis-Perucho,**‡ José Martínez-Lillo,* Dean Smith, Paul M. Forster, Ashkan Salamat and Frederic Poineau*' on s'especifica amb el símbol '‡' que els autors han participat igualment en el treball presentat. Que el doctorant, Adrián Sanchis Perucho, ha tingut una participació rellevant en aquest treball portat a terme en coautoria, realitzant la purificació de la mostra $(NH_4)_2[ReF_6]$, que constitueix l'estudi de l'article, amb la seua posterior caracterització per infraroig en tal d'assegurar la seua puresa en la preparació i posterior estudi de les propietats magnètiques mitjançant els magnetòmetres SQUID i PPMS. Així mateix, cal destacar l'aprenentatge del doctorant en la interpretació i tractament de les dades experimentals obtingudes per la magnetometria, els quals són importants per a la seua formació.

Per últim, deixem constància que els resultats ací publicats no han sigut emprats implícita o explícitament per cap dels coautors en la realització d'una altra Tesi doctoral.

Paterna, Juny de 2023

FRANCISCO JOSE\|MARTINEZ\|LILLO

Firmado digitalmente por FRANCISCO JOSE\|MARTINEZ\|LILLO
Nombre de reconocimiento (DN): cn=FRANCISCO JOSE\|MARTINEZ\|LILLO, serialNumber=73565126V, givenName=FRANCISCO JOSE, sn=MARTINEZ LILLO, ou=CIUDADANOS, o=ACCV, c=ES
Fecha: 2023.06.05 19:44:17 +01'00'

Francisco José Martínez Lillo

FRANCISC O\|LLORET\| PASTOR

Firmado digitalmente por FRANCISCO\|LLORET\|PASTOR
Fecha: 2023.06.05 10:34:44 +02'00'

Francisco Lloret Pastor

https://doi.org/10.1039/D0RA10325J

From page 77 to page 86

Article 2

Magnetochemistry, **2020**, *6(2)*, 20

DECLARATION

Francisco José Martínez Lillo, Professor Titular del Departament de Química Inorgànica de la Universitat de València i **Francisco Lloret Pastor**, Catedràtic del Departament de Química Inorgànica de la Universitat de València

Certifiquen que:

En el treball titulat *Field-Induced Single-Ion Magnet Phenomenon in Hexabromo- and Hexaiodorhenate(IV) Complexes*, els autors i el seu ordre és 'Carlos Rojas-Dotti, **Adrián Sanchis-Perucho**, Marta Orts-Arroyo, Nicolás Moliner,Ricardo González*, Francesc Lloret and José Martínez-Lillo*'. Que el doctorant, Adrián Sanchis Perucho, ha tingut una participació rellevant en el treball realitzat en coautoria apareixent com a segon autor. El doctorant ha col·laborat en els aspectes pràctics de la síntesi i correcta cristal·lització dels compostos reportats en forma de monocristalls adequats per a la difracció de raigs-X sobre monocristall, així com en la resolució de les dades estructurals i caracterització per raigs-X en pols. També cal destacar l'aprenentatge en la interpretació i tractament de les dades experimentals obtingudes per mitjà dels magnetòmetres SQUID i PPMS.

Per últim, deixem constància que els resultats ací publicats no han sigut emprats implícita o explícitament per cap dels coautors en la realització d'una altra Tesi doctoral.

Paterna, Juny de 2023

FRANCISCO JOSE|MARTINEZ|LILLO

Firmado digitalmente por FRANCISCO JOSE|MARTINEZ|LILLO
Nombre de reconocimiento (DN): cn=FRANCISCO JOSE|MARTINEZ|LILLO, serialNumber=73565126V, givenName=FRANCISCO JOSE, sn=MARTINEZ LILLO, ou=CIUDADANOS, o=ACCV, c=ES
Fecha: 2023.06.05 19:52:11 +01'00'

Francisco José Martínez Lillo

FRANCISCO|LLORET|PASTOR

Firmado digitalmente por FRANCISCO|LLORET|PASTOR
Fecha: 2023.06.05 10:35:20 +02'00'

Francisco Lloret Pastor

https://doi.org/10.3390/magnetochemistry6020020

From page 91 to page 104

Article 3

CrystEngComm, **2021**, *23*, 8579-8587

https://doi.org/10.1039/D1CE01337H

From page 107 to page 125

Article 4

Inorganics, **2023**, *11*, 78

https://doi.org/10.3390/inorganics11020078

From page 129 to page 145

Article 5

CrystEngComm, **2018**, *20*, 4575-4581

DECLARATION

Francisco José Martínez Lillo, Professor Titular del Departament de Química Inorgànica de la Universitat de València i **Francisco Lloret Pastor**, Catedràtic del Departament de Química Inorgànica de la Universitat de València

Certifiquen que:

En el treball titulat *Halogen···halogen interactions in the self-assembly of one-dimensional 2,2'-bipyrimidine-based* $Cu^{II}Re^{IV}$ *systems*, els autors i el seu ordre és 'Donatella Armentano,* **Adrián Sanchis-Perucho**, Carlos Rojas-Dotti* and José Martínez-Lillo*'. Que el doctorant, Adrián Sanchis Perucho, ha tingut una participació rellevant en el treball realitzat en coautoria apareixent com a segon autor. El doctorant ha col·laborat en els aspectes pràctics de la síntesi i correcta cristal·lització del compost $\{[ReCl_4(bpym)CuBr_2]\cdot CHCl_3\}_n$ reportat en forma de monocristalls adequats per a la seua resolució estructural, així com en la caracterització per mitjà de infraroig i raigs-X en pols, juntament amb l'anàlisi elemental de C, H i N. També cal destacar l'aprenentatge en la preparació, mesura, interpretació i tractament de les dades experimentals obtingudes per mitjà del magnetòmetre SQUID.

Per últim, deixem constància que els resultats ací publicats no han sigut emprats implícita o explícitament per cap dels coautors en la realització d'una altra Tesi doctoral.

Paterna, Juny de 2023

FRANCISCO JOSE|MARTINEZ|LILLO

Firmado digitalmente por FRANCISCO JOSE|MARTINEZ|LILLO
Nombre de reconocimiento (DN): cn=FRANCISCO JOSE|MARTINEZ|LILLO, serialNumber=73565126V, givenName=FRANCISCO JOSE, sn=MARTINEZ LILLO, ou=CIUDADANOS, o=ACCV, c=ES
Fecha: 2023.06.05 20:00:47 +01'00'

Francisco José Martínez Lillo

FRANCISCO|LLORET|PASTOR

Firmado digitalmente por FRANCISCO|LLORET|PASTOR
Fecha: 2023.06.05 10:35:59 +02'00'

Francisco Lloret Pastor

https://doi.org/10.1039/C8CE00996A

From page 151 to page 169

CHAPTER 3

IRIDIUM

3.1 Theoretical magnetic model for a d^5 ion system

The fundamental term of a d^5 free ion is ^{6}S, in the same way it was deduced for a d^3 in the past section 2.1. Moreover, for $5d$ metal ions with a six coordinated environment, it is well known that the octahedral ligand field is always strong, hence it will have high Δ_{O_h} values. Thus, a d^5 electronic configuration is defined by a low-spin state term $^2\mathrm{T}_{2\mathrm{g}}\left(t_{2g}^5\right)$. For the following model, the coupling with higher excited states and the thermally populated ground state is assumed to be negligible, so only the $^2\mathrm{T}_{2\mathrm{g}}$ term will be considered. The wave-functions belonging to this term are presented in Table 3.1.

Table 3.1: O_h symmetry adapted wave-functions for a $^2\mathrm{T}_{2\mathrm{g}}$ term from a d^5 system.

ψ_i	
1	$\lvert 1,-1/2\rangle$
2	$\lvert -1,1/2\rangle$
3	$\lvert 1,1/2\rangle$
4	$\lvert -1,-1/2\rangle$
5	$\frac{1}{\sqrt{2}}\{\lvert 2,1/2\rangle - \lvert -2,1/2\rangle\}$
6	$\frac{1}{\sqrt{2}}\{\lvert 2,-1/2\rangle - \lvert -2,-1/2\rangle\}$

In the previous Chapter it was confirmed that for a d^3 metal ion no first-order spin-orbit coupling was possible in an octahedron or a tetragonally distorted octahedral environment. Such a situation is observed when all the integrals of the form $\left\langle \psi_i \middle| \widehat{L}_u \middle| \psi_i \right\rangle$ and $\left\langle \psi_i \middle| \widehat{L}_u \middle| \psi_j \right\rangle$ elements of the matrix are zero, ψ_i and ψ_j being wave-functions associated with the ground state, $\widehat{L}_u$ the orbital angular momentum operator with $(u = x, y, z)$ indicating its three components. When this condition is not fulfilled for at least one direction, x, y or z, the first-order spin-orbit coupling cannot be ignored, and the matrix presents values different from zero. Thus, the degeneracy of the ground state will be partially removed by first-order spin-coupling effects. In the case of a d^5 metal ion under octahedral symmetry without distortion, the spin-orbit coupling splits the $^2\mathrm{T}_{2\mathrm{g}}$ term into the E'' $(J = 1/2)$ doublet and G' $(J = 3/2)$ quadruplet (considering the double group, O'), being the doublet the ground state for $\lambda < 0$. This information is summarised in Figure 3.1.

The Hamiltonian to consider in order to quantitatively calculate the spin-orbit energies of each level is presented in (3.1), where it is introduced a new factor, κ, to equation (1.60). This term, generally called orbital reduction factor, is incorporated

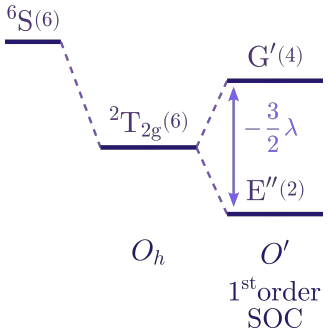

Figure 3.1: Energy diagram for a ^{6}S term in an octahedral symmetry with first-order spin-orbit coupling. The numbers in parenthesis show the total degeneracy.

to the operator for taking into account the delocalisation of the unpaired electrons from the metal to the ligands, which reduces the role of the angular momentum. Hence, the effect of the spin-orbit coupling and consequently the Zeeman effect in the future. Its value is compressed between 1 and 0, where for $\kappa = 1$ the reduction of the orbital angular momentum is neglected as there is no covalency with the ligands. On the other hand, for values zero or close to zero, the two levels E″ and G′ will be accidentally degenerated ($\kappa\lambda = 0$), and it is not longer legitimate to treat the Zeeman as a perturbation with respect the spin-orbit coupling, as the last one has no effect. Thus, too low values of κ have no physical sense on this model. Nevertheless, the inclusion of κ in the spin-orbit Hamiltonian is considered a formalism from a theoretical point of view, as it is always together with λ. So, if it was to be omitted λ will modify its value to adapt it.

$$\widehat{\mathcal{H}}_{SOC} = \kappa\lambda\widehat{L}\widehat{S} \tag{3.1}$$

The evaluation of all possible matrix elements of the ^{2}T$_{2g}$ term gives the secular determinant (3.2). In this case, there are some off-diagonal elements and it is necessary to solve each sub-determinant, indicating that some functions are going to mix by first-order effects. In fact, the first-order spin-orbit coupling lead to two possible values for the energy, $E = \kappa\lambda$ for E″ doublet, and $E = -\frac{\kappa\lambda}{2}$ for G′ quadruplet. No further second-order corrections from levels in an other excited terms will be considered as it was pointed at the beginning. As an example, the evaluation of ψ_3 is presented in (3.3), where it can be seen how after applying the spin-orbit operator over the function, it has a part which belongs to ψ_6, so ψ_3 and ψ_6 will mix by first-order effects.

$$\begin{array}{c|cccccc}
\widehat{\mathcal{H}}_{SOC} & |\psi_1\rangle & |\psi_2\rangle & |\psi_4\rangle & |\psi_5\rangle & |\psi_3\rangle & |\psi_6\rangle \\
\hline
\langle\psi_1| & -\frac{\kappa\lambda}{2} - E & 0 & 0 & 0 & 0 & 0 \\
\langle\psi_2| & 0 & -\frac{\kappa\lambda}{2} - E & 0 & 0 & 0 & 0 \\
\langle\psi_4| & 0 & 0 & \frac{\kappa\lambda}{2} - E & -\frac{\kappa\lambda}{\sqrt{2}} & 0 & 0 \\
\langle\psi_5| & 0 & 0 & -\frac{\kappa\lambda}{\sqrt{2}} & 0 - E & 0 & 0 \\
\langle\psi_3| & 0 & 0 & 0 & 0 & \frac{\kappa\lambda}{2} - E & \frac{\kappa\lambda}{\sqrt{2}} \\
\langle\psi_6| & 0 & 0 & 0 & 0 & \frac{\kappa\lambda}{\sqrt{2}} & 0 - E
\end{array} = 0 \tag{3.2}$$

$$E_3^{(1)} = H_{33} = \left\langle \psi_3 \middle| \lambda \widehat{L}\widehat{S} \middle| \psi_3 \right\rangle = \frac{\kappa\lambda}{2} \langle \psi_3 | \psi_3 \rangle + \kappa\lambda \langle \psi_3 | 2, -1/2 \rangle = \frac{\kappa\lambda}{2} \tag{3.3}$$

The calculation of the effects of the spin-orbit coupling are not yet complete, since it is necessary to calculate all the new wave-functions associated to G$'$ and E$''$ levels. The functions are determined as lineal combinations of the zero-order ones with their respective mixing coefficients. These are obtained by substituting each of the energies into the set of equations, which gave rise to the secular determinant. As an example, the equation system that will give ϕ_3 and ϕ_6 after mixing ψ_3 and ψ_6, is presented in (3.4). The substitution of the two energy values gives the relation between the mixing coefficients. Actually, the substitution of $E = \kappa\lambda$ will give the coefficient relation for the function from the E$''$ level, and $E = -\frac{\kappa\lambda}{2}$ the coefficients relation for the one that belongs to G$'$. Indeed, exactly the same results will be obtained regardless of the equation used.

$$\begin{cases} \left(\dfrac{\kappa\lambda}{2} - E^{(1)}\right) c_3 + \dfrac{\kappa\lambda}{\sqrt{2}}\, c_6 = 0 \xrightarrow{E^{(1)}=\kappa\lambda} \dfrac{c_6}{c_3} = \dfrac{1}{\sqrt{2}} \\ \dfrac{\kappa\lambda}{\sqrt{2}}\, c_3 + (0 - E^{(1)})\, c_6 = 0 \xrightarrow{E^{(1)}=\kappa\lambda} \dfrac{c_6}{c_3} = \dfrac{1}{\sqrt{2}} \end{cases} \tag{3.4}$$

Afterwards, the wave-functions are normalised, so that $\langle \phi_i | \phi_i \rangle$ equals one. For instance, ϕ_6, which is a wave-function corresponding to energy $E = \kappa\lambda$, has its normalization constant calculated in (3.5)

$$\langle \phi_6 | \phi_6 \rangle = N \left[\langle \psi_3 | + \frac{1}{\sqrt{2}} \langle \psi_6 | \right] \cdot N \left[|\psi_3\rangle + \frac{1}{\sqrt{2}} |\psi_6\rangle \right] = 1 \Rightarrow N = \sqrt{\frac{2}{3}} \tag{3.5}$$

Employing this methodology for the rest of equations all wave-functions are calculated and grouped as presented in (3.6) and (3.7) for the two levels. In this way, the new set of functions will give a secular determinant that has been diagonalised, where the energy of each one is easily obtained by (1.35).

$$\underset{\left(E = -\frac{\kappa\lambda}{2}\right)}{\mathrm{G}'} \begin{cases} \phi_1 = \psi_1 \\ \phi_2 = \psi_2 \\ \phi_3 = \dfrac{1}{\sqrt{3}} \left\{ \psi_3 - \sqrt{2}\psi_6 \right\} \\ \phi_4 = \dfrac{1}{\sqrt{3}} \left\{ \psi_4 + \sqrt{2}\psi_5 \right\} \end{cases} \tag{3.6}$$

$$\underset{(E = \kappa\lambda)}{\mathrm{E}''} \begin{cases} \phi_5 = \sqrt{\dfrac{2}{3}} \left\{ \psi_4 - \dfrac{1}{\sqrt{2}}\psi_5 \right\} \\ \phi_6 = \sqrt{\dfrac{2}{3}} \left\{ \psi_3 + \dfrac{1}{\sqrt{2}}\psi_6 \right\} \end{cases} \tag{3.7}$$

The magnetic interaction will be treated as a perturbation of the wave-functions and energies obtained by the spin-orbit coupling. Thus, in the case of the octahedral symmetry, it is necessary to apply the isotropic Zeeman Hamiltonian (1.24) in order to determine quantitatively how the two levels will interact with the magnetic field.

Nevertheless, the introduction of the κ factor modifies the orbital angular momentum term as expressed in (3.8).

$$\widehat{\mathcal{H}}_Z = \mu_B H \left(\kappa \widehat{L}_z + g \widehat{S}_z\right) \tag{3.8}$$

The treatment of the two set of wave-functions with (3.8) Hamiltonian, leads to (3.9) and (3.10) secular determinants for G' and E'' levels, respectively. Certainly, as there is no mixing by first-order Zeeman effects the first-order energies are easily obtained and the functions remain the same. Moreover, when $\kappa = 1$ there is not first-order interaction on the quadruplet level, otherwise some splitting is expected. On the other hand, the doublet breaks its degeneracy regardless the κ value. It is worth noting that the g value was approximated to 2 in the calculations.

$$\begin{array}{c|cccc|}
\widehat{\mathcal{H}}_Z & |\phi_1\rangle & |\phi_2\rangle & |\phi_3\rangle & |\phi_4\rangle \\
\hline
\langle\phi_1| & -(1-\kappa)\mu_B H - E & 0 & 0 & 0 \\
\langle\phi_2| & 0 & (1-\kappa)\mu_B H - E & 0 & 0 \\
\langle\phi_3| & 0 & 0 & -\frac{(1-\kappa)\mu_B H}{3} - E & 0 \\
\langle\phi_4| & 0 & 0 & 0 & \frac{(1-\kappa)\mu_B H}{3} - E \\
\hline
\end{array} = 0 \tag{3.9}$$

$$\begin{array}{c|cc|}
\widehat{\mathcal{H}}_Z & |\phi_5\rangle & |\phi_6\rangle \\
\hline
\langle\phi_5| & -\frac{(1+2\kappa)\mu_B H}{3} - E & 0 \\
\langle\phi_6| & 0 & \frac{(1+2\kappa)\mu_B H}{3} - E \\
\hline
\end{array} = 0 \tag{3.10}$$

The second-order Zeeman energy corrections for each component of the two levels take the form of (3.11) for G' ($i = 1$ to 4), and (3.12) for E'' ($i = 5$ and 6).

$$E_i^{(2)} = \sum_{j=5}^{6} \frac{\left\langle \phi_j \middle| \widehat{\mathcal{H}}_Z \middle| \phi_i \right\rangle^2}{-\frac{\kappa\lambda}{2} - \kappa\lambda} \tag{3.11}$$

$$E_i^{(2)} = \sum_{j=1}^{4} \frac{\left\langle \phi_j \middle| \widehat{\mathcal{H}}_Z \middle| \phi_i \right\rangle^2}{\kappa\lambda + \frac{\kappa\lambda}{2}} \tag{3.12}$$

Besides, how the Zeeman interaction modifies the energy diagram is presented in Figure 3.2, and all calculated first- and second-order energies are summarised on Table 3.2, where it was considered as the zero of energy the first-order spin-orbit coupling for the ground state.

Introducing the zero-field energies and Zeeman coefficients into the Van Vleck formula (1.45) leads to (3.13). The $\chi_M T$ *vs.* $k_B T/\kappa|\lambda|$ plot for $\kappa = 1.0$ and 0.6 is shown in Figure 3.3, where it can be seen how the magnetic susceptibility deviates from the Curie law, and how low κ values reflects as minor $\chi_M T$ values.

$$\begin{gathered}
\chi_M = \frac{N_A {\mu_B}^2}{27 k_B T} \frac{\left[30(1-\kappa)^2 x + 8(2+\kappa)^2\right] + \left[3(1+2\kappa)^2 x - 8(2+\kappa)^2\right] \exp\left(\frac{-3x}{2}\right)}{x\left[2 + \exp\left(\frac{-3x}{2}\right)\right]} \\
x = \frac{\kappa\lambda}{k_B T}
\end{gathered} \tag{3.13}$$

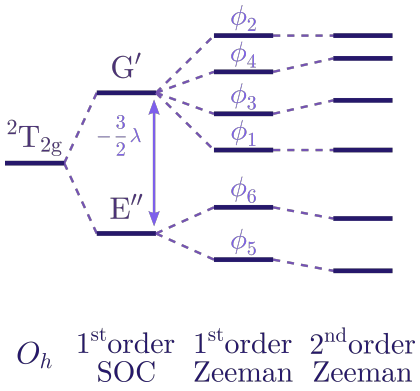

Figure 3.2: Energy diagram of a $^2T_{2g}$ term under an octahedral symmetry exhibiting spin-orbit coupling and Zeeman effect. The diagram is not at scale.

Table 3.2: First and second Zeeman coefficients for a d^5 ion under octahedral symmetry.

ϕ_i	$E_i^{(0)}$	E_i'/μ_B	$E_i''/{\mu_B}^2$
$1,2$	$-\frac{3\kappa\lambda}{2}$	$\pm(1-\kappa)$	0
$3,4$	$-\frac{3\kappa\lambda}{2}$	$\pm\frac{(1-\kappa)}{3}$	$-\frac{4(2+\kappa)^2}{27\kappa\lambda}$
$5,6$	0	$\pm\frac{(1+2\kappa)}{3}$	$\frac{4(2+\kappa)^2}{27\kappa\lambda}$

As it was pointed in Chapter 2, perfectly octahedral environments are rather unlikely being the tetragonal distortion the main cause, so equation (3.13), although it is a pedagogically interesting exercise, few systems will have perfectly octahedral environment to apply it. When the symmetry of the system is lowered to the D_{4h} group by a distortion along the z-axis, it will cause the $^2T_{2g}$ to split into an orbital doublet, ^2E_g, and an orbital singlet, ^2B_g, terms. They will be separated by an energy gap that from now on will be referred as Δ, which is defined as positive if the orbital singlet is the lowest. Besides, if both axial ligands are different, C_{4v} symmetry should be used instead and the parity of the terms omitted.[1] Due to the strong ligand field potential and the spin-orbit coupling acting in $5d$ metal ions, the tetragonal distortion of the octahedral symmetry and the spin-orbit coupling perturbations must be taken into account simultaneously. The resulting energies and wave-functions will be perturbed latter by the magnetic interaction as consequence of being it weaker than the last two.

In Figure 3.4, it can be seen on the left side the energy diagram produced by the ligand field, and on the right side, the one produced by the spin-orbit coupling. The action of both perturbations converge at the centre part of the diagram, where the resulting terms considering the double group, C'_{4v} are two E'' doublets that are mixed together and another E' doublet. Nevertheless, they were labelled as $E''(^2E)$ and $E''(^2B_2)$ to indicate their major components, indicating they are mixtures of what ^2E and $^2B_2$ were before the spin-orbit coupling.

The lowering of symmetry is accounted by the effective operator $\widehat{V}_{tetra}$. The wave-functions are redistributed into the new terms, where ψ_5 and ψ_6 now belong to the singlet ground state $^2B_2$, and the rest to the doublet ^2E. As it was pointed before, the two levels are separated by a quantity named as Δ, which is positive when the zero of

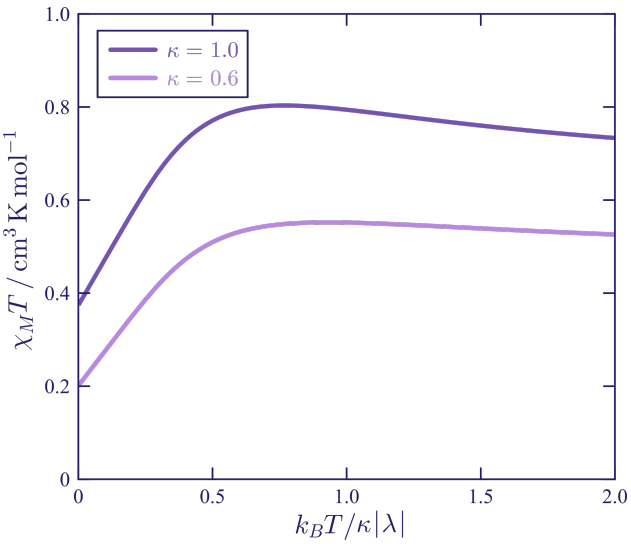

Figure 3.3: $\chi_M T$ *vs.* $k_B T/\kappa|\lambda|$ plot for a d^5 ion in a perfect octahedral environment. The curves are plotted for two values of the orbital reduction factor, namely $\kappa = 1.0$ and 0.6.

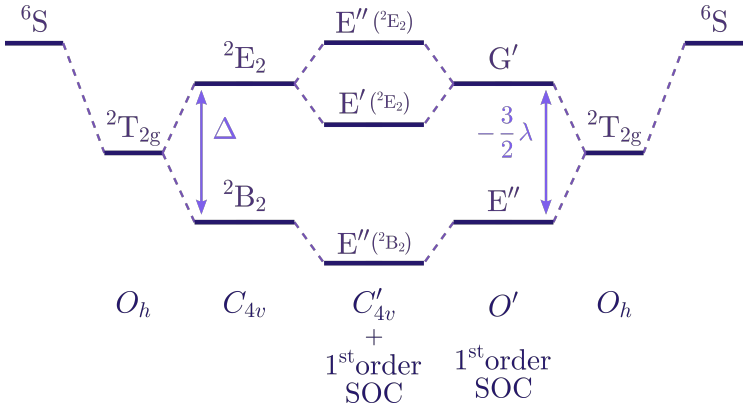

Figure 3.4: Energy diagram for a ^{6}S term in an octahedral symmetry with a tetragonal distortion and spin-orbit coupling.

energy is taken for the singlet ground state. Thus, after applying the $\widehat{V}_{tetra}$ operator over a component of the orbital doublet, it will add a Δ quantity to the energy, whilst it will be zero for the components of the orbital singlet. The Hamiltonian that takes into account the spin-orbit coupling and the tetragonal distortion is given in equation (3.14).

$$\widehat{\mathscr{H}} = \kappa\lambda\widehat{L}\widehat{S} + \widehat{V}_{tetra} \tag{3.14}$$

The secular determinant in (3.15) is equivalent to the one obtained for the octahedral symmetry, but this time with the axial distortion accounted by Δ for the functions belonging to the ^{2}E level. One example of the evaluation of such matrix is given in (3.16), where the first element of the Hamiltonian was treated previously in the octahedral case in (3.3), and the second since it involves a component of the

orbital doublet, $\widehat{V}_{tetra}$ will add a Δ quantity to the energy.

$\widehat{\mathcal{H}}$	$\lvert\psi_1\rangle$	$\lvert\psi_2\rangle$	$\lvert\psi_4\rangle$	$\lvert\psi_5\rangle$	$\lvert\psi_3\rangle$	$\lvert\psi_6\rangle$
$\langle\psi_1\rvert$	$-\frac{\kappa\lambda}{2}+\Delta-E$	0	0	0	0	0
$\langle\psi_2\rvert$	0	$-\frac{\kappa\lambda}{2}+\Delta-E$	0	0	0	0
$\langle\psi_4\rvert$	0	0	$\frac{\kappa\lambda}{2}+\Delta-E$	$-\frac{\kappa\lambda}{\sqrt{2}}$	0	0
$\langle\psi_5\rvert$	0	0	$-\frac{\kappa\lambda}{\sqrt{2}}$	$0-E$	0	0
$\langle\psi_3\rvert$	0	0	0	0	$\frac{\kappa\lambda}{2}+\Delta-E$	$\frac{\kappa\lambda}{\sqrt{2}}$
$\langle\psi_6\rvert$	0	0	0	0	$\frac{\kappa\lambda}{\sqrt{2}}$	$0-E$

$= 0$ (3.15)

$$\begin{aligned} E_3^{(1)} = H_{33} &= \left\langle \psi_3 \middle| \widehat{\mathcal{H}}_{SOC} + \widehat{V}_{tetra} \middle| \psi_3 \right\rangle \\ &= \left\langle \psi_3 \middle| \widehat{\mathcal{H}}_{SOC} \middle| \psi_3 \right\rangle + \left\langle \psi_3 \middle| \widehat{V}_{tetra} \middle| \psi_3 \right\rangle = \frac{\kappa\lambda}{2} + \Delta \end{aligned} \tag{3.16}$$

The sub-determinants are solved, and the energies of the combined effect of the perturbation by spin-orbit and the tetragonal crystal field obtained. The originally six-fold degenerate $^2\mathrm{T}_{2\mathrm{g}}$ term is split into three doubly degenerate levels. Their calculated energies are summarised in (3.17), being ν a new defined convenient parameter called the distortion parameter, which correlates Δ, κ and λ.

$$\begin{gathered} E_1 = E_2 = \kappa\lambda\left(\nu - \frac{1}{2}\right); \quad E_3 = E_4 = \frac{\kappa\lambda}{\sqrt{2}}\, a; \quad E_5 = E_6 = \frac{\kappa\lambda}{\sqrt{2}}\, b; \\ a = \frac{1}{\sqrt{2}}\left(\nu + \frac{1}{2} - Z\right); \quad b = \frac{1}{\sqrt{2}}\left(\nu + \frac{1}{2} + Z\right); \\ Z = \sqrt{\nu^2 + \nu + \frac{9}{4}}; \quad \nu = \frac{\Delta}{\kappa\lambda} \end{gathered} \tag{3.17}$$

A plot of the energy levels as function of the distortion parameter for systems with $\lambda < 0$ is presented in Figure 3.5, where the ground state is always the E'' doublet at $E_{5,6}$ for any value of Δ including positive and negative integers. Furthermore, the energy gap between this ground state and the first excited state, either E'' or E', is larger than $|\lambda|$. Thus, it can be assumed that for systems with a strong spin-orbit coupling parameter as Ir(IV) ($\lambda \approx -5000$ cm^{-1}), this ground Kramer's doublet is the only populated state in the whole temperature range. Hence, the magnetic susceptibility of the compounds can be described taking into account the magnetic properties of only the E'' doublet considered as an effective-spin of 1/2.

The found energies (3.17) are substituted into the set of equations that gave rise to the secular determinant, in order to get the mixing coefficient relations of their corresponding wave-functions. For instance, ϕ_3 presented herein in (3.18) was obtained by substitution of E_3 energy into the equation involving ψ_3 and ψ_6. Thus, after normalisation, the wave-functions corresponding to each energy are established. The resulting functions for the three levels are grouped and summarised in (3.19) to (3.21).

$$\left(\frac{\kappa\lambda}{2} + \Delta - E^{(1)}\right) c_3 + \frac{\kappa\lambda}{\sqrt{2}}\, c_6 = 0 \xrightarrow{E_3 = \frac{\kappa\lambda}{\sqrt{2}}\, a} \frac{c_6}{c_3} = a - \frac{\sqrt{2}}{2} - \frac{\Delta\sqrt{2}}{\kappa\lambda} = -b \tag{3.18}$$

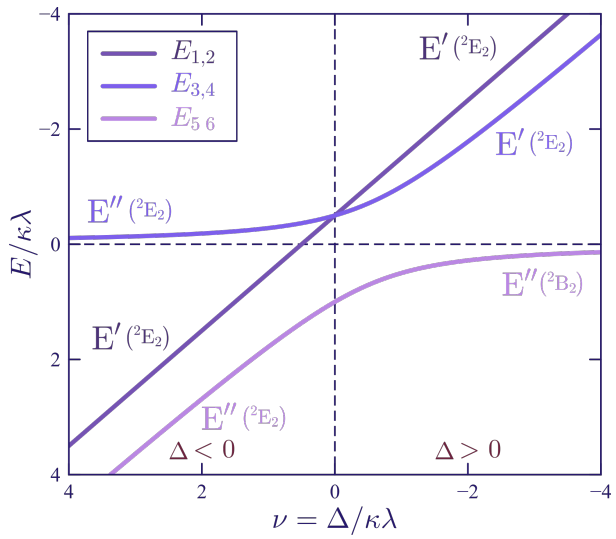

Figure 3.5: Energy levels of the three Kramer's doublets arising from the ground state $^2\mathrm{T}_2$ as a function of the tetragonal distortion parameter ν.

$$\mathrm{E}' \qquad \left[E = \kappa\lambda\left(\nu - \frac{1}{2}\right)\right] \begin{cases} \phi_1 = \psi_1 \\ \phi_2 = \psi_2 \end{cases} \tag{3.19}$$

$$\mathrm{E}'' \qquad \left(E = \frac{\kappa\lambda}{\sqrt{2}}\, a\right) \begin{cases} \phi_3 = \dfrac{1}{\sqrt{1+b^2}}\{\psi_3 - b\psi_6\} \\ \phi_4 = \dfrac{1}{\sqrt{1+b^2}}\{\psi_4 + b\psi_5\} \end{cases} \tag{3.20}$$

$$\mathrm{E}'' \qquad \left(E = \frac{\kappa\lambda}{\sqrt{2}}\, b\right) \begin{cases} \phi_5 = \dfrac{1}{\sqrt{1+a^2}}\{\psi_4 + a\psi_5\} \\ \phi_6 = \dfrac{1}{\sqrt{1+a^2}}\{\psi_3 - a\psi_6\} \end{cases} \tag{3.21}$$

Now that the energies and wave-functions have been obtained, it is time to consider the effect of the magnetic field over the system. As in the spin-orbit coupling, any interaction with the magnetic field between functions from exited terms will be neglected. Moreover, because of the axial symmetry of the system (D_{4h} or C_{4v}), the x- and y-directions are identical. Thus, it is possible to split the Zeeman operator in its parallel (z) and their perpendicular (x or y) components. Introducing κ to the functions (2.12) and (2.13) used previously in Chapter 2, the new Hamiltonians are as follows

$$\widehat{\mathcal{H}}_{Z,\parallel} = \mu_B H\left(\kappa\widehat{L}_z + g\widehat{S}_z\right) \tag{3.22}$$

$$\widehat{\mathcal{H}}_{Z,\perp} = \frac{\mu_B H}{2}\left(\kappa\widehat{L}_+ + \kappa\widehat{L}_- + g\widehat{S}_- + g\widehat{S}_+\right) \tag{3.23}$$

As there are not mixing between functions by first-order Zeeman effect in the parallel component at any of the three levels, all secular determinants are diagonalised and the first-order energies obtained directly equal to H_{ii} integrals. As an example, it is possible to take the secular determinant arising from the first-order

interaction in the parallel component for the E′ level, which is presented in (3.24).

$$\begin{array}{c|cc|} \widehat{\mathcal{H}}_{Z,\parallel} & |\phi_1\rangle & |\phi_2\rangle \\ \hline \langle\phi_1| & -(1-\kappa)\mu_B H - E & 0 \\ \langle\phi_2| & 0 & (1-\kappa)\mu_B H - E \end{array} = 0 \tag{3.24}$$

Besides, expression (3.25) will give the total second-order energy correction coefficients per level. For the doublet at $E^{(0)}_{1,2}$, i has the values 1 and 2, and j the values from 3 to 6. At energy $E^{(0)}_{3,4}$ the appropriate expression is given by (3.25) when, i has the values 3 and 4, and j the values 1, 2, 5, 6. Lastly, for the doublet at an energy $E^{(0)}_{5,6}$, i has the values 5 and 6, and j the values from 1 to 4.

$$\sum_i \sum_j \frac{\left\langle \phi_j \middle| \mu_B H_\parallel \left(\kappa \widehat{L}_z + g\widehat{S}_z\right) \middle| \phi_i \right\rangle^2}{E^{(0)}_i - E^{(0)}_j} \tag{3.25}$$

All Zeeman coefficients required to calculate the parallel magnetic susceptibility are summarised in Table (3.3). Furthermore, the susceptibility expression is presented in (3.26).

Table 3.3: First and second Zeeman coefficients for a d^5 ion under a tetragonal distorted octahedral symmetry in the parallel component.

ϕ_i	$E^{(0)}_i$	$E_i{}'/\mu_B$	$E_i{}''/\mu_B^2$
$1,2$	$\kappa\lambda\left(\nu - \frac{1}{2}\right)$	$\pm(\kappa - 1)$	0
$3,4$	$\frac{\kappa\lambda}{\sqrt{2}}\, a$	$\pm\frac{(\kappa+1-b^2)}{1+b^2}$	$-\frac{2(\kappa+1-ab)^2}{\kappa\lambda(1+a^2)(1+b^2)Z}$
$5,6$	$\frac{\kappa\lambda}{\sqrt{2}}\, b$	$\pm\frac{(\kappa+1-a^2)}{1+a^2}$	$\frac{2(\kappa+1-ab)^2}{\kappa\lambda(1+a^2)(1+b^2)Z}$

$$\begin{aligned} \chi_z = \chi_\parallel &= \frac{N_A {\mu_B}^2}{k_B T} \frac{Q_\parallel}{\exp\left(-\frac{E^{(0)}_1}{k_B T}\right) + \exp\left(-\frac{E^{(0)}_3}{k_B T}\right) + \exp\left(-\frac{E^{(0)}_5}{k_B T}\right)}; \\ Q_\parallel &= \left[E^{(1)}_1\right]^2 \exp\left(-\frac{E^{(0)}_1}{k_B T}\right) + \left\{\left[E^{(1)}_3\right]^2 - k_B T E^{(2)}_3\right\} \exp\left(-\frac{E^{(0)}_3}{k_B T}\right) + \\ &\quad \left\{\left[E^{(1)}_5\right]^2 - k_B T E^{(2)}_5\right\} \exp\left(-\frac{E^{(0)}_5}{k_B T}\right) \end{aligned} \tag{3.26}$$

Following the same procedure, the energies corrections for the perpendicular component are calculated. The first-order Zeeman coefficient for the doublet at energy $E^{(0)}_{1,2}$ give the secular determinant found in (3.27), where it can be seen how the magnetic field does not remove the degeneracy of the level by first-order effects, as there is not interaction. Interestingly, the secular determinant for the doublet at energy $E^{(0)}_{5,6}$ contains non-zero diagonal elements, in contrast with the parallel direction. This means that not only the two-fold degeneracy of this level is removed, but

it also mixes the functions ϕ_5 and ϕ_6 by first-order effects. Its secular determinant is presented in (3.28).

$$\begin{array}{c|cc} \widehat{\mathcal{H}}_{Z,\perp} & |\phi_1\rangle & |\phi_2\rangle \\ \hline \langle\phi_1| & 0-E & 0 \\ \langle\phi_2| & 0 & 0-E \end{array} = 0 \tag{3.27}$$

$$\begin{array}{c|cc} \widehat{\mathcal{H}}_{Z,\perp} & |\phi_5\rangle & |\phi_6\rangle \\ \hline \langle\phi_5| & 0-E & \frac{\left(\sqrt{2}\kappa a-a^2\right)\mu_B H_\perp}{1+a^2} \\ \langle\phi_6| & \frac{\left(\sqrt{2}\kappa a-a^2\right)\mu_B H_\perp}{1+a^2} & 0-E \end{array} = 0 \tag{3.28}$$

The second-order Zeeman energy corrections are calculated using (3.25) with the magnetic moment operator replaced by the perpendicular one (3.23). All Zeeman coefficients required to calculate the perpendicular magnetic susceptibility are summarised in Table (3.4), and its susceptibility expression is presented in (3.29).

Table 3.4: First and second Zeeman coefficients for a d^5 ion under a tetragonal distorted octahedral symmetry in the perpendicular component.

ϕ_i	$E_i^{(0)}$	$E_i{}'/\mu_B$	$E_i{}''/\mu_B^2$
$1,2$	$\kappa\lambda\left(\nu-\frac{1}{2}\right)$	0	$\frac{2}{\kappa\lambda}\left[\frac{(\sqrt{2}-\kappa a)^2}{(1+a^2)(\nu-1.5-Z)}+\frac{(\sqrt{2}-\kappa b)^2}{(1+b^2)(\nu-1.5+Z)}\right]$
$3,4$	$\frac{\kappa\lambda}{\sqrt{2}}\,a$	$\pm\frac{\sqrt{2}\kappa b-b^2}{1+b^2}$	$-\frac{2}{\kappa\lambda}\left[\frac{\left[\kappa(a+b)-ab\sqrt{2}\right]^2}{2Z(1+a^2)(1+b^2)}+\frac{(\sqrt{2}-\kappa b)^2}{(1+b^2)(\nu-1.5+Z)}\right]$
$5,6$	$\frac{\kappa\lambda}{\sqrt{2}}\,b$	$\pm\frac{\sqrt{2}\kappa a-a^2}{1+a^2}$	$\frac{2}{\kappa\lambda}\left[\frac{\left[\kappa(a+b)-ab\sqrt{2}\right]^2}{2Z(1+a^2)(1+b^2)}-\frac{(\sqrt{2}-\kappa a)^2}{(1+a^2)(\nu-1.5-Z)}\right]$

$$\begin{aligned} \chi_x=\chi_y=\chi_\perp &= \frac{N_A{\mu_B}^2}{k_BT}\,\frac{Q_\perp}{\exp\left(-\frac{E_1^{(0)}}{k_BT}\right)+\exp\left(-\frac{E_3^{(0)}}{k_BT}\right)+\exp\left(-\frac{E_5^{(0)}}{k_BT}\right)}; \\ Q_\perp &= -k_BTE_1^{(2)}\exp\left(-\frac{E_1^{(0)}}{k_BT}\right)+\left\{\left[E_3^{(1)}\right]^2-k_BTE_3^{(2)}\right\}\exp\left(-\frac{E_3^{(0)}}{k_BT}\right)+ \\ &\quad \left\{\left[E_5^{(1)}\right]^2-k_BTE_5^{(2)}\right\}\exp\left(-\frac{E_5^{(0)}}{k_BT}\right) \end{aligned} \tag{3.29}$$

Nevertheless, as it was pointed previously with the discussion made in Figure 3.5, for systems with a strong spin-orbit coupling, the susceptibility can be approximated taking into account the magnetic properties of only the ground Kramer's doublet at energy $E_{5,6}^{(0)}$. Thus, the magnetic susceptibility for the parallel and perpendicular components becomes as (3.30), where u corresponds to the $\parallel$ or $\perp$ directions. The total magnetic susceptibility of a powder sample is obtained through equation (2.22)

as introduced in Chapter 2.

$$\begin{gathered}\chi_u = \frac{N_A {\mu_B}^2 {g_u}^2}{4k_B T} + \mathrm{TIP}_u\,; \\ g_\parallel = \left|2\left(\frac{\kappa + 1 - a^2}{1 + a^2}\right)\right|\,; \qquad g_\perp = \left|2\left(\frac{\sqrt{2}\kappa a - a^2}{1 + a^2}\right)\right|\,; \\ \mathrm{TIP}_\parallel = -\frac{2N_A {\mu_B}^2}{\kappa\lambda}\frac{(\kappa + 1 - ab)^2}{(1 + a^2)\,(1 + b^2)\,Z}\,; \\ \mathrm{TIP}_\perp = -\frac{2N_A {\mu_B}^2}{\kappa\lambda}\left[\frac{\left[\kappa(a+b) - ab\sqrt{2}\right]^2}{2Z(1+a^2)(1+b^2)} - \frac{(\sqrt{2} - \kappa a)^2}{(1+a^2)(\nu - 1.5 - Z)}\right]\end{gathered} \tag{3.30}$$

In this sense, the experimental thermal dependence of the $\chi_M T$ product on polycrystalline samples is expected to follow a straight line of the type, $\chi_M T = A + BT$, with A being the Curie constant $\left(\frac{N_A {\mu_B}^2 {g_{av}}^2}{4k_B}\right)$, where $\left(g_{av} = \frac{g_\parallel + 2g_\perp}{3}\right)$, and B the average TIP $\left(\mathrm{TIP}_{av} = \frac{\mathrm{TIP}_\parallel + 2\mathrm{TIP}_\perp}{3}\right)$.

Additionally, for a system with $\lambda < 0$ Figure 3.6a shows the calculated values of the g-factors in the parallel and perpendicular components as a function of the distortion parameter, and different values of the orbital reduction factor. It can be seen how for $\Delta = 0$, g_u becomes isotropic, that is $\left(g_\parallel = g_\perp = 2\right)$ for $\kappa = 1$. When $\nu > 0$ $(\Delta < 0)$, with an increase of the tetragonal distortion, the values of $g_\parallel$ increases whilst those of $g_\perp$ decreases, so $g_\parallel > g_\perp$. In the limit of highly negative values of Δ for $\kappa = 1$, $g_\parallel$ becomes *ca.* 4 whereas $g_\perp \approx 0$, so $g_{av} = 4/3$. In the case where $\nu < 0$ $(\Delta > 0)$, $g_\parallel$ first decreases, reaches a minimum and then increases. For $g_\perp$ the opposite situation occurs, first it increases until reaching a maximum and then it slowly decreases, so $g_\parallel < g_\perp$. In the limit of a strong positive distortion, the g-factors become isotropic again being $g_\parallel = g_\perp = 2$. In both cases, the decrease of κ implies an effective decrease of the g-value. In Figure 3.6b, the average g-values obtained through $\left(g_{av} = \frac{g_\parallel + 2g_\perp}{3}\right)$ are shown for different κ factors.

Lastly, some aspects of the TIP deserve to be discussed. Figure 3.7 shows the behaviour of TIP for different κ values as a function of ν with an estimated value of $\lambda \approx -5000$ cm^{-1}. The maximum average TIP value is reached when $\nu = 0$ $(\Delta = 0)$. Moreover, for $\Delta < 0$, the TIP_{av} is greater than that for $\Delta > 0$. As a noteworthy remark, the values of TIP strongly increases with the decrease of $\kappa\lambda$, that is with the increase of the covalence or the decrease of spin-orbit coupling effects.

The one-dimensional compounds described in Article 7 and Article 8 have been treated roughly considering a chain model with an effective isotropic spin of $S = 1/2$ for Ir(IV) and Cu(II) metal ions, with the spin Hamiltonian described in (1.69). Moreover, for the magnetic study of these chain compounds, an isotropic Zeeman operator as the one in (1.25) was considered, where $g = g_{Cu} = g_{Ir}$. Indeed, the model simplifies the real system, where same g-values are assigned to both metal ions ignoring the orbital contribution present in Ir(IV) along with the ZFS effects that it exhibits. However, there is a lack of an adequate theoretical model that enables to quantitative analyse in detail the magnetic exchange coupling between both metal ions, that is a non-trivial problem. Besides, magnetic exchange coupling between chains by short intermolecular interactions were also neglected, so isolated

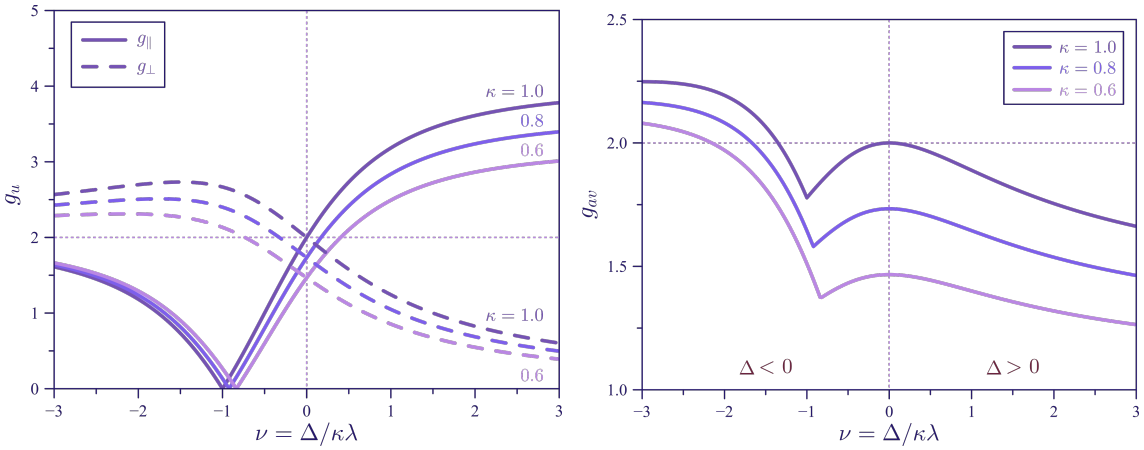

(a) **(b)**

Figure 3.6: Calculated g values ($u = \parallel$ or $\perp$) for a t_{2g}^5 electronic configuration ($\lambda < 0$), as a function of a positive and negative tetragonal distortion (ν), and different values of the orbital reduction factor (κ). For (a) the parallel and perpendicular components, and (b) the average value, being $g_{av} = \frac{g_\parallel + 2g_\perp}{3}$.

chains were considered.

As a result of this considerations, the analysis of the magnetic susceptibility was carried out by means of the Bonner–Fisher numerical expression (1.70) for an antiferromagnetic interaction between Ir(IV) and Cu(II) centres, and through Baker-Rushbrooke numerical expression (1.72) for ferromagnetic interactions between metal ions.

3.2 Ir(IV) coordination chemistry

Iridium compounds can be found in a very wide variety of oxidation states, from -III to IX.[2–4] Although up to the date of this Thesis work, it has never been isolated a stable Ir(-II) compound.[5] Nevertheless, the most common oxidation states are those involving Ir(I) and Ir(III). As a result, due to their unique physical properties these complexes have been intensively studied, where several potential applications in different fields of technological interest, such as catalysis, imaging, sensing or medical therapies have been developed during the last decades.[6–12]

As Ir(I) compounds are generally square planar and Ir(III) octahedral, both oxidation states form complexes with a diamagnetic ground state. In contrast, Ir(IV) in an octahedral or tetragonally distorted octahedral environment has an unpaired electron with an important first-order spin-orbit contribution due to its $^2T_2$ fundamental term, which indeed make its magnetic behaviour less easy to treat when compared with other electronic configurations. Nonetheless, this non-Curie characteristic behaviour that can be display even at room temperature is what makes the Ir(IV) also interesting to explore. Thus, salts of $[IrCl_6]^{2-}$ anion were used in the classic first Electronic Paramagnetic Resonance (EPR) experiments, to demonstrate the delocalization of unpaired electrons onto the chloride ligand, where the unpaired electron spends 30% or more of its time in the ligand orbitals.[13]

From a crystallographic point of view, the most simple structures containing the

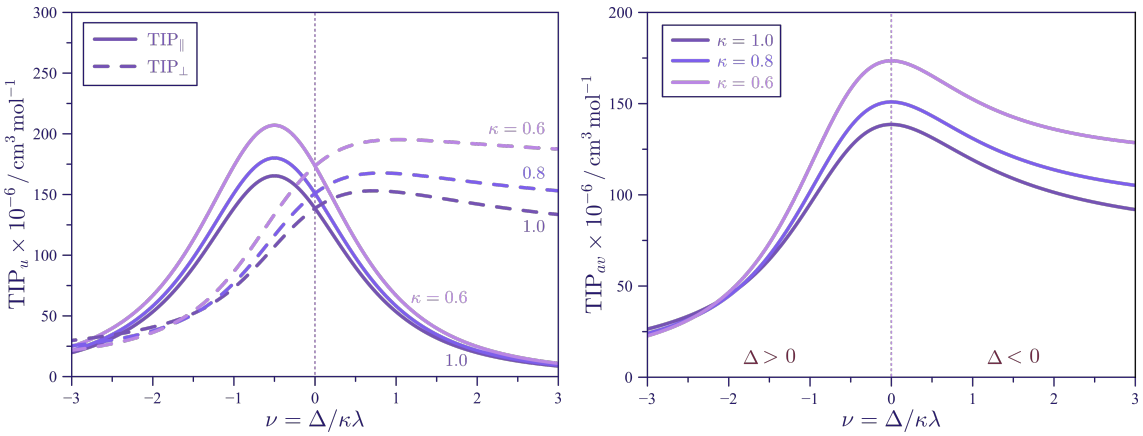

Figure 3.7: Calculated TIP values as a function of ν and κ, for a t_{2g}^5 electronic configuration with $\lambda \approx -5000$ cm^{-1}, under a tetragonal distortion for (a) the parallel and perpendicular components, and (b) the average value, being $\left(\text{TIP}_{av} = \frac{\text{TIP}_{\parallel}+2\text{TIP}_{\perp}}{3}\right)$.

Ir(IV) ion are the hexahalo complexes, $[IrX_6]^{2-}$ (X = F, Cl, and Br), which have been known for a long time, except for the hexaiodo derivative, where the strongly oxidising character of Ir^{4+} makes it difficult to coexist with the reducing I^- anion. Moreover, hexahaloiridate(IV) compounds are known for reducing into their analogous Ir(III) complexes in acid aqueous media or with help of mild reducing agents, such as oxalate, H_2S or Fe^{2+}. Thus, they are normally used in their preparations.[14,15] The mainly factor responsible of the reduction is the increased stability of the Ir(III) ion as consequence of the high stabilization of the low-spin d^6 configuration in octahedral environments. As generally happens with 5*d* transition metals, they are more kinetically inert to undergo ligand substitution reactions, so it is commonly necessary to perform their reactions heating together with a ligand excess. Nevertheless, the ligand substitution of Ir(IV) complexes must be taken carefully as iodine or ligands with phosphorus, arsenic, and sulphur donor atoms are not stable because they reduce Ir(IV) to the Ir(III) state in aqueous and organic solvents.[16–18] Despite of that, it is possible to explore the re-oxidation of the formed Ir(III) complexes to Ir(IV).[19–22]

Salts of hexachloroiridate(IV) are normally prepared by oxidation of metallic iridium with Cl_2, mixed with an alkali metal halide. On the other hand, bromo derivatives are commonly obtained treating the previously prepared chloro analogues with high concentrations of HBr acid.[15,23] Nevertheless, hexachloro- and hexabromoiridate(IV) salts and acids are commercially available and affordable. In contrast, the hexafluoridoiridate(IV) salts are not commercially accessible and they require the use of the chloro or bromo derivatives as starting materials along with BrF_3 or direct F_2 as fluorinating agents.[24,25]

From a magnetism point of view, the susceptibility measurements of different mononuclear hexahaloiridate(IV) salts with several alkali metals, and some organic countercations, are known since more than 70 years ago. However, most of the studies were related only to $[IrCl_6]^{2-}$ species with measurements at room temperature or only down to *ca.* 80 K, with a few exceptions for the $(NH_4)_2[IrCl_6]$ and $K_2[IrCl_6]$ salts, whose measurements were performed down to 2 K. Moreover, the magnetic

behaviour of the hexabromo- and hexafluoroiridate(IV) complexes was rarely investigated.[23,26–28]

More recent studies related to $Na_2[IrCl_6]{\cdot}xH_2O$ species with different grades of hydration ($x = 0$, 2 and 6) have revealed that for the anhydrous and $x = 2$ species, the compounds behave as weak ferromagnets arising from a canted antiferromagnetic disposition. Their ordering temperatures being 7.4 and 2.7 K, respectively, with coercive fields below 1 kØe.[29] Furthermore, when the sodium is replaced by a bulkier cation, the different mononuclear Ir(IV) entities are more isolated and SIM behaviour at low temperature is observed.[25,30] On the other hand, the use of cations able to display electric conductivity together with the hexahaloiridate(IV) entities, could lead to semiconducting charge-transfer salts while keeping the magnetic properties of the Ir(IV) metal ion, as in the case of the $(BEDT\text{-}TTF)_2[IrCl_6]$ compound.[31]

As a noteworthy remark, the use of the $[IrX_6]^{2-}$ entities as metalloligands towards other metallic ions, along with their utility as potential precursor to synthesise new mononuclear complexes, has been scarcely explored. In this regard, $\{IrF_5(\mu\text{-}F)Co_3(dpa)_4 \cdot 2DMF\}_n$ (dpa = 2,2'-dipyridyl-amine) one-dimensional compound, schematised in Figure 3.8, is one of the few examples found in the literature.[32] Perhaps, part of the cause is due to the lack of an adequate theoretical model to treat the magnetic behaviour of these Ir(IV)-based compounds. After all, an appropriate model needs to take into account the different 'g'-values attributed to each paramagnetic ion in heteropolynuclear compounds, along with the ZFS effects from the Ir(IV) ion, besides of the intermolecular interactions that can occur. For these reasons, the analysis in detail of the whole $\chi_M T$ curve is normally precluded in either salts or coordination polymers.[25,29–32]

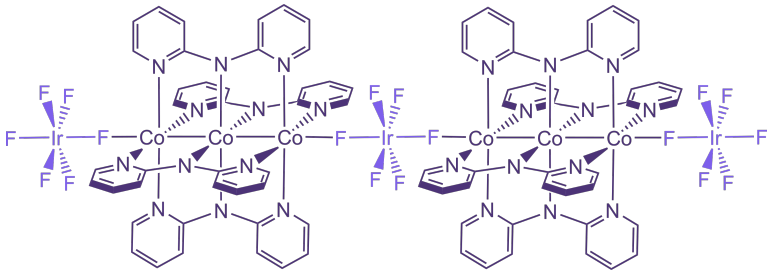

Figure 3.8: Schematic structural representation of the $\{IrF_5(\mu\text{-}F)Co_3(dpa)_4\}_n$ one-dimensional compound. The $[IrF_6]^{2-}$ anionic unit has been highlighted.

3.3 References

(1) P. W. Atkins, M. S. C.; Phillips, C. S. G. *Tables for group theory*; Oxford University Press: Oxford, UK: 2006, p 27.

(2) Wang, G.; Zhou, M.; Goettel, J. T.; Schrobilgen, G. J.; Su, J.; Li, J.; Schlöder, T.; Riedel, S. *Nature* **2014**, *514*, 475–477.

(3) Payne, D. *Nat. Chem.* **2016**, *8*, 392–392.

(4) Yellowlees, L.; Macnamara, K. *Comprehensive Coordination Chemistry II, Vol.6*; Elsevier Science: Pergamon, UK: 2003, pp 147–246.

(5) Ritter, S. K. *Chem. Eng. News* **2014**, *92*, 7.

(6) Vaska, L.; DiLuzio, J. W. *J. Am. Chem. Soc.* **1962**, *84*, 679–680.

(7) Crabtree, R. *Acc. Chem. Res.* **1979**, *12*, 331–337.

(8) Iglesias, M.; Oro, L. A. *Chem. Soc. Rev.* **2018**, *47*, 2772–2808.

(9) Yang, Y.; Zhao, Q.; Feng, W.; Li, F. *Chem. Rev.* **2013**, *113*, 192–270.

(10) Kar, B.; Das, U.; Roy, N.; Paira, P. *Coord. Chem. Rev.* **2023**, *474*, 214860.

(11) Yip, A. M.-H.; Lo, K. K.-W. *Coord. Chem. Rev.* **2018**, *361*, 138–163.

(12) Caporale, C.; Massi, M. *Coord. Chem. Rev.* **2018**, *363*, 71–91.

(13) Griffiths, J. H. E.; Owen, J.; Ward, I. M.; Bleaney, B. *Proc. R. Soc. Lond. A* **1953**, *219*, 526–542.

(14) Fine, D. A. *Inorg. Chem.* **1969**, *8*, 1014–1016.

(15) Fergusson, J. E.; Rankin, D. A. *Aust. J. Chem.* **1983**, *36*, 863–869.

(16) Kauffman, G. B.; Hogarth, J. W.; Dwyer, F. P. *Inorganic Syntheses Vol. 7*; John Wiley and Sons Ltd.: New York, USA: 1963, pp 224–228.

(17) Sharutin, V. V.; Sharutina, O. K.; Senchurin, V. S.; Somov, N. V. *Russ. J. Inorg. Chem.* **2016**, *61*, 969–974.

(18) Mura, P.; Casini, A.; Marcon, G.; Messori, L. *Inorg. Chim. Acta* **2001**, *312*, 74–80.

(19) Cipriano, R. A.; Levason, W.; Pletcher, D.; Powell, N. A.; Webster, M. *J. Chem. Soc., Dalton Trans.* **1987**, 1901–1910.

(20) Cipriano, R. A.; Hanton, L. R.; Levason, W.; Pletcher, D.; Powell, N. A.; Webster, M. *J. Chem. Soc., Dalton Trans.* **1988**, 2483–2490.

(21) Kruszyna, H. G.; Bodek, I.; Libby, L. K.; Milburn, R. M. *Inorg. Chem.* **1974**, *13*, 434–438.

(22) Hoag, C. M.; Hanrahan, R. J. *Int. J. Chem. Kinet.* **2004**, *36*, 623–626.

(23) Norman, V.; Morrow, J. C. *J. Chem. Phys.* **1959**, *31*, 455–459.

(24) Hepworth, M. A.; Robinson, P. L.; Westland, G. J. *J. Chem. Soc.* **1954**, 4269–4275.

(25) Pedersen, K. S. et al. *Nat. Comm.* **2016**, *7*, 12195.

(26) Hepworth, M. A.; Robinson, P. L.; Westland, G. J. *J. Chem. Soc.* **1958**, 611–613.

(27) Sloth, E. N.; Garner, C. S. *J. Chem. Phys.* **1954**, *22*, 2064–2066.

(28) Cooke, A. H.; Lazenby, R.; McKim, F. R.; Owen, J.; Wolf, W. P.; Bleaney, B. *Proc. R. Soc. Lond. A* **1959**, *250*, 97–109.

(29) Bao, S.-S.; Wang, D.; Huang, X.-D.; Etter, M.; Cai, Z.-S.; Wan, X.; Dinnebier, R. E.; Zheng, L.-M. *Inorg. Chem.* **2018**, *57*, 13252–13258.

(30) Liu, S.-B.; Huang, X.-D.; Bao, S.-S.; Kurmoo, M.; Zheng, L.-M. *Cryst. Growth Des.* **2019**, *19*, 4836–4843.

(31) Kepert, C. J.; Kurmoo, M.; Day, P. *J. Mater. Chem.* **1997**, *7*, 221–228.

(32) Cortijo, M.; Bulicanu, V.; Pedersen, K. S.; Rouzières, M.; Bendix, J.; Clérac, R.; Hillard, E. A. *Eur. J. Inorg. Chem.* **2018**, 320–325.

Article 6

J. Coord. Chem., **2022**, *17-18(75)*, 2495-2507

https://doi.org/10.1080/00958972.2022.2117036

From page 189 to page 206

Article 7

Dalton Trans., **2019**, *48*, 13925-13930

Volume 48 | Number 37 | 7 October 2019 | Pages 13891–14208

Dalton Transactions

An international journal of inorganic chemistry

rsc.li/dalton

ISSN 1477-9226

ROYAL SOCIETY OF CHEMISTRY | Celebrating IYPT 2019

PAPER

Adrián Sanchis-Perucho and José Martínez-Lillo

Ferromagnetic exchange interaction in a new Ir(IV)–Cu(II) chain based on the hexachloroiridate(IV) anion

https://doi.org/10.1039/C9DT02884F

From page 210 to page 218

Article 8

Dalton Trans., **2022**, *51*, 3323-3330

https://doi.org/10.1039/D1DT04384F

From page 221 to page 236

3.4 Additional information

Compounds $(NBu_4)_2[IrX_6]$ (X = Cl and Br), presented in Article 7 and Article 8, respectively, have been fitted with the magnetic model provided in section 3.1. As expected, a straight line is observed for these compounds, being the sharp decrease at low temperatures in the chloro derivative mostly due to the occurrence of weak intermolecular interactions through Cl···Cl contacts. For this reason, a more satisfactory match of the experimental $\chi_M T$ curve is achieved through equation (3.30) with the introduction of the Weiss constant as $(T-\theta)$, in order to take into account the intermolecular magnetic interactions. The best least-squares fit of the data for both compounds is shown in Figure 3.9, where the R values are 8.0×10^{-6} and 1.2×10^{-5} for chloro and bromo derivatives, respectively, being R the agreement factor described as $\sum_i \left[(\chi_M T)_i^{calcd} - (\chi_M T)_i^{obs}\right]^2 / \sum \left[(\chi_M T)_i^{obs}\right]^2$. Their fit values are summarised in Table 3.5, where additionally, the previous Curie-Weiss fit parameters for the chloro derivative have also been included for comparison, which are in agreement with those obtained herein. Unfortunately, due to the strong correlation

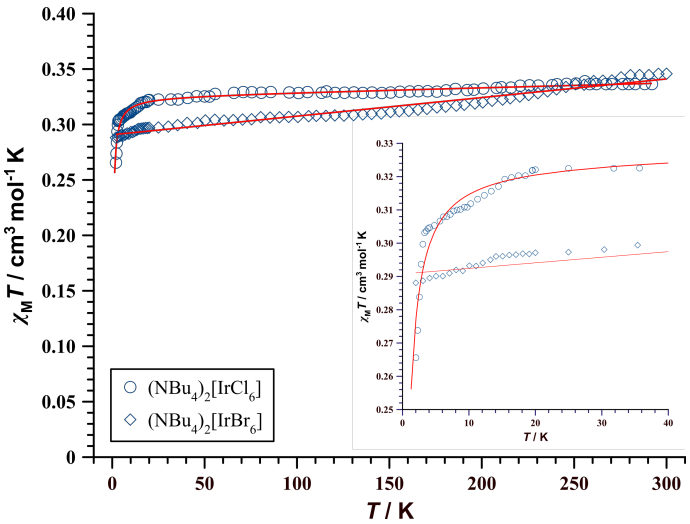

Figure 3.9: Thermal variation of the $\chi_M T$ product for $(NBu_4)_2[IrX_6]$ (X = Cl and Br). The solid red line represents the best-fit of the experimental data (see text), and the inset shows on detail the low temperature domain.

Table 3.5: Best-fit magnetic parameters for $(NBu_4)_2[IrX_6]$ (X = Cl and Br) compounds.

Compound	C / cm^{3}mol^{-1}K	g_{av}	θ / K	TIP$\times 10^{-6}$ / cm^{3}mol^{-1}
X = Cl	0.325 (0.335)[a]	1.87 (1.90)[a]	−0.35 (−0.9)[a]	41.7 (-)[a]
X = Br	0.291	1.76	-	167.8

[a] In parenthesis previously reported values in Article 7.

between κ, λ and Δ parameters acting in the whole $\chi_M T$ range describing a straight line, it is hard to asses the parameters for validating the model. Moreover, because of the large correlation existing between diamagnetism and TIP, the experimental

magnetic susceptibility measurements must be carefully corrected for the diamagnetism of the constituent atoms and also for the sample holder, in order to avoid big errors in the κ, λ and Δ determination.

As it was seen in Figure (3.6a), the sign of Δ can be confirmed from the g-factors, so it would be sensible to perform EPR experiments to the samples. Moreover, well resolved signals in the EPR spectra will lead to unambiguous determination of the values of the g-factors, so more information will be available and a better fit of all parameters will be possible.

CHAPTER 4

HOLMIUM

4.1 Theoretical magnetic model for a f^{10} ion system

Free rare earth ions can present partially occupied $4f$ orbitals and, hence, potential magnetically active electrons. However, those electrons are very efficiently shielded by inner fully occupied orbitals, chiefly the $5s^2$ and $5p^6$ orbitals that came before in energy to the $4f$. As consequence, these $4f$ orbitals are almost uninvolved with bonds between a rare earth ion and its nearest neighbours. Therefore, the influence of the environment on the magnetic properties is much less pronounced for a rare earth compound that for the previously seen $5d$ compounds. On the other hand, it is important to take into account that the polyelectronic spin-orbit coupling constant value, $|\lambda|$, is larger than for $3d$ ions. For this reason, the bielectronic repulsion will be considered first, and thus the energy terms from a Russell-Saunders approach will be obtained. Secondly, the spin-orbit coupling effects may partially removed the degeneracy of the ground term into vary J states. In order to keep track of S, L and J for every term in a lanthanide metal ion, they will be written as ${}^{(2S+1)}L_J$ from now on. Lastly, the action of the ligand field potential when the symmetry of the system is low enough, may split the several M_J components from a ${}^{(2S+1)}L_J$ term into different levels and significant ZFS effects may arise. For this reason, despite of being the ligand field less energetic than the interelectronic repulsion and the spin-orbit coupling, the distortion of the symmetry of the system is the ultimately responsible of splitting the ${}^{(2S+1)}L_J$ ground state required for the magnetic anisotropy of the lanthanide metal ions.

Nevertheless, as consequence of the weak ligand field, it is possible to obtain a good first approximation close to the real average value of $\chi_M T$ at room temperature, where the ligand field effects can be neglected. Thus, from a free ion perspective with spin-orbit effects, the magnetic susceptibility formula presented in (4.1) follows the Curie law. Remarkably, its derivation is rigorously parallel to the derivation for (1.47).

$$\chi_M = \frac{N_A {\mu_B}^2 {g_J}^2}{3k_B T} J(J+1); \qquad g_J = \frac{3}{2} + \frac{S(S+1) - L(L+1)}{2J(J+1)} \tag{4.1}$$

The presence of excited states not too far in energy from the ground state would add a significant TIP contribution to the magnetic susceptibility. This contribution has been calculated as

$$\text{TIP} = \frac{2N_A {\mu_B}^2 (g_J - 1)(g_J - 2)}{3\lambda} \tag{4.2}$$

Besides, the molar magnetisation can also be described for a free ion with spin-orbit coupling effects, in the same way it was deduced previously for a free ion

without these effects in section 1.2. Its expression is shown in equation (4.3), where $B(y)$ represents the Brillouin function previously defined in (1.51), but with J instead of S in this case.

$$M = N_A g_J \mu_B J B(y); \qquad y = \frac{g_J \mu_B S}{k_B T} H \tag{4.3}$$

Although for most of the lanthanide ions the measured $\chi_M T$ at room temperature are rather close to the calculated values with equation (4.1), the situation is quite different when there are thermally populated excited states, like for example in Sm(III) ($4f^5$), Sm(II) or Eu(III) ($4f^6$) systems. Nevertheless, that is not the case for the Ho(III) metal ion, and is out of the scope of this dissertation. Moreover, it does not mean that the free ion approximation allows to interpret all the details of the magnetic properties for the rest of lanthanides. In most cases, the situation is much more complex. Indeed, as the temperature is lowered the splitting effects on the ${}^{(2S+1)}L_J$ ground state due to the ligand field potential will be of great importance. If the ligand field has an axial distorted symmetry, which is the most likely for molecular compounds, it will give rise to a number of components separated by a difference of a few tens to few hundreds of wavenumbers, depending on the multiplet width. When the width is small enough, all the components arising from the ${}^{(2S+1)}L_J$ term are statically populated at room temperature and the free ion approximation applies. However, as the temperature is lowered, the components of higher energy are successively depopulated and the free ion approximation becomes less and less valid. This may have two consequences. First, the magnetic susceptibility does not follow the Curie law. Second, the system becomes more and more anisotropic on cooling. Indeed, the magnetic anisotropy always increases as the temperature is lowered. Moreover, when the multiplet width is larger, the higher in energy M_J components are not statistically populated even at room temperature. Hence, the system may present a significant magnetic anisotropy. In such cases, the fact that the average value of $\chi_M T$ is close to the value predicted in the free ion approximation may be somewhat fortuitous.

In the case of Ho(III) complexes, the energy term corresponding to a $4f^{10}$ electronic configuration is ${}^5\mathrm{I}$ ($S = 2$ and $L = 6$), which was deduced in the same way it was done for $5d$ metal ions in the past Chapters. Moreover, the polyelectronic spin-orbit coupling constant has a negative value, hence, the lower energy state is the one with the highest value of J. Thus, the ground state corresponds to the ${}^5\mathrm{I}_8$ term. The most near excited state, ${}^5\mathrm{I}_7$, is well separated from ${}^5\mathrm{I}_8$, to *ca.* 4300 cm^{-1}. As a result, the ground state can be considered the only one populated even at room temperature. Any deviation of the calculated magnetic susceptibility by the free ion approximation from the observed values in Ho(III) compounds are attributed to the action of the ligand field potential on the ${}^5\mathrm{I}_8$ ground state. Indeed, as the spin multiplicity $(2S+1)$ is an odd number, the ground state will split into eight Kramer doublets (M_J from $\pm$ 1 to $\pm$ 8) and one singlet $M_J = 0$ due to the combined effect of the spin-orbit coupling and an axial distortion of the symmetry. In Figure 4.1 is depicted the energy diagram of an Ho(III) with $M_J = 0$ as its ground state.

Following the free ion with spin-orbit coupling approximation, the g_J and $\chi_M T$ values calculated at room temperature from equation (4.1) for Ho(III) compounds are expected to be 5/4 and 14.07 $\mathrm{cm}^3\mathrm{mol}^{-1}\mathrm{K}$, respectively.

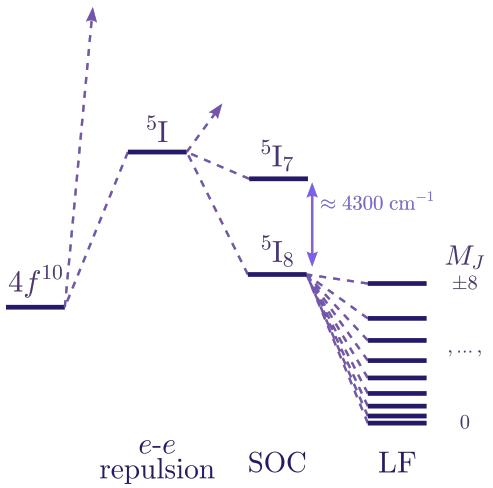

Figure 4.1: Energy diagram with sequential perturbations for Ho(III) compounds, where it is considered a $M_J = 0$ as ground state. From left to right, *e-e* repulsion stands for the bielectronic interaction, SOC for the spin-orbit coupling and LF for the ligand field potential with an axial distortion. The Zeeman interaction splits every M_J component. The diagram is not at scale.

On the other hand, the occurrence of magnetic anisotropy can also be demonstrated from the magnetisation curves, where the saturation of the magnetisation achieved will be different from the one expected by the free ion approximation, as long as the several components of the ground state present different magnetic moments, and as consequence, different contributions to the total magnetic behaviour of a system. Moreover, in order for the temperature to be able to change the populations between components, the energy separation between them due to the anisotropy must not be too high. Additionally, the M *vs.* H/T curves or isothermal curves, show the magnetisation without the effect of the temperature. Thus, in anisotropic systems different isothermal magnetisations curves do not superpose between them, as consequence of being the various components, with different populations, depending on the temperature before applying the external field. In contrast, in isotropic systems all components share the same populated state before applying the external field and, therefore, they are independent of the temperature and the isothermal magnetisations curves do superpose.

Nevertheless, the simulation of the magnetic properties outside the free ion approximation is possible, but the first requirement is to describe the effect of the ligand field in a satisfying fashion. For rare earth compounds the electrostatic model seems to be suitable. Thus, the LF potential describes the effect of the electric field due to the surrounding ligands acting on the lanthanide ion, splitting the electronic ground state multiplet of the free ion, described by its total angular momentum, J, into their M_J components depending on the symmetry. Following the Stevens formalism, the Hamiltonian of this interaction is presented in (4.4), where the equivalent operators $\widehat{O}_k^q$ are denoted as Stevens operators and expressed as polynomials of the total angular momentum operators, k is the operator order restricted up to $k \leq 7$ for f-electrons with q going from $-k$ to k, as a result, the ranges of k and q are limited to a maximum of 27 parameters. $\langle r^k \rangle$ are the radial part factors, A_k^q are numerical parameters that depend on the nature of the ligand shell, being the products $A_k^q \langle r^k \rangle$

the parameters to be determined in the data fit, and θ_k are the Stevens coefficients tabulated for the different f^n configurations and for the different k values. The operators with k even (0, 2, 4, 6) are responsible for the ligand field splitting, hence the ones used for the magnetic description, whereas those with k odd (1, 3, 5, 7) are responsible for the intensity of the induced electric dipole transitions in optical spectroscopy.[1–6]

$$\widehat{\mathcal{H}}_{LF} = \sum_{k,q} A_k^q \langle r^k \rangle \theta_k \widehat{O}_k^q \tag{4.4}$$

Equation (4.4) is a convenient way of calculating the energies from the ground state $|J, M_J\rangle$ wave-functions, where the corresponding matrix elements can be easily computed if the mixing between different J multiplets, second-order interactions, are neglected. Moreover, the magnetic perturbation is evaluated together with the ligand field splitting through an anisotropic Zeeman operator over the $|J, M_J\rangle$ functions, similar to the one used in (2.12) and (2.13) for the parallel and perpendicular component, respectively. Nevertheless, when the basis set is restricted to the ground state multiplet, it provides a reasonable description of the magnetic properties, but it fails in describing another interesting property of lanthanides as optical absorption or luminescence, which have different multiplets as initial and final states. In this ligand field approach, however, the chemical intuition tends to vanish with parameters that does not have, *a priori*, correlation with parameters with physical meaning.

Nonetheless, the ligand field Hamiltonian in (4.5) along with the Zeeman operator was used for a full description of the magnetic susceptibility curve of the Ho(III) compound described in Article 9, where the ligand field symmetry determines which parameters of the 27 combinations of k and q are non-zero. For a D_{3h} symmetry, the only non-zero parameters responsible for the crystal field splitting are presented in equation (4.5). A complete table of allowed parameters as a function of their point-group symmetry is listed elsewhere.[1,3]

$$\widehat{\mathcal{H}}_{LF} = A_2^0\langle r^2\rangle\theta_2\widehat{O}_2^0 + A_4^0\langle r^4\rangle\theta_4\widehat{O}_4^0 + A_6^0\langle r^6\rangle\theta_6\widehat{O}_6^0 + A_6^6\langle r^6\rangle\theta_6\widehat{O}_6^6 \tag{4.5}$$

Moreover, the relevant Stevens operators used for a D_{3h} symmetry are gathered in Table 4.1. A more complete table of Stevens operators can be found in the literature.[2,3,5]

Table 4.1: Relevant Stevens $\widehat{O}_k^q$ operators for D_{3h} symmetry expressed in terms of $\widehat{J}_z$, $\widehat{J}_+$ and $\widehat{J}_-$ polynomials.

k	q	$\widehat{O}_k^q$
2	0	$3\widehat{J}_z^2 - J(J+1)$
4	0	$35\widehat{J}_z^4 - [30J(J+1) - 25]\widehat{J}_z^2 + 3J^2(J+1)^2 - 6J(J+1)$
		$231\widehat{J}_z^6 - [315J(J+1) - 735]\widehat{J}_z^4$
6	0	$+[105J^2(J+1)^2 - 525J(J+1) + 294]\widehat{J}_z^2$
		$-5J^3(J+1)^3 + 40J^2(J+1)^2 - 60J(J+1)$
6	6	$\frac{\widehat{J}_+^6 + \widehat{J}_-^6}{2}$

4.2 Magneto-caloric effect and refrigeration

The Magneto-caloric effect (MCE) is the temperature variation of a material subjected to a magnetic field variation under adiabatic conditions, produced by a change on the magnetic entropy of the material.[1,7–9]

In order to explain the origin of the magneto-caloric effect, it is necessary to relate the magnetic variables as magnetisation, M, and the external field, H, to entropy, S_E, and temperature, T, by the use of thermodynamics. To begin with, the definition of entropy of a system in statistical thermodynamics is of the form $S_E = k_B \ln(\Omega)$, where Ω represents the accessible, and non-degenerate, states. Since a magnetic moment of spin S has $(2S+1)$ magnetic levels, the entropy content per mole of substance associated with the magnetic degrees of freedom between $T = 0$ and $T = \infty$ becomes (4.6), where R is the gas constant, and S represents the effective spin with $(2S+1)$ describing the multiplicity of the states taking part in the magnetic process.

$$S_m = R \ln(2S+1); \quad R = k_B N_A \tag{4.6}$$

When a magnetic material is magnetised by the application of an external magnetic field, it changes its magnetic order, hence its magnetic entropy, S_m. However, in adiabatic conditions the total entropy of the system must remain constant during the magnetic field change, then ΔS_m must be compensated for by an equal but opposite variation of the entropy associated with the lattice, resulting in a change in the temperature of the material, ΔT_{ad}. As consequence, both ΔS_m and ΔT_{ad} represent the characteristic parameters of the MCE. In Figure 4.2 there is a representation of the process, where it is easy to see that if the magnetic change ΔH reduces the magnetic entropy ($\Delta S_m < 0$), then ΔT_{ad} is positive, whereas for $\Delta H > 0$, ($\Delta S_m > 0$ and ΔT_{ad} is negative.

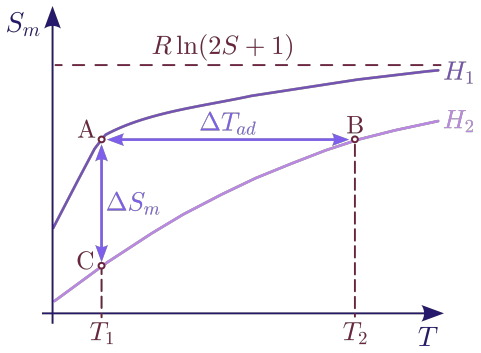

Figure 4.2: Molar magnetic entropy as a function of temperature illustrating the existence of the magneto-caloric effect for two different fields, being $H_1 < H_2$. The adiabatic process, A $\rightarrow$ B, providing ΔT_{ad}, and the isothermal magnetization, A $\rightarrow$ C, providing ΔS_m. The maximum magnetic entropy is also indicated.

In order to establish the relationship between H, M and T to the MCE terms, ΔT_{ad} and ΔS_m, the Maxwell equation (4.7) for the magnetic entropy is considered

for the MCE evaluation.[10]

$$\left[\frac{\partial S_m(T,H)}{\partial H}\right]_T = \left[\frac{\partial M(T,H)}{\partial T}\right]_H \tag{4.7}$$

Integrating (4.7) for an isothermal process, it is obtained (4.8), which indicates that ΔS_m is proportional to both the derivative of magnetisation with respect to temperature at constant field and to the field variation. A numerical approach can be used, but the accuracy of ΔS_m calculated from the magnetisation experiments depends on the accuracy of the measured M, T and H parameters, replacing the differentials by the measured variations (ΔM, ΔT, ΔH).

$$\Delta S_m(T,\Delta H) = \int_{H_i}^{H_f} \left[\frac{\partial M(T,H)}{\partial T}\right]_H dH \tag{4.8}$$

An interesting application of the MCE is that they can be used for refrigerating purposes through a process known as adiabatic demagnetisation. First, the magnetocaloric material is placed in a thermally insulated (adiabatic) environment and the magnetic field is applied to carry the adiabatic magnetisation. The material heats up due to the above-mentioned MCE and the produced heat is extracted by a exchange media, while the magnetic field is held constant. Once the material has cooled down to the starting temperature, it is brought back to the adiabatic conditions and then the magnetic field is removed. In this way, as the total entropy of the system must not change, and the magnetic entropy of the system has increased, the lattice entropy must decrease, and as a result, the material is cooled by adiabatic demagnetisation. The material is then put in contact with whatever wants to be refrigerated, heating itself. Thus, a cooling cycle can then be realised in an iterative process, as the one depicted in Figure 4.3.

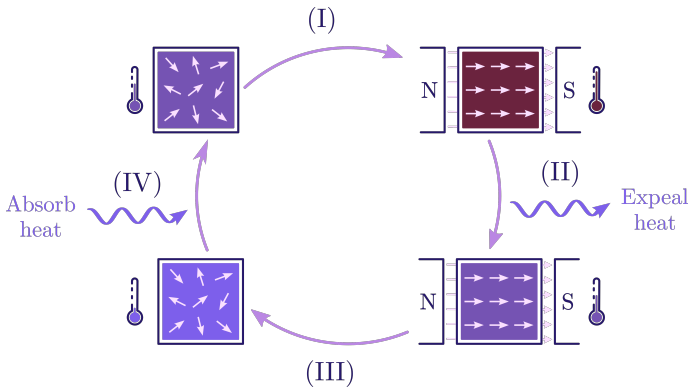

Figure 4.3: Illustration of a thermodynamic cycle with a magnetic refrigerator with classical spin representation. The cycle consists of four steps. In step (I), the adiabatic magnetisation is carried by an external field that orders the spin system under adiabatic conditions heating the material. In step (II), the adiabatic conditions are broken for the extraction of the heat. In step (III) the adiabatic conditions are back and the adiabatic demagnetisation is performed by removing the external magnetic field, which leads to the cooling of the material. Step (IV) closes the cycle by putting the cooled material again in thermal contact, but this time with the media that is wanted to cool.

All magnetic systems intrinsically present MCE as they are able to align their magnetic moments with the external field. However, the intensity of the effect depends on the properties of each material. As for example, if they present intermolecular interactions. Ferromagnetic exchange coupling obtains better performance than non-interacting coupling with a small magnetic field and in a high temperature regime, whereas antiferromagnetic interactions result in the lowest ΔS_m values. For paramagnetic systems, according to the relationship between temperature and magnetization, the MCE becomes effective in this type of compounds only at very low temperatures.

On the other hand, the (4.6) relationship makes clear that a molecule should exhibit a large total effective spin to be a good candidate for producing an efficient cooling, because a high density of the low-lying spin states carries a large entropy change. In the literature are reported spin values up to 83/2.[11] However, even though a high spin value is a relevant point, it is not enough by itself to determine a significant MCE. A fundamental characteristic to have into account is the absence of an anisotropy barrier. For this reason, isotropic Gd compounds constitutes good candidates as cryogenic magnetic coolants.[12]

Nevertheless, in Figure 4.4 it is shown S, L and J values for all Ln(III), where Ho(III) has the biggest J of all lanthanides after the spin-orbit coupling. In this way, the effective available spin states is increased with a magnetic entropy up to $S_m = R \ln(2J+1) = 23.6\ \mathrm{J\,mol^{-1}\,K^{-1}}$ for $J = 8$. However, because of the magnetic anisotropy that the Ho(III) ground state presents the maximal magnetic entropy is reduced, and as a result its magnetic cooling properties are limited.

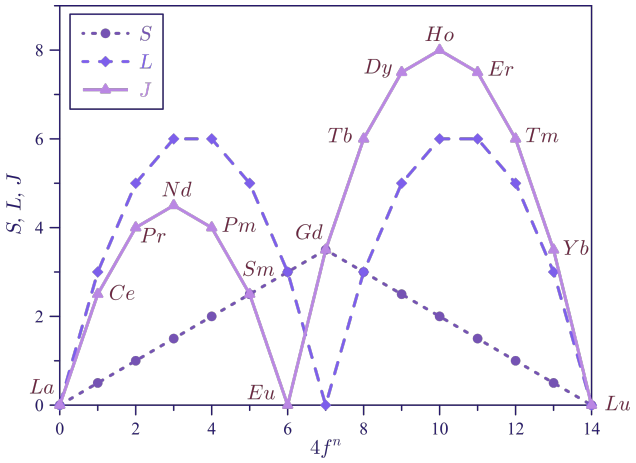

Figure 4.4: S, L and J for $4f^n$ ions according to Hund's rules. In this plot, n is the number of electrons in the $4f^n$ orbital, where all the represented lanthanides were considered to be in (III) oxidation state.

4.3 References

(1) Benelli, C.; Gatteschi, D. *Introduction to Molecular Magnetism: From Transition Metals to Lanthanides*; Wiley-VCH Verlag GmbH & Co. KGaA: Weinheim, Germany: 2015.

(2) Jiang, S.-D.; Wang, B.-W.; Gao, S. *Molecular Nanomagnets and Related Phenomena*; Gao, S., Ed.; Springer: Heidelberg, Germany: 2015.

(3) Richard A. Layfield, M. M. *Lanthanides and Actinides in Molecular Magnetism*; Wiley-VCH: New York, USA: 2015.

(4) Stevens, K. W. H. *Proc. Phys. Soc. A* **1952**, *65*, 209.

(5) Rudowicz, C.; Karbowiak, M. *Coord. Chem. Rev.* **2015**, *287*, 28–63.

(6) Dreiser, J. *J. Phys.: Condens. Matter* **2015**, *27*, 183203.

(7) Evangelisti, M.; Brechin, E. K. *Dalton Trans.* **2010**, *39*, 4672–4676.

(8) Liu, J.-L.; Chen, Y.-C.; Guo, F.-S.; Tong, M.-L. *Coord. Chem. Rev.* **2014**, *281*, 26–49.

(9) Reis, M. S. *Coord. Chem. Rev.* **2020**, *417*, 213357.

(10) Földeàki, M.; Chahine, R.; Bose, T. K. *J. Appl. Phys.* **1995**, *77*, 3528–3537.

(11) Ako, A. M.; Hewitt, I. J.; Mereacre, V.; Clérac, R.; Wernsdorfer, W.; Anson, C. E.; Powell, A. K. *Angew. Chem. Int. Ed.* **2006**, *45*, 4926–4929.

(12) Zheng, Y.-Z.; Zhou, G.-J.; Zheng, Z.; Winpenny, R. E. P. *Chem. Soc. Rev.* **2014**, *43*, 1462–1475.

Article 9

Inorg. Chem., **2021**, *60*, 12719-12723

DECLARATION

Francisco José Martínez Lillo, Professor Titular del Departament de Química Inorgànica de la Universitat de València i **Francisco Lloret Pastor**, Catedràtic del Departament de Química Inorgànica de la Universitat de València

Certifiquen que:

En el treball titulat *Holmium(III) Single-Ion Magnet for Cryomagnetic Refrigeration Based on an MRI Contrast Agent Derivative*, els autors i el seu ordre és 'Borja Rodríguez-Barea, Júlia Mayans, Renato Rabelo, **Adrián Sanchis-Perucho**, Nicolás Moliner, José Martínez-Lillo,* Miguel Julve, Francesc Lloret, Rafael Ruiz-García, and Joan Cano*'. Que el doctorant, Adrián Sanchis Perucho, ha tingut una contribució fonamentalment de caràcter cristal·logràfic, portant a cap el desenvolupament de l'estratègia de mesura i la recol·lecció de les dades de difracció de raigs-X sobre monocristall, així com el refinament de les dades cristal·logràfiques per a la seua resolució estructural.

Per últim, deixar constància que els resultats ací publicats no han sigut emprats implícita o explícitament per cap dels coautors en la realització d'una altra Tesi doctoral.

Paterna, Juny de 2023

FRANCISCO JOSE|MARTINEZ|LILLO

Firmado digitalmente por FRANCISCO JOSE|MARTINEZ|LILLO
Nombre de reconocimiento (DN): cn=FRANCISCO JOSE|MARTINEZ|LILLO, serialNumber=73565126V, givenName=FRANCISCO JOSE, sn=MARTINEZ LILLO, ou=CIUDADANOS, o=ACCV, c=ES
Fecha: 2023.06.05 20:06:18 +01'00'

Francisco José Martínez Lillo

FRANCISCO|LLORET|PASTOR

Firmado digitalmente por FRANCISCO|LLORET|PASTOR
Fecha: 2023.06.05 10:38:03 +02'00'

Francisco Lloret Pastor

https://doi.org/10.1021/acs.inorgchem.1c01905

From page 251 to page 278

CONCLUSIONS AND PERSPECTIVES

In the last part of this Thesis work, the conclusions and more important results that have been reached will be summarised for each Chapter, along with some perspective for future works.

Chapter 2 is dedicated to the study of Re(IV)-based complexes. The synthesis, crystal structures and magnetic properties of nine species have been studied and reported across five publications, three of them were dedicated to the hexahalorhenate(IV) family members, whilst the last two are focused on the $[ReCl_4(bpym)]$ compound and its use as a metalloligand.

In the first set, the $(NH_4)_2[ReF_6]$ compound was characterised as a system that exhibits metamagnetism and SIM behaviour in the same system, an attribute unusual in molecular compounds based on $5d$ metal ions reported so far. The metamagnetic phenomena is due to a field-induced antiferromagnetic-to-paramagnetic ordering transition, being the antiferromagnetic interaction mainly *via* F···F contacts. Further studies of the hexahalorhenate(IV) entities with bulky counter-cations as $(PPh_4)^+$ or protonated ciprofloxacin antibiotic as a potentially interesting biological complex have been investigated. Because of the bulkiness of these cations, the $[ReX_6]^{2-}$ (X = Cl, Br or I) anions are found to be isolated, and as consequence, favouring the slow relaxation of the magnetisation phenomena in all these salts. To this regard, $(PPh_4)_2[ReBr_6]$ system exhibits the highest energy barrier of the $[ReX_6]^{2-}$ family ($U = 30.1$ cm^{-1} at 5000 G). Furthermore, $[H_2cip][Hcip][ReCl_6]Cl \cdot H_2O$ and $[Hcip]_2[ReBr_6]$ salts constitute the first magnetoestructural studies performed on compounds based on protonated ciprofloxacin and a paramagnetic $5d$ ion.

In future works, it would be interesting to keep exploring the synthesis of new salts combining the physical properties of the anionic $[ReX_6]^{2-}$ entities with potentially interesting cations in one molecule. Thus, the final materials may be able to perform multiple functions with an unusual combination of physical properties, or even a mutual interplay-synergy-of the properties involved.

The study on the second set starts with the direct impact that the solvent of crystallisation, MeCN or CH_3COOH and H_2O, has upon the final magnetic properties of the known unsolvated $[ReCl_4(bpym)]$ complex. Short intermolecular Cl···Cl contacts are present in both solvated compounds that preclude SIM behaviour. Besides, in contrast with the unsolvated system, they do not exhibit magnetic ordering through spin-canting phenomenon. Nevertheless, it was proven how it is possible to alter the magnetic behaviour of this type of Re(IV) complexes by changing the crystallisation solvent. On the other hand, the use of the $[ReCl_4(bpym)]$ system towards simple copper salts resulted into two novel one-dimensional coordination polymers, in which the dinuclear $[ReCl_4(\mu\text{-bpym})CuX_2]$ units (X = Cl or Br) are linked through double Cu-X-Cu halide bridges generating chains. In this way, these compounds constitute the first reported examples of doubly halogen-bridged and bipyrimidine-based Cu(II) chains including a paramagnetic $5d$ metal ion. Their magnetic studies revealed several magnetic exchanges through intermolecular interactions, mainly *via* Re-Cl···Cl-Re contacts. However, intramolecular interactions take place between Re(IV) and

Cu(II) ions through the bpym ligand and between Cu(II) ions mediated by halogen atoms, with the overall interaction being antiferromagnetic.

Following this research line, it would be interesting to expand the Re(IV) metalloligand compounds family. To this regard, *cis* and *trans* isomers of the $[ReCl_2(ox)_2]^{2-}$ system have already been synthesised, and their use towards another metallic centres is expected to generate new two- or three-dimensional networks connected through the two bridging bis-bidentate oxalate ligands. Furthermore, a Re(IV) system combining two different bridging ligands in one molecule, such as bpym and ox, could lead to an interesting selective metalloligand due to the different nature of both ligands.

Chapter 3 is focused on the investigation of iridium compounds in two different oxidation states. One publication features three novel Ir(III) bpym-based systems, whilst the other two are dedicated to six systems based on the magnetically active Ir(IV) ion.

The obtained $NBu_4[IrBr_4(bpym)]$ and the two $[IrBr_3(bpym)(MeCN)]$ polymorphs, represent three of the few mononuclear bpym-based Ir(III) compounds that have been reported up to date. Interestingly, the polymorphism phenomenon was encountered when different crystallisation solvents were employed. Moreover, the viability of oxidation of these systems to Ir(IV) was preliminary explored through chemical methods with a robust stability of the Ir(III) oxidation state. The cyclic voltammetry study performed on the salt complex shown a reversible Ir(III)-Ir(IV) pair, whereas no reversible process was observed for the polymorphs in the studied conditions.

The synthesis, crystal structure and magnetic properties of several Ir(IV)-based compounds have been investigated. The first steps to treat the DC magnetic behaviour of the mononuclear $(NBu_4)_2[IrX_6]$ (X = Cl or Br) systems have been reported. On the other hand, the study of the AC magnetic properties of these salts reveals SIM behaviour, constituting two of the few reported examples based on the Ir(IV) metal ion. Moreover, it was proven the suitability of the hexahaloiridates(IV) units as building blocks in a synthetic processes to lead to new mixed magnetic systems. To this regard, $\{IrCl_5(\mu\text{-}Cl)Cu(Viim)_4\}_n$ constitutes the first reported system based on Ir(IV) and Cu(II) and enables us to get for the first time the J value of the magnetic interaction between this $3d$-$5d$ couple. Three more one-dimensional coordination polymers of formula $\{IrBr_5(\mu\text{-}Br)Cu(L)_4\}_n$ (L = Meim, Viim or Buim) were obtained and magnetostructurally characterised. The compounds with the Meim and Viim ligands displayed antiferromagnetic behaviour, whereas the one with Buim displays a ferromagnetic coupling between Ir(IV) and Cu(II) metal ions across the bromide bridges.

As a perspective to future works, a collaboration with the University of Angers (France) is already underway to explore Ir(IV) multifunctional systems. Specifically, the crystallisation of the chiral conductor (*R,R,R,R*)-TM-BEDT-TTF [(*R,R,R,R*)-tetramethyl-bis(ethylenedithio)-tetrathiafulvalene] together with the anionic $[IrX_6]^{2-}$ (X = Cl or Br) entities. On the other hand, the ligand substitution of the hexahaloiridates(IV) by bpym or ox could lead to novel Ir(IV) metalloligands as the ones previously observed with the Re(IV) metal ion. Thus, new interesting magnetically active systems could be formed with these bis-bidentate ligands acting as bridges towards other metal ions and their properties studied.

Chapter 4 is committed to the synthesis, crystal structure and magnetic properties of one compound based on the Ho(III) metal ion with the DTPA ligand. Thus, the last work of this Thesis is dedicated to the novel $Na_2[Ho(DPTA)(H_2O)] \cdot 8H_2O$ system, which behaves as a SIM. It also exhibits a moderate MCE in a wide temperature range, from *ca.* 2 to 20 K, with a strong field-dependent magnetic entropy maxima between the liquid helium and hydrogen temperatures. Despite their limited cryogenic magnetic refrigeration performance, the results illustrate the potential of magnetically anisotropic Ho(III)-based SIMs as prototypes of molecular cryomagnetic coolants operating near the strategically relevant hydrogen liquefaction temperature.

Following the Ho(III) compound example, further investigations on cryogenic magnetic refrigeration are being conducted on other members of the lanthanides series. In this regard, we look towards Nd(III) and Er(III) metal ion based complexes, which also presents high J values.

APPENDIX A

RESUM

En el present resum es troba descrit l'abast i principals objectius d'aquesta Tesi juntament amb la seua metodologia. Alhora, el lector es guiat a través dels principals resultats. La Tesi es troba estructurada bàsicament en quatre Capítols, els quals són, una introducció que proporciona una visió general dels conceptes bàsics del Magnetisme Molecular, seguit de tres Capítols més, dos dels quals estan dedicats als composts basats en ions metàl·lics $5d$, en concret el Re(IV), Ir(III) i Ir(IV), mentre que l'últim es centra en l'Ho(III), un ió metàl·lic de la sèrie $4f$. Finalment, hi ha un Capítol final que serveix com a conclusió dels resultats que poden ser extrets dels anteriors amb algunes propostes per a futures investigacions.

El Capítol 1 aprofundeix en el coneixement fonamental relacionat amb el Magnetisme Molecular des del punt de vista de la mecànica quàntica, on el moment orbital i d'espín donen lloc a moments magnètics, la relació dels quals amb la termodinàmica estadística condueix al comportament magnètic de les mostres macroscòpiques. Tanmateix, l'expressió deduïda dependeix del coneixement de la funció de l'energia per a tots els estats tèrmicament poblats. Per a un determinat sistema aquestes poden ser desconegudes, per aquest motiu és habitual dependre d'unes quantes aproximacions. La fórmula de Van Vleck és capaç de reproduir la susceptibilitat magnètica d'una mostra sempre i quan el camp magnètic es considere una petita pertorbació del sistema inicial. També es mostra com l'aproximació tan sols es manté a alta temperatura, on l'energia produïda pel camp magnètic extern és menor que la tèrmicament disponible. A més a més, l'equació de Van Vleck és valida tan sols per a sistemes paramagnètics on $M = 0$ quan $H = 0$. D'aquesta manera, s'explica el comportament paramagnètic de sistemes simples.

En una segona part introductòria, es presenta la interacció entre el moment angular orbital i d'espín que presenta un àtom, i com això dóna lloc a l'acoblament espín-òrbita dels moments magnètics, el qual és interpretat a través de dos esquemes energètics diferents. El primer es coneix com a model L-S i s'empra per a elements lleugers, i el segon com a model j-j per a àtoms més pesats. L'anomenat efecte de ZFS pot sorgir per la combinació de l'acoblament espín-òrbita i la simetria del sistema, d'aquesta manera donant lloc al desdoblament dels diferents nivells d'energia sense cap aplicació d'un camp magèntic extern. Aquests sistemes esdevenen magnèticament anisòtrops. Una altra interacció magnètica apareix rellevant depenen de la distància entre els diferents centres metàl·lics i la temperatura del sistema. Aquestes interaccions poden ser principalment per ordenaments ferromagnètics o antiferromagnètics, les quals no poden ser ignorades per cap sistema paramagnètic a suficient baixa temperatura. Les interaccions febles poden ser fàcilment preses en compte amb el paràmetre de Weiss (θ). A més a més, per a sistemes on no hi ha un moment angular orbital associat a l'estat fonamental dels ions metàl·lics que interactuen, aquesta pot ser tractada amb un Hamiltonià d'intercanvi espín-espín, que inclou la correlació entre els centres metàl·lics escollits mitjançant una constant d'intercanvi magnètic (J).

Al final del Capítol 1 es consideren les mesures dinàmiques de la susceptibilitat

magnètica i com la redistribució dels dipols magnètics requereix una certa quantitat de temps que depén de la freqüència del camp extern aplicat i la temperatura. Es revisen breument els sistemes amb un sol temps de relaxació o una distribució d'ells mitjançant el model de Debye generalitzat, juntament amb els mecanismes de relaxació més comuns que poden tenir lloc. Pel que fa a l'estudi de la dinàmica d'espín, s'introdueix el primer sistema reportat en mostrar cicles d'histèresi magnètica interessants a nivell molecular i aquests són comparats amb els clàssics obtinguts amb compostos ferromagnètics.

Les propietats magnètiques de les espècies que contenen ions metàl·lics $4f$, i especialment $5d$, s'han explorat relativament menys en comparació amb els sistemes $3d$. Això prové de la dificultat per fer front als acoblaments espín-òrbita més forts que presenten els àtoms més pesats, que esdevé un factor d'influència directa en l'anisotropia magnètica que els caracteritza. Com a conseqüència, si bé el coneixement detallat dels mecanismes d'intercanvi relacionats amb els ions $3d$ està considerablement avançat, hi ha menys comprensió de la correlació magnètica en sistemes $4f$ i $5d$. D'aquesta manera, els Capítols següents es centren principalment en la química de coordinació i caracterització de sistemes basats en els ions metàl·lics de Re(IV), Ir(III), Ir(IV) i Ho(III). L'abast d'aquesta investigació pretén tant estudiar el comportament magnètic de complexos mononuclears, com millorar la nostra comprensió de l'intercanvi magnètic d'espècies que contenen aquests ions metàl·lics, alhora que s'explora noves aplicacions potencials per a aquests sistemes. Per assolir aquest objectiu, totes aquestes línies de treball es centren a compartir una metodologia des d'un punt de vista sintètic dins del camp del Magnetisme Molecular, on els composts obtinguts es caracteritzen principalment per un espectre infraroig preliminar seguit d'una anàlisi elemental dels percentatges de C, N i H juntament amb les proporcions dels elements pesats. Posteriorment, les seues estructures es resolen mitjançant la difracció de raigs-X sobre monocristall i els seus patrons són comparats amb la resta de la mostra per difracció de raigs-X en pols, en tal de confirmar la seua homogeneïtat. A més a més, per a mostres magnèticament actives es realitza la mesura de les seues propietats magnètiques sobre mostres molturades, i juntament amb les dades estructurals es realitza una correlació amb el comportament magnètic.

El Capítol 2 està dedicat a l'estudi de sistemes basats en ions metàl·lics de Re(IV), el qual es escollit pel seu alt efecte de ZFS i el seu valor efectiu d'espín. A més a més, la manca de contribució orbital per als complexos Re(IV) octaèdrics constitueix un avantatge respecte a altres elements, on es produeixen efectes espín-òrbita de primer i segon ordre. Per tant, els sistemes de Re(IV) són relativament més fàcils d'ajustar mitjançant models teòrics. Es poden obtenir molts resultats interessants dels complexos de Re(IV). A la literatura es poden trobar composts amb propietats remarcables, com el comportament de SIM, que s'espera que presenten entitats de Re(IV) aïllades, mentre que els composts polinuclears contribueixen a un millor coneixement de l'intercanvi magnètic entre diferents centres metàl·lics, on també poden sorgir fenòmens de SMM. D'altra banda, també s'han observat altres fenòmens magnètics singulars, com *spin-canting*, anti-, ferro-, ferri- o metamagnetisme en sistemes que contenen aquest l'ió metàl·lic.

Els treballs publicats dins d'aquest Capítol es poden dividir en dues parts. El primer està dedicat a l'estudi de les propietats magnètiques de les espècies mononuclears aniòniques $[ReX_6]^{-2}$ (X = F, Cl, Br, I), mentre que una segona part està

dedicada al compost neutre $[ReCl_4(bpym)]$ (bpym = 2,2'-bipirimidina).

Com a part d'una col·laboració amb la *University of Nevada* (Las Vegas), el treball presentat, a l'Article 1, descriu la sal d'amoni de l'entitat aniònica $[ReF_6]^{-2}$. Aquest sistema presenta dos comportaments magnètics, metamagnetisme i relaxació lenta de la magnetització coexistint junts, un atribut inusual en els sistemes moleculars basats en ions metàl·lics de la sèrie $5d$ reportats fins ara. Aquest sistema cristal·litza en el grup espacial trigonal $P\bar{3}m1$. Els àtoms d'hidrogen del catió amoni no es tenen en compte durant el procediment de refinament, tanmateix, les seues posicions més favorables es calculen mitjançant mètodes de DFT, mostrant que es pot produir un desordre en sals d'amoni. Aquestes distorsions escurcen algunes distàncies H···F emfatitzant els enllaços d'hidrogen. Els càlculs d'enllaç per DFT de l'anió $[ReF_6]^{-2}$ en la seua geometria experimental mostren la presència d'enllaços Re-F σ, que són gairebé iònics. La seua comparació amb l'anió en fase gasosa proporciona unes longituds mitjanes d'enllaç Re-F més llargues, de manera que la diferència es deu a les forces d'empaquetament. La sal també es caracteritza per espectroscòpia Raman, on el desdoblament dels pics Raman es correlaciona amb la simetria de l'anió $[ReF_6]^{-2}$.

D'altra banda, l'estudi de les propietats magnètiques mitjançant mètodes DC revela un ordenament antiferromagnètic dels portadors d'espín mitjançant interaccions intermoleculars febles F···F (*via* Re-F···F-Re) i N···F (*via* Re-F···N···F-Re) amb un màxim en la representació χ_M *vs.* T. El màxim disminueix a mesura que s'apliquen camps magnètics més alts, la qual cosa suggereix l'aparició d'una transició d'ordenació antiferromagnètica a paramagnètica induïda pel camp, típica dels sistemes metamagnètics. La corba de magnetització mesurada a 2 K dóna també suport a aquest comportament, ja que els valors de M augmenten amb el camp aplicat amb un punt d'inflexió tènue a un camp crític. Per a estudiar més a fons les propietats magnètiques de la sal $(NH_4)_2[ReF_6]$, s'han realitzat mesures de susceptibilitat magnètica AC, que mostren senyals incipients fora de fase a molt baixa temperatura, la qual cosa és indicativa d'un sistema amb relaxació lenta de la magnetització.

Pel que fa a aquest treball en concret, el qual firme com a quart coautor amb igual participació que el segon i el tercer, la meua aportació personal s'ha centrat principalment en la purificació de la mostra $(NH_4)_2[ReF_6]$ proporcionada pels nostres col·laboradors, juntament amb la seua caracterització mitjançant espectroscòpia infraroja, preparació, mesura i tractament de les dades experimentals obtingudes mitjançant els dispositius SQUID i PPMS.

Les sals $(PPh_4)_2[ReX_6]$ [PPh_4^+ = tetrafenilfosfoni, X = Br o I], es descriuen a l'Article 2, el qual està elaborat en col·laboració amb la *Universidad de la República* (Uruguai), aquests són un dels pocs exemples descrits a la literatura de compostos mononuclears basats en l'ió metàl·lic Re(IV) que mostren una relaxació lenta de la magnetització induïda pel camp. Les sals cristal·litzen en el sistema triclínic amb el grup espacial $P\bar{1}$ i les seues estructures estan formades per cations voluminosos $(PPh_4)^+$ que mantenen ben separats els anions hexahalorenat(IV) entre ells.

Les mesures de susceptibilitat magnètica DC a diferents temperatures mostren un comportament molt semblant per als dos compostos, típic dels sistemes de Re(IV) que es troben aïllats magnèticament. La disminució dels valors de $\chi_M T$ a baixa temperatura són principalment a causa dels alts efectes de ZFS que posseeix aquest ió metàl·lic. D'altra banda, les mesures magnètiques AC revelen la presència de

senyals fora de fase per als dos compostos en el rang de baixa temperatura quan s'aplica un camp magnètic extern de 1000 o 5000 G. Tanmateix, la dinàmica de relaxació que presenten els dos compostos no es veu igualment afectada pels camps externs, essent 5000 G l'òptim per al bromo derivat, tal com suggereix la presència de més màxims en χ'' que apareixen a freqüències més altes, mentre que el seu nombre disminueix per al iodo complex al mateix camp. Els valors obtinguts del paràmetre α en les representacions Cole-Cole suggereixen una distribució estreta dels temps de relaxació d'aquests complexos de Re(IV) mononuclears. Pel que fa a les dades experimentals $\ln\tau$ *vs.* $1/T$, aquestes s'ajusten tenint en compte que la relaxació de la magnetització és impulsada per un únic mecanisme Orbach. Per a una descripció més precisa de tota la corba, en el cas del bromo derivat es considera un conjunt de quatre mecanismes de relaxació entre l'espín i la xarxa cristal·lina, aquest són Orbach, Direct, Raman i QTM. Notablement, el bromo complex presenta la barrera energètica més alta de la família $[ReX_6]^{-2}$.

La meua contribució a aquest treball, on aparec com a segon coautor, s'ha centrat en els aspectes pràctics de la síntesi i la cristal·lització adequada dels compostos reportats per als posteriors estudis de difracció de raigs-X sobre monocristall. També he participat en la mesura i resolució de les dades estructurals, juntament amb la caracterització per raigs-X en pols, així com en la interpretació i processament de les dades experimentals obtingudes mitjançant els magnetòmetres SQUID i PPMS.

Els últims sistemes relacionats amb les espècies d'hexahalorenat(IV) d'aquesta Tesi tenen com a objectiu mantenir les interessants propietats magnètiques que mostra aquest ió metàl·lic, alhora que s'afegeixen noves funcionalitats al material final mitjançant l'ús d'un catió amb potencial interés biològic amb les entitats aniòniques $[ReX_6]^{-2}$ (X = Cl, Br). D'aquesta manera, dos nous compostos de Re(IV) amb fórmula $[H_2cip][Hcip][ReCl_6]Cl \cdot H_2O$ i $[Hcip]_2[ReBr_6]$ (cip = ciprofloxacin) són reportats a l'Article 3. Constituint aquests compostos el primer estudi magnetoestructural realitzat sobre sistemes basats en l'antibiòtic protonat ciprofloxacin i un ió paramagnètic de la sèrie 5*d*.

El cloro derivat cristal·litza al grup espacial $P2_1/c$, mentre que el bromo complex al grup *Pbca*. A més, aquests sistemes mononuclears de Re(IV) aïllats són possibles gràcies als voluminosos cations protonats de ciprofloxacin. Per a una millor comprensió de les forces electroestàtiques que mantenen l'empaquetament cristal·lí, s'han calculat i analitzat les superfícies d'Hirshfeld per ambdós sals, on es veuen reflectides la varietat d'interaccions que tenen lloc a les seues xarxes cristal·lines.

Les mesures de susceptibilitat magnètica DC mostren un comportament molt similar per als dos compostos, típic dels sistemes mononuclears que contenen un ió de Re(IV) aïllat magnèticament. No es detecta cap màxim de la susceptibilitat magnètica a la gràfica χ_M *vs.* T a baixa temperatura, cosa que indica l'absència d'interaccions antiferromagnètiques significatives. Per tant, la disminució detectada en les representacions $\chi_M T$ *vs.* T es deurà principalment als efectes de ZFS, que són molt significatius en sistemes mononuclears de Re(IV). Les mesures de susceptibilitat magnètica AC a baixa temperatura revelen senyals fora de fase induïdes pel camp per als dos sistemes de sals, on les representacions $\ln\tau$ *vs.* $1/T$ s'obtenen a un camp extern òptim de 5000 G. En primer lloc, es poden ajustar les dades tenint en compte que la relaxació de la magnetització només implica un procés Orbach, però és possible una reproducció més precisa de tota la corba experimental tenint

en compte els mecanismes Direct i Raman.

En la següent part, s'explora la substitució directa de dos lligands clorur de la entitat $[ReCl_6]^{-2}$ per un lligand bpym, com una estratègia diferent per sintetitzar nous sistemes emprant el complex com a lligand. Tanmateix, a l'Article 4, es reporta l'efecte del dissolvent de cristal·lització sobre el compost $[ReCl_4(bpym)]$, i com canvien les seues propietats magnètiques en contrast amb el sistema no solvatat.

$[ReCl_4(bpym)] \cdot MeCN$ i $[ReCl_4(bpym)] \cdot CH_3COOH \cdot H_2O$ cristal·litzen al sistema monoclínic amb els grups espacials $P2_1/n$ i $P2_1/c$, respectivament. Tots dos sistemes presenten contactes curts Re-Cl···Cl-Re formant una xarxa cristal·lina que allotja les molècules de dissolvent. A més a més, també es produeixen interaccions intermoleculars entre $[ReCl_4(bpym)]$ i els seus dissolvents de cristal·lització. Per avaluar tots aquests contactes s'han calculat les superfícies d'Hirshfeld i s'han analitzat les seues empremtes digitals.

Pel que fa a les propietats magnètiques d'ambdós compostos, les importants interaccions antiferromagnètiques entre les diferents entitats de Re(IV) a través de l'espai impedeixen que es produïsca el fenomen de la relaxació lenta de la magnetització. Tots dos sistemes mostren un comportament magnètic similar amb una reducció dels valors $\chi_M T$ amb la disminució de la temperatura com a resultat de les interaccions antiferromagnètiques entre ions de Re(IV), així com a causa de l'efecte de ZFS. No es detecta cap màxim de susceptibilitat magnètica per a cap dels dos compostos. En canvi, les propietats magnètiques del sistema sense dissolvent de cristal·lització són molt diferents, mostrant un ordre magnètic mitjançant *spin-canting*. D'aquesta manera, és possible ajustar el comportament magnètic d'aquest tipus de complexos de Re(IV) canviant el dissolvent de cristal·lització.

L'ús del metal·loligand $[ReCl_4(bpym)]$ cap a un ió metàl·lic paramagnètic com el Cu(II) es reporta a l'Article 5, juntament amb els nostres col·laboradors de la *Università della Calabria* (Itàlia). En ell es tracten dos polímers de coordinació unidimensionals amb fórmula general $\{[ReCl_4(\mu\text{-bpym})CuX_2] \cdot Solv\}_n$, que presenten diferents estructures cristal·lines depenent de X i Solv. Concretament, quan X = Cl i Solv = H_2O, el sistema cristal·litza en el grup espacial $P2_1/c$, mentre que quan X = Br i Solv = $CHCl_3$, cristal·litza en el $P2_1/n$ grup espacial. Tots dos sistemes estan formats per unitats dinuclears $[ReCl_4(\mu\text{-bpym})CuX_2]$, que s'uneixen entre si mitjançant ponts d'halogen Cu-X-Cu dobles, generant així cadenes amb molècules de dissolvent presents en les seues respectives xarxes cristal·lines. D'aquesta manera, aquests compostos constitueixen els primers exemples reportats de cadenes de Cu(II) basades en la bipirimidina i doble pont d'halogen que inclouen un ió metàl·lic paramagnètic $5d$.

Les interaccions intermoleculars del tipus Re-Cl···Cl-Re i X···π estan presents per a tots dos compostos, però el cloro derivat també presenta enllaços d'hidrogen connectant els àtoms terminals de clor de les unitats dinuclears. D'aquesta manera, es poden produir diversos intercanvis magnètics mitjançant diferents interaccions intermoleculars, però principalment mitjançant contactes *via* Re-Cl···Cl-Re. També es produeixen interaccions intramoleculars entre els ions de Re(IV) i Cu(II) a través del lligand bpym i entre ions de Cu(II) mediats per àtoms d'halogen. Les dades de susceptibilitat magnètica obtingudes mitjançant mesures DC mostren com els valors de $\chi_M T$ disminueixen a mesura que es redueix la temperatura, principalment a causa de les interaccions moleculars antiferromagnètiques i els efectes de ZFS. La

presència de màxims en les representacions χ_M *vs.* T donen suport inequívocament a l'ocurrència d'intercanvis antiferromagnètics entre els ions metàl·lics implicats.

A causa de la complexitat dels sistemes que presenten un ió metàl·lic altament anisòtrop com el Re(IV) i a causa dels diferents intercanvis magnètics que tenen lloc, hi ha una manca d'un model teòric adequat per avaluar completament la corba de susceptibilitat magnètica experimental. No obstant això, es fan dos tipus de tractaments en el rang de temperatura de 20-300 K, on hi ha un bon comportament lineal de la representació ${\chi_M}^{-1}$ *vs.* T. En el primer, les dades s'ajusten a l'expressió de Curie-Weiss, on la magnitud i signe negatiu de la constant de Weiss dóna suport al fet que es produeixen interaccions antiferromagnètiques significatives en ambdós sistemes. En el segon, es realitza una simulació isòtropa de les dades experimentals amb dos constants d'acoblament d'intercanvi diferents per a la interacció Cu(II)-Cu(II) i Re(IV)-Cu(II). El valor calculat de l'intercanvi Cu(II)-Cu(II) indica un acoblament antiferromagnètic relativament fort, mentre que es produiria un acoblament antiferromagnètic molt menys intens entre els ions de Re(IV) i Cu(II) en ambdós compostos.

En aquesta col·laboració, que firme com a segon coautor, la meua contribució ha estat centrada en els aspectes pràctics de sintetitzar i cristal·litzar adequadament el compost $\{[ReCl_4(\mu\text{-bpym})CuBr_2] \cdot CHCl_3\}_n$ per a la seua resolució estructural. També he participat en la seua caracterització mitjançant difracció de raigs-X en pols, espectroscòpia infraroja i anàlisi elemental de percentatges C, H, N juntament amb la preparació, mesura, interpretació i processament de dades experimentals obtingudes mitjançant el magnetòmetre SQUID.

D'altra banda, els treballs que tracten sobre compostos basats en l'iridi es recullen al Capítol 3. Tot i que els sistemes d'Ir(III) s'han investigat intensament a causa de les seues potencials aplicacions tecnològiques en àrees com la catàlisi, imatge i sensors, els complexos d'Ir(IV) s'han mantingut en gran mesura sense explorar. Pel que fa a aquesta Tesi es centrarà en el desenvolupament de nous compostos d'Ir(IV) amb l'objectiu de conéixer millor la seua química i propietats. A diferència de les espècies d'Ir(III), l'Ir(IV) és un ió metàl·lic paramagnètic en simetria octaèdrica o octaèdrica distorsionada, amb propietats magnètiques prometedores a causa del seu alt efecte de ZFS, que confereix als compostos basats en l'Ir(IV) amb anisotropia magnètica. A més a més, com és un ió metàl·lic de la sèrie $5d$ tindrà una deslocalització significativa de la seua densitat electrònica sobre els lligands, provocant així una millora de les propietats magnètiques en compostos polinuclears en comparació amb els seus anàlegs de la sèrie $3d$. No obstant això, el seu terme fonamental $^2T_2$ combinat amb el seu elevat acoblament espín-òrbita fan que aquests sistemes siguen molt difícils de ser analitzats.

En aquesta Tesi s'han emprat les sals alcalines d'hexahaloiridat(IV) comercialment disponibles com a reactius de partida per a l'intercanvi de lligands i cations. Els contracations voluminosos com $(NBu_4)^+$ no només confereixen propietats pràctiques al compost final, com solubilitat en una gran varietat de dissolvents, sinó que també condueixen a sistemes interessants que poden presentar una relaxació lenta de la magnetització. A més a més, aquestes noves sals sintetitzades són emprades en la preparació de nous sistemes polinuclears d'Ir(IV) mitjançant l'ús de les unitats $[IrX_6]^{2-}$ (X = Cl, Br) com a components del compost final, juntament amb altres ions paramagnètics de la sèrie $3d$, com per exemple el Cu(II), on els derivats

d'imidazol també s'empren com a lligands auxiliars per bloquejar les seues posicions de coordinació equatorial.

D'altra banda, l'intercanvi de lligands en aquests sistemes esdevé un repte des del punt de vista sintètic, principalment per la fàcil reducció que presenten les espècies d'Ir(IV) cap als seus anàlegs d'Ir(III), els quals són més estables. Pel que fa a la substitució de dos lligands bromur per una bpym, a l'Article 6, es tracta l'estudi de tres noves estructures cristal·lines basades en l'Ir(III) i la bpym, on s'observa el fenomen del polimorfisme quan s'utilitzen diferents dissolvents de cristal·lització. Tan sols uns pocs treballs tracten sobre el polimorfisme cristal·lí dins de la química de l'Ir(III). A més a més, cal destacar que tan sols s'han reportat fins ara unes poques estructures cristal·lines de compostos mononuclears d'Ir(III) amb bpym. El compost $NBu_4[IrBr_4(bpym)]$ cristal·litza al grup espacial $P2_1/c$, i $[IrBr_3(bpym)(MeCN)]$, als grups espacials $P2_1/n$ i $P2_12_12_1$. Les interaccions intermoleculars del tipus C-H···N i C-H···Br febles estan presents en la sal. En canvi, els polimorfs presenten contactes π···Br, C-H···Br i Br···Br per estabilitzar les seues estructures supramoleculars. A més a més, també s'han analitzat les seues estructures cristal·lines mitjançant els programes SHAPE i CrystalExplorer.

L'oxidació d'aquests nous compostos d'Ir(III) a Ir(IV) emprant espècies químiques s'ha estudiat preliminarment amb mescles estequiomètriques de diversos oxidants en dissolucions aquoses àcides. Així i tot, els complexos d'Ir(III) van demostrar ser estables contra aquest tipus d'oxidació. Per altra banda, es van investigar amb cura les propietats electroquímiques d'aquests compostos. La voltamperometria cíclica en aquests sistemes mostra el comportament reversible del parell Ir(III)-Ir(IV) en el rang 10-500 $mV\,s^{-1}$ per a la sal $NBu_4[IrBr_4(bpym)]$, mentre que no s'observen pics reversibles per als altres sistemes.

D'altra banda, també s'ha explorat una nova estratègia per a la preparació de nous materials magnètics basats en l'Ir(IV) i ions metàl·lics paramagnètics de la sèrie $3d$ mitjançant l'ús de les unitats $[IrX_6]^{-2}$ (X = Cl, Br) com a metal·loligands cap al Cu (II). A l'Article 7, es presenten els resultats pel que fa a les espècies amb X = Cl, on s'han caracteritzat estructuralment i magnèticament el reactiu de partida $(NBu_4)_2[IrCl_6]$ i la cadena heterobimetàl·lica d'Ir(IV) i Cu(II) de fórmula $\{IrCl_5(\mu\text{-}Cl)Cu(Viim)_4\}_n$ (Viim = 1-vinilimidazol), la qual constitueix el primer sistema reportat basat en els ions Ir(IV) i Cu(II). Tots dos complexos cristal·litzen al grup espacial $C2/c$. Tanmateix, a causa dels voluminosos contracations en el sistema mononuclear, les unitats $[IrCl_6]^{-2}$ estan ben aïllades entre elles. D'altra banda, l'empaquetament cristal·lí del compost unidimensional connecta les diferents cadenes entre si mitjançant interaccions π···π, les quals acaben adoptant una disposició perpendicular entre elles.

La representació $\chi_M T$ *vs.* T per al compost mononuclear s'ajusta a l'equació de Curie-Weiss fins a *ca.* 50 K. Addicionalment, fora d'aquesta publicació, la corba de $\chi_M T$ s'ajusta a tot el rang de temperatures amb el model teòric proposat en aquesta Tesi. D'altra banda, la mateixa representació per al sistema unidimensional es reprodueix amb un model aproximat tenint en compte una cadena amb un espín efectiu isotròpic de $S = 1/2$, on es presenta un acoblament ferromagnètic entre els ions Cu(II) i Ir(IV). D'aquesta manera, és la primera vegada que s'avalua la interacció magnètica entre aquest parell d'ions metàl·lics quan es troben units a través d'un pont clorur. A més a més, per a avaluar les senyals fora de fase induïdes

per un camp magnètic extern, es realitzen mesures de susceptibilitat magnètica AC sobre el compost mononuclear. El seu procés de relaxació s'ajusta mitjançant un mecanisme Orbach en la part lineal de la representació $\ln\tau$ *vs.* $1/T$ i tota la corba es reprodueix quan es considera un mecanisme Direct i Raman.

D'altra banda, l'Article 8 recopila els resultats obtinguts amb la unitat $[IrBr_6]^{-2}$, essent aquesta publicació l'últim treball comprés en el Capítol 3. L'estructura cristal·lina del compost $(NBu_4)_2[IrBr_6]$ es troba prèviament publicada, mentre que la seua corba experimental de $\chi_M T$ s'ajusta amb el model teòric introduït en aquesta Tesi. El complex amb entitats d'hexabromoiridat(IV) aïllades presenta una relaxació lenta de la magnetització, confirmada a través de les mesures de susceptibilitat magnètica AC. Aquest complex es converteix en el cinqué SIM reportat basat en l'ió Ir(IV). Com en el cas del compost mononuclear $(NBu_4)_2[IrCl_6]$, la representació $\ln\tau$ *vs.* $1/T$ mostra un rang lineal ben reproduït mitjançant un mecanisme Orbach, el qual considera un sol temps de relaxació. En canvi, tota la corba es reprodueix quan es considera un mecanisme Direct i Raman.

L'ús de l'entitat mononuclear $[IrBr_6]^{2-}$ cap a ions Cu(II) juntament amb lligands auxiliars, també és explorada per al bromo derivat. D'aquesta manera, s'han estudiat estructuralment i magnèticament tres nous complexos unidimensionals de fórmula $\{IrBr_5(\mu\text{-Br})Cu(L)_4\}_n$ (L = Meim, Viim o Buim, essent Meim = 1-metilimidazol i Buim = 1-butilimidazol). Aquests cristal·litzen als grups espacials $P\bar{1}$, $C2/c$ i $Pccn$, respectivament. En els compostos obtinguts amb Meim i Viim, es troben importants contactes Ir-Br···Br-Ir i interaccions π···Br entre cadenes. En canvi, el volum dels grups butil dels lligands Buim manté les cadenes completament separades entre si.

Com en el cas del compost unidimensional obtingut amb el cloro derivat, les dades de susceptibilitat magnètica DC es tracten de forma aproximada tenint en compte el model d'una cadena amb un espín efectiu isotròpic de $S = 1/2$. Per als complexos obtinguts amb els lligands Meiim i Viim, les representacions $\chi_M T$ *vs.* T mostren un acoblament antiferromagnètic entre els ions metàl·lics Cu(II) i Ir(IV) a baixa temperatura. En canvi, s'observa un acoblament ferromagnètic dominant per al compost obtingut amb Buiim.

Els elements del bloc de les terres rares han obtingut un interés rellevant a causa de les seues propietats electròniques, magnètiques i òptiques úniques. Per exemple, els complexos mononuclears d'ions Ln(III) que presenten una relaxació lenta de la magnetització, els anomenats SIM de lantànids, s'han donat a conéixer en diverses àrees de la nanociència i la nanotecnologia. A més a més, a causa de les seues conegudes propietats de coherència magnetotèrmica i quàntica, els derivats mononuclears de Gd(III), Dy(III) i Ho(III) són exemples representatius d'aplicacions prometedores de SIMs basats en lantànids tant com a refrigerants criomagnètics moleculars, com emprats en tecnologies de processament d'informació quàntica. En conseqüència, el Capítol 4 explora les propietats i les aplicacions potencials de l'Ho(III) del bloc de les terres rares.

A més a més, quan es busquen materials moleculars amb diverses propietats físiques que es pugen utilitzar en diferents aplicacions tecnològiques, una bona estratègia és seleccionar una molècula de partida que ja dispose d'una. Per aquest motiu, la nostra atenció s'ha dirigit cap al grup de complexos mononuclears que contenen ions Ln(III) (Ln = Gd, Dy, Ho) i lligands poliaminocarboxilats lineals o cíclics, els quals s'utilitzen habitualment com a agents de contrast en la ressonància

magnètica.

A l'Article 9, es mostren els nostres primers resultats sobre la síntesi, caracterització estructural i propietats fisicoquímiques generals d'un nou complex d'Ho(III) de fórmula $Na_2[Ho(DPTA)(H_2O)] \cdot 8H_2O$ (DPTA = Dietiletriamina-N, N, N', N'', N''-pentaacetat), així com una investigació preliminar de la dependència del comportament magnètic sota un camp magnètic DC i AC. El compost cristal·litza al grup espacial $P2_1/n$ i consta de dos ions d'Ho(III) cristal·logràficament independents, ambdós amb un índex de coordinació de nou i geometries distorsionades similars, segons els càlculs del programa SHAPE entre un prisma trigonal triapicat i un antiprisma quadrat monopicat. Les entitats dinuclears es connecten entre si mitjançant ions Na^+ donant una estructura tridimensional, on en els seus petits porus rectangulars hi ha la majoria de les molècules d'aigua de cristal·lització.

Les mesures de susceptibilitat magnètica DC mostren com els valors de $\chi_M T$ disminueixen contínuament al baixar la temperatura, essent una característica principalment atribuïda als efectes del LF que provoca la divisió dels diferents M_J de l'estat fonamental $^5I_8$. Aquest fet es troba recolzat per la no superposició de les corbes de magnetització isotèrmiques. D'altra banda, també s'han estudiat les propietats magnètiques dinàmiques, revelant senyals fora de fase amb i sense aplicar un camp magnètic extern. L'anàlisi de les representacions χ' i χ'' *vs.* ν en un rang de freqüències d'1-10 kHz es realitza mitjançant l'equació de Debye generalitzada, mostrant una ampla distribució dels temps de relaxació. La representació $\ln \tau$ *vs.* $1/T$ és reproduïda amb un sol mecanisme Orbach amb valors dins del rang dels pocs exemples de SIM d'Ho(III) reportats. A més a més, malgrat el seu limitat rendiment en la refrigeració magnètica criogènica, els resultats magnetotèrmics il·lustren el potencial estratègicament rellevant dels SIM basats en ions magnèticament anisotròpics com l'Ho(III), en qualitat de prototips de refrigerants criomagnètics moleculars que operen prop de la temperatura de liqüefacció de l'hidrogen.

La meua contribució a aquest treball, la qual firme com a quart coautor, s'ha centrat des d'un punt de vista fonamentalment de caràcter cristal·logràfic, portant a cap el desenvolupament de l'estratègia de mesura i la recol·lecció de les dades de difracció de raigs-X sobre monocristall, així com el refinament de les dades cristal·logràfiques per a la seua resolució estructural.